PhD Dissertation

International Doctorate School in Information and
Communication Technologies

DIT - University of Trento

MEMS PIEZORESISTIVE MICRO-CANTILEVER ARRAYS FOR SENSING APPLICATIONS

Andrea Adami

Advisor:
Dr. Leandro Lorenzelli
Fondazione Bruno Kessler (Trento)

Copyright © 2010 Andrea Adami

Abstract

In several application fields there is an increasing need for a diffused on-field control of parameters able to diagnosis potential risks or problems in advance or in early stages in order to reduce their impact. The timely recognition of specific parameters is often the key for a tighter control on production processes, for instance in food industry, or in the development of dangerous events such as pollution or the onset of diseases in humans. Diffused monitoring can be hardly performed with traditional instrumentation in specialised laboratories, due to the time required for sample collection and analysis. In all applications, one of the key-points for a successful solution of the problem is the availability of detectors with high-sensitivity and selectivity to the chemical or biochemical parameters of interest. In this paradigm, MEMS technologies are emerging as realisation of miniaturised and portable instrumentation for agro-food, bio-medical and material science applications with high sensitivity and low cost.

Among different options, cantilever micro-mechanical structures are one of the most promising technical solution for the realisation of MEMS detectors with high sensitivity. This thesis deals with the development of cantilever-based sensor arrays for chemical and biological sensing and material characterisation. In addition to favourable sensing properties of single devices, an array configuration can be easily implemented with MEMS technologies, allowing the detection of multiple species at the same time, as well as the implementation of reference sensors to reject both physical and chemical interfering signals. In order to provide the capability to operate in the field, solution providing simple system integration and high robustness of readout have been preferred, even at the price of a lower sensitivity with respect to other possibilities requiring more complex setups. In particular, piezoresistive readout has been considered as the best trade-off between sensitivity and system complexity, due to the easy implementation of readout systems for resistive sensors and to their high potential for integration with standard CMOS technologies. In this general framework, this thesis reports the activities related to the development of piezoresistive cantilever arrays for portable applications. In particular, modelling of devices and fabrication processes were performed in order to select the best design and technologies for implementation of gravimetric and stress sensors, as well as procedures for material characterisation. Different case-studies were chosen for the development of devices. In agrofood field, activity were focused on the detection of amines, used as markers of fish spoilage during fish supply chain, while in bio-medical field cantilever were targeted to the detection of specific DNA sequences for portable diagnostic systems. Finally, thin TiO_2 film characterisation based on micromechanical structure where implemented as a tool for analysis of deposition quality. All devices were fabricated by the BioMEMS research unit of FBK (Fondazione Bruno Kessler - Center for Materials and Microsystems, Trento), using FBK clean room facilities.

Keywords

Microcantilever sensors, MEMS technologies, gas sensors, DNA detectors, materials characterisation

Contents

1. INTRODUCTION 1

1.1. THE CONTEXT: APPLICATION-ORIENTED PORTABLE AND MINIATURISED SYSTEMS 1

1.2. THESIS CONTENT AND INNOVATIVE ASPECTS 2

1.3. STRUCTURE OF THE THESIS 4

2. STATE OF THE ART 6

2.1. INTRODUCTION 6

2.2. CANTILEVER SENSORS 8

2.3. CANTILEVER NANOMECHANIC RESPONSE FOR DNA SENSING 12

2.4. CANTILEVERS FOR MATERIAL CHARACTERISATION 16

2.5. CANTILEVER TECHNOLOGIES 18

3. PIEZORESISTIVE CANTILEVER DEVICES 20

3.1. MECHANICAL PROPERTIES 20

3.2. PIEZORESISTIVE READ-OUT 22

3.2.1 Monocrystalline Si 22

3.2.2 Polysilicon 23

3.2.3 Strain gauges 23

3.2.4 Resistor geometrical efficiency: resistor and passivation thicknesses 24

3.2.5 Thermo-mechanical and electrical noise and SNR ratio 25

3.3. RESONATING CANTILEVER SENSORS 25

3.4. STATIC CANTILEVER SENSORS 28

3.5. TECHNOLOGIES FOR CANTILEVER FABRICATION 29

3.5.1 Fabrication process of 10 µm-thick silicon microcantilevers 29

3.5.2 Fabrication process of 2 µm-thick silicon microcantilevers 33

3.5.3 Development of 340nm beams 34

4. DEVELOPMENT OF MICROCANTILEVER DETECTORS FOR GRAVIMETRIC SENSING 42

4.1. ANALYTICAL MODELLING 42

4.2. FINITE ELEMENT (FE) MODELLING 45

4.2.1 Static analysis 45

4.2.2 Modal analysis 46

4.2.3 Stress-stiffening 48

4.2.4 Under-etch effect 49

4.2.5 Read-out optimization 50

4.2.6 Mass sensitivity and resolution 52

4.3. CANTILEVER DESIGN 54

4.3.1 Design of 10µm devices 54

4.3.2 Design of 2µm devices *56*
4.4. ELECTRO-MECHANICAL CHARACTERISATION OF DEVICES 57
4.5. DEVICE SENSITIVITY 61
4.5.1 Estimation of cantilever performances *65*
4.5.2 Sensitivity tests *66*
4.6. DISCUSSION 68
5. DEVELOPMENT OF MICROCANTILEVER DETECTORS FOR STRESS SENSING 70
5.1. ANALYTICAL MODELLING AND TECHNOLOGY COMPARISON 70
5.2. FE MODELLING 77
5.3. DESIGN 79
5.4. DISCUSSION 81
6. MATERIAL CHARACTERISATION WITH MICRO CANTILEVER DETECTORS 82
6.1. MODELLING AND DESIGN OF STRUCTURES FOR MATERIAL CHARACTERISATION 83
6.2. MEASUREMENT METHOD 86
6.3. TiO_2 FILMS 87
6.4. EXPERIMENTAL RESULTS 88
6.5. DISCUSSION 92
7. CONCLUSIONS 94
ACKNOWLEDGMENTS 96
BIBLIOGRAPHY 97
APPENDIX A: LIST OF RELATED PUBLICATIONS 107
APPENDIX B: OTHER RELATED PUBLICATIONS 110

Chapter 1

1. Introduction

1.1. The context: application-oriented portable and miniaturised systems

In several applications, there is an increasing need for a diffused on-field control of parameters able to diagnosis potential risks or problems in advance or in early stages in order to reduce their impact. The timely recognition of specific parameters is often the key for a tighter control on production processes, for instance in food industry, or in the development of dangerous events such as pollution or the onset of diseases in humans. Diffused monitoring can be hardly performed with traditional instrumentation in specialised laboratories, due to the time required for sample collection and analysis. One of most interesting example of benefits coming from diffused analysis is the biomedical field, where the need for patient-oriented healthcare systems and the high cost of hospitalization, lead to the need of moving from treatment to prevention, also by means of the screening of critical parameters. This will enable the possibility to perform preliminary medical screening for disease prevention and for limiting the access to hospital structures to the cases where deeper investigation and treatments are needed. The timely detection of a small set of parameters might improve the prevention of diseases and improvement of the patient's quality of life, as well as personalised diagnosis and treatments.

In the agrofood field, the quality control of production and supply chain are currently based on in-depth tests performed in centralised laboratories on a small sample of products. Miniaturised and autonomous systems may lead to a tighter control of the production and supply chain by performing a fast pre-screening on a larger sample of products, able to select critical issues to be addressed with in depth analyses with expensive and time consuming laboratory tests. Similarly, thin film technologies are gaining a huge development in several fields ranging from electronics to industrial coatings; thus, there is a clear interest in the development of thin film characterisation platforms, allowing the fast analysis of mechanical properties of deposited films, possibly during the deposition process itself, and with low cost instruments.

These needs can be fulfilled by the rapid development of both information and MEMS technologies. Microfabrication technologies are expected to produce new low cost and widely diffused analytical procedures based on portable devices, by means of integrated system providing a large number of functionality in small systems. In all applications, one of the key-points for a successful solution of the problem is the availability of detectors with high-sensitivity, selectivity and reproducibility to the chemical or biochemical parameters of interest. In order to compete with well-known and established solution, one of main fea-

ture of new systems is the capability to perform specific tests on the field with fast response times and low costs; in this perspective, a fast measurement of reduced number of parameters is to be preferred to a straightforward "clone" of laboratory instrumentation. Moreover, the detector must also provide robustness and reliability for real-world applications, with low costs and easiness of use. In this paradigm, MEMS technologies are emerging as realisation of miniaturised and portable instrumentation for agro-food, biomedical and material science applications with high sensitivity and low cost. In fact, MEMS technologies can allow a reduction of the manufacturing cost of detectors, by taking advantage of the parallel manufacturing of large number of devices at the same time; furthermore, MEMS devices can be potentially expanded to systems with high level of measurement parallelism. Device costs are also a key issues when devices must be for "single use", which is a must in application where cross-contamination between different measurement is a major cause of system failure and may cause severe consequences, such as in biomedical application.

1.2. Thesis content and innovative aspects

The objective of this thesis is the development and optimisation of innovative design, technologies and approaches for the realisation of microcantilever devices for portable systems. In particular, chemical and biological sensing and material characterisation were selected as case studies to evaluate the performances of this class of devices, which is one of the most promising technical solution for the realisation of detectors with high sensitivity. In fact, in addition to favourable sensing properties of single devices, an array configuration can be easily implemented with MEMS technologies, allowing the detection of multiple species at the same time, as well as the implementation of reference sensors to reject both physical and chemical interfering signals.

Different approaches and technologies for the realisation of high sensitivity detectors with integrated readout were investigated starting from the most promising approach in the literature, in order to provide an alternative to commonly used optical readout systems. Such high sensitivity systems are, in fact, poorly suitable for robust portable systems due to their complexity. After a preliminary evaluation, piezoresistive readouts have been considered as the best trade-off between sensitivity and system complexity, due to the easy implementation of readout systems and to their high compatibility with standard CMOS technologies for the integration of signal processing capabilities on-chip. On the other hand, piezoresistive readouts usually have lower sensitivity than optical methods. Thus, optimised devices are needed in order to allow an appropriate device exploitation. The implementation strategy has been performed after an analysis of mechanical and sensing properties of microcantilever, also depending of technological options for their realisation. Different approaches, dealing with both static and resonant operation, have been selected for gas sensing applications, DNA hybridisation sensing and material characterisation).

Performances of devices has been investigated by analytical and numerical modelling of both structures and readout elements, in order to optimise both fabrication technology and design. In particular, optimal implant parameters for the realisation of piezoresistors have been evaluated with process simulation performed with Athena Silvaco simulation software, while ANSYS has been used to analyse the best design for devices and the effect of some technology-related issues, such as the effect of underetch during the release of the beams or residual stresses. Static and modal analyses of cantilever bending in different conditions have been performed, in order to evaluate the mechanical performances of the device, and results have been compared with the experimental characterisation.

With regard to gas sensing applications, the development has been oriented to resonant sensors, where the adsorption of analytes on a adsorbent layer deposited on the cantilever leads to shift of resonance frequency of the structure, thus providing a gravimetric detection of analytes. The detection of amines, as markers of fish spoilage during transport, has been selected as a case-study for the analysis of these sensors. The sensitivity of devices has been measured, with results compatible with the models.

Cantilever structures are also suitable for bioaffinity-based applications or genomic tests, such as the detection of specific Single Nucleotide Polymorphisms (SNPs) that can be used to analyse the predisposition of individuals to genetic-based diseases. In this case, measurements are usually performed in liquid phase, where viscous damping of structures results in a severe reduction of resonance quality factor, which is a key-parameter for the device detection limit. Then, cantilever working in "bending mode" are usually preferred for these applications. In this thesis, the design and technologies have been optimised for this approach, which has different requirements with respect to resonant detectors. The interaction of target analytes with properly functionalised surfaces results in a bending of the cantilever device, which is usually explained by a number of mechanism ranging from electrostatic and steric interaction of molecules to energy-based considerations. In the case of DNA hybridisation detection, the complexity of the molecule interactions and solid-liquid interfaces leads to a number of different phenomena concurring in the overall response. Main parameters involved in the cantilever bending during DNA hybridisation has been studied on the basis of physical explanations available in the literature, in order to identify the key issues for an efficient detection.

Microcantilever devices can also play a role in thin film technologies, where residual stresses and material properties need to be accurately measured. Since cantilever sensors are highly sensitive to stress, their use is straightforward for this application. Moreover, apart from their sensitivity, they also have other advantages on other methods for stress measurements, such as the possibility to perform on-line measurements during the film deposition in an array configuration, which can be useful for combinatorial approaches for the development of thin film materials libraries. In collaboration with the Plasma Advanced Materials (PAM) group of the Bruno Kessler Foundation, the properties of TiO_2 films deposited by sput-

tering has been investigated as a case study for these applications. In addition to residual stress, a method for measuring the Young's modulus of the deposited films has been developed, based on the measurement by means of a stylus profilometer of beam stiffness increase due to TiO_2 film. The optimal data analysis procedure has been evaluated in order to increase the efficiency of the measurement.

In conclusion, this work describes the development of MEMS-based microcantilever devices for a range of different applications by evaluating the best technological implementations and optimised design. Experimental testing of realised devices demonstrated the feasibility of innovative high performance piezoresistive sensors, also enabling their exploitation in large number of applications for portable analysis systems, which are expected to increase their diffusion in the next years.

1.3. Structure of the Thesis

This thesis begins with the description of the state of the art related to microcantilever sensors in ***Chapter 2 "State of the art"***. Starting from early development of cantilevers for Atomic Force Microscopy, an overview of main properties and applications of cantilever for sensing application is presented, highlighting the main results and the advantage of using this class of devices in integrated systems for portable applications (*Paragraphs 2.1*). Then, a more detailed analysis of technical details of devices in the literature is reported, focusing on aspects such as methods for read-out and actuation, advantages and disadvantages of resonant or static operation and functional layers (*Paragraph 2.2*). Being DNA detection one of the most demanding applications, *Paragraph 2.3* is devoted to the analysis of nanomechanical interaction between DNA strands and functionalised cantilever, which must be optimised for an appropriate DNA detection with cantilevers. In *Paragraph 2.4*, an analysis of advantages and application of cantilevers to thin film characterisation is presented and compared with other miniaturised structure for material characterisation. Finally, in *Paragraph 2.5*, an overview of main technological approaches for cantilever sensors fabrication is reported.

In ***Chapter 3 "Piezoresistive cantilever devices"***, an analysis of physical properties of piezoresistive cantilever structure is reported, including mechanical properties (*Paragraph 3.1*), piezoresistive materials (*Paragraph 3.2*), general physics involved in transduction methods (*Paragraph 3.3*) and FBK technologies for cantilever fabrications (*Paragraph 3.4*). In the later paragraph, the Finite Element modelling and activities related to the optimisation of technologies are reported, as well as an overview of technologies developed by the FBK BioMEMS group.

Chapter 4 "Development of microcantilever detectors for gravimetric sensing" reports specific modelling (*Paragraphs 4.1 and 4.2*) and design activities (*Paragraph 4.3*) performed to realise optimised cantilever sensors for gas sensing purpose. In *Paragraph 4.4*, the electromechanical characterisation of realised devices allows the validation of modelling activities. The *Paragraph 4.5* deals with the analysis of

properties of sensitive phthalocyanines thin films deposited by the University of Valladolid in the framework of the GOODFOOD Project, and device sensitivity to amines.

In ***Chapter 5 "Development of microcantilevers detectors for stress sensing"***, modelling activities finalised to the evaluation of different technological options, selection of best approach and design optimisation are reported in *Paragraphs 5.1 and 5.2*, while design activities are reported in *Paragraph 5.3*.

Chapter 6 "Material characterisation with micro cantilever detectors" reports the activities performed in collaboration with the Plasma and Advanced Materials Research Unit of FBK in the field of material characterisation with microcantilever devices, starting from modelling and design of devices (*Paragraph 6.1*) and adopted experimental methods for Young's Modulus and residual stress measurement on thin TiO_2 films (*Paragraph 6.2*). Results reported in *Paragraph 6.3* demonstrate the suitability of proposed methods for the characterisation of thin film structures.

In ***Chapter 7 "Conclusions"*** main activities and results are reported and discussed. ***Acknowledgments***, ***Bibliography*** and ***Annexes*** sections complete this thesis.

Chapter 2

2. State of the Art

2.1. Introduction

The development of cantilever sensors stems from the Scanning Tunnelling Microscopy (STM) and Atomic Force Microscopy (AFM) techniques, in which thin cantilever structures are used for scanning the topography of a surface. These technologies were developed in early eighties at the IBM Research Laboratory in Zurich [Binning 1982, Binning 1986] and, beside the assignment of the Nobel Prize for physics in 1986 for the design of the STM, they provided the scientific, technological and experimental background for the development of microfabricated devices with thin structures, useful insights of beams physics at micrometric scale and first actuation and readout systems. At first STM was developed to study the topography of conducting surfaces by measuring the tunnelling current flowing between the surface and a sharp tip, thus providing a high resolution imaging of the surface. In order to provide the high accuracy positioning of the measurement head, 3D piezoelectric stages were used to scan the surface and to control the tip spacing from the surface. In order to circumvent the limitation to conducting surfaces, AFM was developed, using a micrometric cantilever with ultra-compliant spring constant as a force sensors able to measure the weak force interaction between the cantilever tip and the atoms of the surface. For this application, the beam is provided with a sharp tip interacting with the surface under examination; the interatomic force results in a deflection of the beam, which is typically measured with optical lever methods. Thus, in AFM, the elastic properties of the beam play the key role for the analysis and high deflection resolution is needed, which also apply to sensing applications described later. Moreover, while in the static procedure the measurement of force is related to deflection of the beam, the dynamic mode of operation was also developed. In this case, the tip is vibrated near its resonance frequency and frequency, amplitude and phase of vibration are modified by the interaction with the surface. The implementation of these methods led to the development of system for the actuation of beams and for the measurement of dynamic properties of devices, which were later applied for sensing applications using gravimetric measurements. Starting from this background, first attempts to use cantilever for sensing purposes could take advantage of already available laboratory instrumentation and focus on the optimisation of devices, sensitive layers and instrumentation for specific applications.

In this perspective, cantilever detectors have been applied to a wide range of application fields, from gas sensing for safety to genomics [Ziegler 2004, Datskos 2004, Waggoner 2007], also taking advantage of MEMS technologies for mass production, which make them potentially low cost – high performances devices [Raiteri 2001, Baller 2000, Rasmussen 2003, Datskos 2004]. Sensitivity to specific analytes can be

achieved by coating the beam surface with proper sensitive films, ranging from polymeric coatings (PEUT, Phtalocyanines, etc.) for gas sensing applications to DNA oligonucleotide probes for bioaffinity detection.

In addition to the production of high performance detectors such as cantilever sensors, microfabrication technologies are expected to take advantage of miniaturised devices in order to integrate low cost and efficient systems providing functionalities ranging from detection to sample handling and pre-treatment. These systems are expected to find a wide diffusion for innovative portable tools enabling the possibility to perform preliminary medical screening for disease prevention or on-field analysis of parameters of interest for environmental or agrofood applications. In fact, the current trend in the BioMEMS devices (i.e. Micro-Electro-Mechanical-Systems for biologic or biomedical applications) is oriented to low cost Microsystems, including integrated sensors with biological components [Bashir 2004], microfluidic modules [Linder 2007, Abgrall 2007] and signal elaboration capability. Nano-on-micro methodologies are enabling the realisation of biosensors combining both functionalisation technologies (Self Assembled Monolayers, oligonucleotides, antigen-antibody receptors, nanostructurated materials, etc.), able to grant high selectivity and sensibility towards the molecules of interest, and microsystems for sample handling and signal read-out and treatment [Bashir 2004]. Innovative architectures for diagnostic aimed to improve the system integration and to optimise the signal resolution demand a deep investigations of various critical parameters in order to exploit the high selectivity of bioaffinity interactions towards the molecules of interest, also because of the small sample sizes (and high costs of reagents) typical in this applications. For instance, the use of a microfabricated detection module, coupled with a microfluidic module may lead to the realisation of an integrated low cost Lab-on-a-Chip (LOC) for point-of-care (POC) applications with sample handling functionality. In the biosensor field, cantilevers can compete with other detection methods including electrochemical, electromechanical, waveguide-based and Plasmon Surface Resonance. Electrochemical methods such as potentiometric systems based on microelectrodes and Ion Sensitive FET (ISFETs) are present in the literature, showing high sensitivity and the capability of detecting single-base mismatches. The FET-based devices take advantage of the intrinsic charge of DNA strands adsorbed on gate dielectric of a field-effect transistor in order to modulate the channel [Fritz 2002, Kim 2004, Ingebrandt 2007]. Other methods, such as devices based on Plasmon Surface Resonance (PSR), can lead to high sensitivity for various bioaffinity tests, including DNA hybridisation [Abdulhaim 2008]. Laboratory instrumentations are already available on the market (e.g. see Biacore, www.biacore.com); however, due to the measurement principle, which require optical excitation and detection, often with precision alignments, this method is less easily implemented in integrated systems and portable devices [Abdulhaim 2008].

2.2. Cantilever sensors

The working principle of cantilever sensors is based on analytes adsorption on sensitive surface, which usually leads to both an induced superficial stress and an increase of cantilever's mass. Thus, measurements can be performed according to two different methods, which are the deflection mode and the resonance mode [Ziegler 2004, Datskos 2004, Waggoner 2007]. Since both methods deal with beam deflection, sometimes they can be performed contemporaneously [Battiston 2001]. The sensing materials deposited as functional layer on cantilevers need to either provide an high analyte bulk adsorption for gravimetric approaches or high surface density of analyte adsorption for stress measurements. In the first case, the adsorption is proportional to the thickness of the sensing film, which is typically a polymeric material with chemical affinity to analytes and is therefore able to provide a selective adsorption. Another approach for gravimetric sensing is the use of nanostructured materials with high specific surface. In this case, the large gas-solid surface allows using material with surface reactivity with analytes, thus avoiding problems related to diffusion. The typical example of this approach is the use of carbon nanotubes adsorbent for sensing purposes. Both polymeric and nanostructured materials are typically lowly selective to specific analytes and thus array configurations are often found for the implementation of e-nose systems in which responses of sensors with slightly different sensitivity to analytes are combined and analysed to extrapolate the presence of analytes through elaboration and data mining techniques. The most commonly used approaches includes Principal Component Analysis (PCA), [Baller 2000, Capone 2003]. Other approaches might use a separation methods such as gas chromatography to provide time-resolved measurement of the different analytes in a mixture, thus using a non-selective detector [Chapman 2007]. With this approach the selectivity is provided by the pre-treatment of the sample, only requiring a high sensitivity detector. For stress-based sensing, instead, thin surface coatings such as Self Assembled Monolayers (SAM) of biochemical compounds are commonly used, one example being immobilised single DNA strands in genomic applications. A large number of biological application can be addressed by cantilever structures with specific functional layers, based for instance on gene – antigens interactions. The two approaches have both advantages and disadvantages and the choice is usually related to the application requirements.

In the resonance mode, resonance frequencies can be estimated by the simplified models reported in the literature [Ziegler 2004, Datskos 2004, Waggoner 2007], where the structure is modelled with a simple spring-mass oscillator. The spring constant K is related to physical and geometrical properties of the beam and resonance frequency f_0 for the first resonance mode is related to beam stiffness, density and vibration damping. The resonance frequency is also dependant on the residual stresses of materials [Ren 2004, Zhang 2004/2]. With this approach, the sensor mass sensitivity ($S_m = 1/f_0 \cdot \Delta f/\Delta m$) is inversely proportional to beam thickness and density. Then higher sensitivities can be achieved from thin, low-density devices. The quality factor Q is another important parameter of the resonance, which depends on the vis-

cous damping of the cantilever vibration. The resolution of resonance frequency detection and amplitude of the output signal for a given actuation are strictly related to the quality factor. Thus, the efficiency of resonance methods is strongly affected in liquid environments, making the deflection mode more less attractive for such applications. Despite the low quality factor, resonant cantilever devices were used for biosensing applications in liquid environment, for instance for the detection of proteins by using an antigen-antibody strategy [Lee 2004]. The resonance mode allows detection limit as low as single DNA molecule mass when used in ultra-high vacuum conditions, as reported by some papers [Ilic 2005, Yang 2000]. These approaches, although interesting, can be hardly used in practical conditions for portable diagnostic purposes. Recently, an hybrid system has been developed, in which the liquid sample is flown through an hollow cantilever, thus taking advantage of the higher quality factor achievable in gas or vacuum conditions [Burg 2007]. In order to reduce this drawback, an improvement of the quality factor can be also achieved by using a feedback system for the actuation, where the signal read from the cantilever is fed to the actuator. This has been demonstrated to improve the read-out efficiency of orders of magnitude [Vidic 2003, Passian 2003], making this approach usable also in liquid phase.

Actuation can be performed with several approaches, including integrated and discrete piezoelectric devices, electrostatic and magnetic induction set-up [Lee 2004/2]. In order to provide low stiffness devices with integrated actuation, an interesting approach using lateral vibration of nanomechanical beams was described in [Villaroya 2006], using capacitive actuation of poly-silicon beams.

Sensitive layers for gas sensing are often implemented by using thin film polymers, such as the cantilever array reported in [Battiston 2001], using carboxymethylcellulose, polyvinylalcohol, polyvinylpyridine, polyvinylchloride, polyurethane, polystyrene, polymethylmethacrylate to detect and discriminate mixtures of different alcohols by the comparison of bending and resonance shift detection, coupled with data analysis methods. Cantilever structures have also been used to detect pollutants such as mercury [Rogers 2003] or explosives such as trinitrotoluene (TNT), also providing an interesting tool to study their adsorption/desorption properties [Muralidharan 2003].

Being the theoretical sensitivity mainly dependant on the beam linear density, large cantilevers are expected to provide lower resonance frequencies with the same relative variation as response to analyte adsorption. In fact, some papers in the literature demonstrate the suitability of such approach for gas sensing [Fadel 2004]. The real device resolution is however set by the frequency detection resolution, which is in turn inversely proportional to quality factor. Being the quality factor mainly dependant on beam width (pls. see Paragraph 3.3), long and narrow beams can provide good frequency resolution. Moreover, the higher resonance modes have demonstrated an increase of quality factor with respect to first mode [Jin 2006, Ghatkesar 2008, Tseytlin 2005]. With the opposite approach, the implementation of nanometric cantilevers for resonant detection is presented in [Li 2007], where the realisation of nanocantilevers al-

lowed the realisation of nanosensors. The extreme miniaturisation of devices to nanoscale can reduce the viscous damping of beams at atmospheric pressure, thus resulting in high Q factors and resolution in operative conditions. Similar technologies provided an interesting application to the realisation of nanocantilever-based detectors for mass spectrometry with single molecule resolution [Roukes 2007].

In the deflection mode, measurements are performed by monitoring the cantilever bending resulting from analyte-induced stress on single-side functionalised devices. The cantilever bending is related to both induced stress and geometrical and physical properties of the beam, according to the well-known Stoney's equation for the bending of thick substrates resulting from residual stresses in deposited thin films [Stoney 1909]. In accordance with this approach, the best sensitivity to an applied stress in terms of deflection amplitude can be achieved with devices with high compliance, which can be obtained with thin beams and a low elastic modulus. The drawback of high compliance structure is thermal vibrational noise that may limit the ultimate resolution of devices. In fact, in a damped cantilever in thermal equilibrium brownian motion causes a random deflection of the beam, which can be modelled with a fluctuation force with spectral density proportional to square root of acoustic resistance [Gabrielson 1993, Butt 1995]. Thus, large suspended structures are more prone to noise. The deflection methods applies to both liquid and gas applications, although the frequency mode is usually preferred in gas sensing because of the better accuracy in the measurements of relative frequency shifts. Gas sensing with deflection mode cantilever arrays, however, has been demonstrated by several works including [Baller 2000], in which 8 cantilevers covered with 8 different polymers are able to detect and discriminate alcohols and solvent mixtures by using a PCA approach coupled with Artificial Neural Network (ANN) algorithms. More recent work on the topic include for instance [Yoshikawa 2009], where different polymer (namely poly-vinyl alcohol (PVA), poly-ethylene imine (PEI), poly-acryl amide (PAAM), and poly-vinyl pyrrolidone (PVP)) are used to selectively detect vapours of volatile organic compounds including alkanes with different chain length from 5 (n-pentane) to 14 (n-tetradecane). Gas sensing can be performed with both thin films and monolayers. For instance, detection of TNT adsorbed on a polymeric layer (namely SXFA-[poly(1-(4-hydroxy-4-trifluoromethyl-5,5,5-trifluoro)pent-1-enyl)methylsiloxane]) or thiol-based self assembled monolayers has been demonstrated with detection limits in the order of hundreds or tens of ppt [Pinnaduwage 2004, Li 2006]. The interest for such low detection limit can be found in several fields such as safety and security, environmental monitoring and agrofood. Due to the surface-based nature of stress detection, main applications for the deflection mode can be however found in biosensor field, where measurements are usually performed in liquid phase, and performances of resonance mode detection are strongly reduced. Main biosensor classes deals with either antigen-antibody or DNA hybridisation for obtaining a high selectivity to quantities of interest [Fritz 2008]. DNA detection has received great attention after the demonstration of single-nucleotide polymorphism (SNP) detection in [Fritz 2000], also due to the fast developments of genetics in biology and medicine. Thus, the need for fast and low cost analysis systems has led to a wide literature on the topic, reporting detection limits for DNA oligonucleotides as

low as 100pM [Stackowiack 2006] and 10pM in non-amplified RNA sensing [Zhang 2006]. The presence of concurring phenomena not related to the DNA sensing, also requires strategies for the minimisation of parasitic effects. A reference beam, with the same structure of the measurement beam but different functionalisation, is commonly used for the rejection of spurious deformations, mainly due to thermal effect (i.e. deflection of the thermal bimorph structure formed by the beam material and gold adhesion layer, due to their different thermal expansion coefficients) or non-specific adsorption of DNA or compounds on the active surface. This strategy is one of the most effective for dealing with real measurements and the literature also demonstrate the possibility to work with a high background of non-specific molecules in solution, which is one of most important parameters for biosensors in real applications. The use of cantilever sensors using antigens-antibody interactions for the detection of proteins and bacteria is also diffused in the literature. The lower stability of such molecules is one drawback of this approach [Fritz 2008], which has not been investigated in detail in this work.

Several read-out methods for cantilever deflection have been proposed in literature, including laser beam deflection, piezoresistive and piezoelectric reading, and electrostatic or electromagnetic based methods [Datskos 2004]. For static detection, which is usually preferred in liquid phase, optical read-out methods are the most commonly used, due to their high sensitivity. Nevertheless, this approach has several drawbacks, mainly due to the system complexity to assure the collimation of the laser beam, of the cantilever device and the detector and to the sensitivity to opacity and beam refraction in the liquid sample. Other methods, such as piezoresistivity-based methods can be easily implemented in a microfabrication process and then it shows great advantages in term of integrability of the device, especially for portable applications [Mukhopadhyay 2005]. Alternative approaches for increasing the bending sensitivity of the electromechanical structure include recent results on MOSFET stress detection, allowing both high sensitivity and ease of integration [Shekhawat 2006]. Piezoresistivity, which is related to a stress-induced change of carrier mobility in semiconductors, can be used for stress-sensing elements with different approaches [Creemer 2001], including resistors, diodes and field-effect transistors. Since the physical phenomenon is the same for the methods, usually comparable sensitivities are obtained with the three different types of sensing elements, although MOSFET stress detectors operated in weak inversion conditions can show higher sensitivity, due to channel modulation effects at the dielectric-semiconductor interface [Shekhawat 2006, Lange 2003, Wang 1993]. Other diffused readout methods are capacitive and piezoelectric sensing. Capacitive sensing is particularly suitable for gas sensing, since it allows direct actuation and detection in resonance mode [Li-2006/2, Villarroya 2006], and it can also provide good sensitivity in static mode operation. The narrow gaps between structure and readout electrode, however, can be the cause of stitching issues in liquid phase and an increase of damping in gas applications. Piezoelectric detection can be used for actuation [Minne 1995], as well for coupled actuation and sensing in resonance mode [Lee 2004/2]. The need for piezoelectric materials, which may be non-compatible with equipments and CMOS devices

are one of the strongest limits to their diffusion. In liquid phase usually the electrical insulation of such materials is an additional point of concern. Other approaches to device actuation may be based on magnetic or thermal actuation [Lange 2002, Li 2009], the latter being more suitable for low- frequencies application due to device specific heat and heat exchange rates.

2.3. Cantilever nanomechanic response for DNA sensing

Although the response of static cantilever sensors to DNA hybridisation is unanimously attributed to the stress induced on their surface by DNA interactions, the chemical/physical explanation of the origin of such stresses on microcantilever structures is still not fully understood, due to the complexity of the interaction of DNA with the surface, electrolytes and between DNA strands on the surface. Despite a wide agreement on a set of different chemical / physical phenomena contributing to the cantilever deflection and on the importance of the grafting density of DNA and experimental conditions in general, the phenomenon dominating the induced stress is different in the several papers available in the literature [Mukhopadhyay 2005, Liu 2003, Wu 2001, Alvarez 2004, Zhang 2008, Stachowiak 2006, Hansen 2001, McKendry 2002]. The different experimental conditions, in fact, can result in a change of the relative weight of the different phenomena involved in the overall response, which can in turn modify both the intensity and the sign of the response. Then, for a successful implementation and operation of stress-based biosensor, a deep knowledge of nano-mechanical aspects related to DNA grafting and hybridisation is required, especially to address the detection of single nucleotide mismatch in DNA with this class of devices.

DNA strands are complex molecules with very peculiar properties. In order to understand the origin of cantilever deflection, some physical properties must be considered, especially in the electrical and mechanical domain. From the electrical point of view, DNA has an intrinsic charge related to the phosphate group in the chain backbone, thus resulting in an electrostatic repulsion between adjacent strands and the presence of solvation layers in an electrolytic solution. Both effects related to charge are affected by the buffer ionic strength, which can reduce the length of interaction between charges. Consequently, the cantilever deflection is dependent on the buffer ionic strength (and then hybridisation buffer concentration) [Wu 2001, Mukhopadhyay 2005]. A further secondary effect of charge is the variation of the coverage density achievable at different buffer concentrations, due to the previously mentioned electrostatic/solvation interaction during the immobilisation [Stachowiak 2006]. Since the variation of the grafting density is unanimously considered one of the key parameters for the efficiency of nanomechanical sensors [Stachowiak 2006], a proper selection of the immobilisation buffer is required to obtain good sensitivity, usually involving buffers with high ionic strength to reduce the electrical interactions during the grafting procedure.

Steric hindrance is one of parameter involved in nanomechanical response [McKendry 2002]. From the mechanical point of view, there is a significant difference between the flexible single strands of DNA and the more rigid double strand. A parameter commonly used to describe the rigidity of a molecular chain is the "persistence length" ρ, which is the typical length of the molecule which can be described by a rigid rod rather than a fully flexible chain with a random configuration. In the case of DNA, the persistence length varies between 0.75nm and 50÷80nm upon hybridisation, due to the change of configuration from single strand to double strand. The variation of rigidity is correlated to the variation of conformational entropy of the molecule, which can be used as a parameter for modelling the DNA behaviour during hybridisation and calculate the related cantilever bending. Regarding ssDNA chains, it is possible to evaluate the average size of the chain in solution, given the probe length N and persistence ρ in nm, by the gyration radius parameter R_g [Alvarez 2004]:

$$R_g=(0.43\ N\ \rho\ /3)^{0.5} \qquad [nm] \qquad 2.1$$

This parameter is of paramount importance for evaluating the length of interaction between adjacent chains immobilised on a surface, due to the changes of conformation of the chain; for instance, a 27-mer chain has a gyration diameter $2R_g$ = 3.4nm [Alvarez 2004]. Then, this parameter may provide a first evaluation of the probe density needed in order to obtain a proper nanomechanical response.

The different effect are usually accounted by energetic methods, where the free energy of the system is modelled as a sum of contribution from the different phenomena, and related to the mechanical energy stored by the bended beam. At least qualitative prediction of cantilever response as a function of experimental conditions (probe length, coverage density, DNA target concentration, ionic strength of the reaction buffer, et.) can be performed by using such models.

DNA binding to a substrate is commonly performed by means of the very stable and selective gold-sulphur link, which can be easily implemented by adding a thiol group to the DNA strand and a gold layer on the device surface. The binding energy is often accounted for an addictive bending effect during the DNA immobilisation. For low coverage, this is often the dominating effects, leading to a response to immobilisation only, and almost no response during the hybridisation [Alvarez 2004]. In general, the immobilisation produces a wide response, with a downward bending due to an equivalent compressive stress. In this case all the phenomena are contributing to the bending, since electrostatic repulsion, hydration and conformation entropy are minimised by a downward bending. When hybridisation is performed, the conformational term is reduced by the stiffer configuration of dsDNA, while the charge effects are increased. For this reason, according to the ionic strength of the buffer, the beam can bend upward if the conformational term is dominating (high ionic strength) or downward if the electrical effects higher (i.e. at low ionic strength). The sign and the intensity of the response to hybridisation are also depending on the graft-

ing density but, as a rule of thumb, they can be considered to be one order of magnitude weaker than response to immobilisation.

Extensive characterisations of grafting density, as a function of immobilisation buffer and probe length have been presented in [Stachowiak 2006], showing an increasing grafting density for buffers with higher ionic strength, with a steep increase at low concentration due to the predominance of osmotic forces, and a lower variations at high ionic strength due to the predominance of hydration forces. The grafting density is also influenced by the length of the probes, with a reduction for longer probes. All the models and experimental results in the literature point out that probe density is one of main key point for the efficiency of the device. Several evaluation techniques are available for investigating the probe density and the hybridisation efficiency, ranging from radio labelling (e.g. ^{32}P in [Alvarez 2004]), fluorescence-based methods [Stachowiak 2006] and label free approaches such as SPR-based measurements [Alvarez 2004]. Immobilisation densities around $(1\div2)10^{13}$ molecules/cm^2 typically provide chains near enough to give a significant nanomechanical response [Wu 2001], while in [Alvarez 2004] the $3\ 10^{12}$ molecules/cm^2 density did not provide a good response. In the latter case, the average distance between molecules is around 6 nm, which is larger than the typical length of interaction (3÷4 nm), on the contrary of results in [Wu 2001], where the average distance is around 2.3nm. When density is low, the only option is to use low buffer concentration in order to extend the length of electrical interaction, while length of interaction for conformational terms is almost independent from these conditions.

The hybridisation density and efficiency are of course strictly related to probe density on the substrate. Interestingly, at high immobilisation densities the efficiency of the hybridisation is reduced due to the close strand packing, which contrast the target strand from reaching the hybridisation position on the immobilised probes [Stachowiak 2006], with stronger reduction for longer probes. In any case, the overall hybridisation density is increasing with the immobilisation density, since the reduction in the hybridisation efficiency is not high enough for overcoming the advantage of a higher number of probes on the substrate. When dealing with "nanomechanical" sensors, a distinction must be provided between the hybridisation efficiency and sensor response, since some cases are reported [Mukhopadhyay 2005, Alvarez 2004] in which a successful hybridisation did not correspond to a mechanical response. In these devices, the positive effect of high immobilisation densities is much more effective than high hybridisation efficiencies on low-density ssDNA SAMs, due to the need for short strand-to-strand spacing in order to develop nanomechanical responses. Thus, the hybridisation efficiency is sometimes a parameter of reduced importance. For instance, the presence of so-called spacers, which are additional chain inserted between the thiol group and the "real" DNA probe, is quite common in papers, in order to improve the coverage density of the ssDNA probes and hybridisation efficiency. Since the presence of linkers is also contributing to the nanomechanical response of the device, a reduction of the mechanical response is reported [Mukhopadhyay 2005] even if the hybridisation efficiency is higher, possibly due to the presence of both

a ssDNA and a dsDNA section after hybridisation, thus reducing the average contributions of the interaction terms.

Furthermore, in [Stachowiak 2006], the mechanical deflection of cantilever is shown to be almost independent from the probe length, when the immobilisation density is taken into account and target and probes have the same length. Thus, in this case the response of the cantilever seems to be affected by the probe length only indirectly because of a reduction of the grafting density for longer probes. In [Hagan 2002, Wu 2001, Hansen 2001], however, it is shown that at fixed probe length the response to target strand with different lengths is different.

When the detection of single nucleotide mismatch is required, some further aspects must be taken into account, especially related to the effect of SNP on the mechanical response of the system, and to the robustness of the cantilever method in real LOC systems. In [Hansen 2001], the effect of the position of a SNP in the probe strands is evaluated, leading to different responses. The proposed explanation is the partial hybridisation happening in the region from the strand end to the position of the SNP, thus resulting in a mixed ss/dsDNA structure. The loose end of the target strand not hybridised produces the SNP detection mechanism, which is accordingly dependent on SNP position. Thus, the design of probes must be defined in order to position the SNP in a proper region of the probe. Furthermore, in long probes (> 16-mer) the sensitivity to SNP is reduced, due to the partial hybridisation of the loose target probe after the SNP with the remaining complementary nucleotides of the probe strand. In LOC applications, real conditions present some additional challenges, due to the non-controlled length of DNA target strands, which can influence the mechanical response of cantilever, due to the excess region of the target strands with respect to the region hybridised on the probe.

The nanomechanical response of cantilever is then related to the DNA status (single or double strand, surface density, length) on the surface and the nanomechanical interactions upon hybridisation or de-hybridisation can be detected with cantilever sensors. Some papers in the literature [Biswal 2006, Biswal 2007] have demonstrated the possibility to detect the de-hybridisation of DNA upon the application of temperature sweep. The change of DNA conformation is clearly detectable as a step response superimposed to the linear response related to bimetallic beam behaviour of devices. De-hybridisation temperature can also provide useful insights of DNA strand nature. This approach can be considered as a nanomechanical study of thermodynamic properties of DNA upon hybridisation / de-hybridisation, which, although not widely diffused in the literature, might demonstrate a strong potential for improving the confidence of DNA detection with cantilevers in real applications, where the uncontrolled length of DNA strands to be detected may results in incorrect results. In fact, a temperature scan can potentially distinguish between complete or partial DNA match and binding of unspecific strand or interferents.

The immobilisation of DNA self-assembled layers is one of the key issues for a successful realisation of DNA detectors. Several chemical procedures can be used, taking advantage of the recent advances in technologies for microarray production. The most commonly used immobilisation chemistry is based on sulphur-gold covalent bonding, due to the easy availability of gold film on devices and thiolated organic compounds, its chemical stability and the high specificity of this chemical bonding. The need for a deposition method that can be scaled to large arrays with several different functionalisation on the same chip leads to the evaluation of either contact or non-contact spotting techniques used for microarrays and ELISA system. Papers in the literature also present incubation-based deposition of sensitive layer on cantilever, by inserting the cantilever array in an appropriate capillary array filled with reagents [Fritz 2008].

2.4. Cantilevers for material characterisation

The use of thin materials for MEMS and microelectronics applications requires an in-depth knowledge of mechanical, electrical and morphological properties of the material, especially when working with thin films. In order to optimize the deposition techniques for highly reliable protective coatings in terms of mechanical parameters, measurement techniques able to evaluate mechanical properties are required. Even if commercially available instrumentations are able to perform the analysis of mechanical properties of materials (e.g. nanoindentation techniques, measurement based on Stoney's formula for the evaluation of residual stresses on thick substrates, interferometric methods), large errors can be obtained when film thickness is approaching the nanometer range. Furthermore, the evaluation of material stiffness by means of nano-indenters is prone to large errors when thin film materials are deposited [Cai 1995, Fisher]. Moreover, the small dimensions, thin film materials and free-standing structures often prevent the direct adaptation of standard testing methods for bulk materials [Srikar 2003]. The recent advances in microfabrication technologies have led to the development of a range of MEMS-based devices which can be used in the field of thin film metrology and characterization [Yi 1999], one prominent example being microcantilevers for atomic force microscopy (AFM) [Humphris 2005]. Bending and tension test may be implemented in MEMS structure, where suspended beam are pulled with several methods such as integrated electrostatic actuators, or a pressure load applied to suspended membranes [Srikar 2003]. Resonance of suspended structures with controlled dimensions might be also used to define the stiffness and mass of materials, as commonly done for the calibration of AFM probes or thickness control during film deposition through microbalances. External load may also be applied to suspended structures through several laboratory instrumentation such as nanoindenters, AFM, profilometers [Weihs 1988]. Static structures such as lancets and suspended structures with tilted arm geometries may be used for residual stress characterisation on wafer, allowing a direct evaluation of stresses by a simple optical inspection [Bagolini 2004]. In order to increase the sensitivity of Stoney's method for the measurement of thin film materials, suspended circular structures with reduced dimension can be used with optical interferometric detection [Tang 2007].

Recently microcantilevers have also been proposed as a tool for the characterization of thin film parameters such as Young's modulus and residual stress with great resolution and accuracy [McShane 2006, He 2005]. In the cited literature, the used approach deals with the use of profilometers (optical and stylus) for measuring the bending of a thin suspended structure, which is related to the stress in a thin film deposited on the structure. The use of a mechanical profilometer also allows the evaluation of the deformation of the structure for a given applied force and thus of the stiffness variation due to the deposited thin film.

The method is based on the measurement of the deflection of a cantilever, which is coated with a thin film of the material to be characterized. Mechanical properties of the thin film are, in fact, responsible for the bending of the beam. Among various possibilities reported in the literature, optical interferometry [Wehrmeister 2007] and methods based on optical reflection of a collimated laser beam [Mertens 2005, Waggoner 2007] can provide deflection measurement with high resolution. Beam bending can also be measured by mechanical profilometers or AFM equipments, which, in addition, allow the evaluation of the structure deflection for a given applied force and thus of the stiffness variation due to the deposited thin film [Humphris 2005, McShane 2006]. Both AFM and optical methods usually need high precision alignment between instrumentation and micromachined structures, making these systems unsuitable for online measurements and rather complex to be setup.

A different approach consists in the integration of the deflection sensing elements on the cantilever. Although more demanding from the point of view of the cantilever fabrication, this method provides two major advantages: the first one is the simplification of the measurement procedure, because, in principle, only an electrical measurement is required and the second one is the possibility of an on-line measurement during the deposition of a thin film. Different implementations for the integration of the sensing elements are available, such as piezoresistive, piezoelectric or capacitive [Waggoner 2007]. Piezoresistive approach has some benefits with respect to other methods. From the cost and system complexity perspective, large arrays of piezoresistive cantilevers can be easily integrated in microfabrication technologies, allowing a high degree of parallelism in measurements and a strong reduction of production costs. The compatibility with CMOS technologies may also enable the on-chip integration of signal conditioning and readout electronics [Yu 2007]. Yet, when low cost devices for single use are needed, devices with integrated sensing elements can be coupled with external CMOS readout electronics to provide a compromise between performances and costs. Moreover, the complicated setup typical of most optical methods, using high-precision alignments, are not required. The method is also suitable for on-line measurement of stresses, while other methods cannot be easily used in an equipment for material depositions. On the other hand, piezoresistors usually have a lower deflection resolution with respect to methods based, for instance, on optical lever detection with Position Sensitive Detectors (PSD), but resolution is still high enough for most of applications where residual stresses in thin film need to be measured.

The procedure for the data extraction must be optimized in order to increase the measurement accuracy and robustness and in order to overcome some practical issues. Also secondary effects, such as the influence of beam length, Poisson ratio and anticlastic effects have been studied in the literature [Butt 1995, Vidic 2003].

2.5. Cantilever technologies

The technological approaches described in the literature provide an overview of advantages, drawbacks and achievable results with the piezoresistive materials described in previous paragraphs. In particular, approaches using thin film structures and poly-silicon resistors can be found in [Rasmussen 2003], while in [Mukhopadhyay 2005], silicon nitride cantilever with silicon resistors are realised. The later technology also led to the creation of a spin-off company of the Technical University of Denmark providing small cantilevers arrays as well as the instrumentations for arrays functionalisation and readout (Cantion, www.cantion.com).

Another common approach for realising structures with tight control on the thickness involve the use of SOI (Silicon on Insulator) wafers, for both realising silicon cantilevers with implanted resistors or using the BOX (Buried Oxide) layer for the mechanical structure and the device layer for the realisation of the resistors [Rasmussen 2004, Yu 2007, Yu 2008, Choudhury 2007]. As already highlighted in the materials section, the doping of choice for structure with applied uniform stress is n-type [Rasmussen 2004], due to the higher response. Similar technologies, developed at National Competence Center for Nanoscale Science (NCCR) in Basel and at the IBM Research Laboratory in Rüschlikon/Zurich resulted in the foundation of the Concentris GMBH (www.concentris.ch), working with silicon cantilevers arrays for several application. Chips are similar to those presented in several scientific paper such as [Fritz 2008]. IBM also developed a technological platform, named “Millipede”, for the development of large cantilevers arrays for storage purposes. Heaters, thermometers, electrodes for electrostatic actuation are integrated on cantilevers, which are used to write bits as holes on a thermoplastic polymeric layer through thermal and mechanical methods. Although the application is different, the 1024 cantilever chip presented in [Vettiger 2002] demonstrated the feasibility of very large arrays and might also be applied to sensing applications.

More recently, polymeric beams (thus with Young’s modulus orders of magnitude lower then silicon-based materials such as crystalline Si, silicon oxide and nitride) have been realized [Calleja 2005], featuring gold strain-gauges elements for deflection detection [Johansson 2005, Thaysen 2002]. Although the appealing mechanical properties of polymeric materials (for instance such SU-8), this approach still suffer of the limited choice of sensing materials that can be implemented on the device (e.g. gold strain gauges), usually providing really low sensitivity. Alternative implementation of piezoresistive elements with high compliance deals with polymeric material to either direct implementation of strain gauges using conduc-

tive polymers [Lillemose 2008] or polymeric matrix with embedded conducting particles [Shui 1996] or wires [Gammelgaard 2006].

More complex technological approach oriented to the integration of sensing elements and standard CMOS electronics have been reported. Some works [Verd 2005, Barrettino 2007] use post-processing steps on standard CMOS processes for realising the suspended structure, for instance by using the well/substrate junction as an etch stop for wet etching techniques [Barrettino 2007] or by using the standard poly-silicon layers available in standard CMOS for the realisation of the sensing elements. Since in this approach the thickness achievable is too high for biosensing applications and control on the etching procedure is somehow non optimal, latest approaches exploit CMOS processes realised directly on SOI wafers to ease the post processing steps needed for the realisation of micromechanical structure [Yu 2007, Yu 2008].

Regarding the general design approaches, the configuration using a double resistor reference on bulk and a reference cantilever is by far the most used and the reference beam is definitively needed in order to discriminate the real signals from the non-specific interaction in the solution [Fritz 2000]. Different width/length ratio of the beams can be implemented according to the selected technology, and in particular there is the possibility to realise short beams (W/L around 1) and sensing elements covering almost all the beam surface when using poly-Si, p-type or n-type (100) resistors [Mukhopadhyay 2005], while for n-type (110) resistor a higher W/L ratio is required in order to minimised the sensitivity reduction at the root [Choudhury 2007].

Chapter 3

3. Piezoresistive cantilever devices

3.1. Mechanical properties

In both resonance and deflection modes, the microcantilever response is related to the mechanical properties of the beam. In single material suspended beams, the beam stiffness S for a given rectangular section can be calculated as:

$$S = \frac{1}{12} E \cdot W \cdot t^3 \qquad 3.1$$

where E is the Young's Modulus, t and W respectively the thickness and the width of the beam.

Real devices, however, need a more complex structure in order to allow the electrical insulation of sensing elements and to provide a suitable surface for the deposition of the sensitive layer; then, the beams usually have a multilayer rather than a single layer structure. This results in some modification of beam properties, due to different densities and mechanical properties of materials and to residual stresses. Moreover, the effect of residual stress of materials results in a beam bending, according to the overall momentum on the section. The mechanical behaviour of microcantilever structures can be described by the equations [Mallick 1993]:

$$\begin{Bmatrix} N \\ M \end{Bmatrix} - \begin{Bmatrix} N_R \\ M_R \end{Bmatrix} + \begin{Bmatrix} N_T \\ M_T \end{Bmatrix} = \begin{bmatrix} A & B \\ B & C \end{bmatrix} \cdot \begin{Bmatrix} \varepsilon^0 \\ k^0 \end{Bmatrix} \qquad 3.2$$

where $\boldsymbol{\varepsilon}_0$ and k_0 are the mid-plane strain and warping of the multilayer, and:

$$\{N_R\} = \sum_{i=1}^{n} (h_i - h_{i-1}) \cdot \{\sigma_{Ri}\} \qquad 3.3$$

$$\{M_R\} = \frac{1}{2} \sum_{i=1}^{n} \left(h_i^2 - h_{i-1}^2\right) \cdot \{\sigma_{Ri}\}$$

are the loads equivalent to residual stresses of materials, N_T, M_T are the loads equivalent to thermal deformation and N, M are the external loads on the section. The components A, B and C of the beam stiffness are defined as:

$$[A] = \sum_{i=1}^{n} \left([Q] \cdot \left(h_i - h_{i-1}\right)\right) \qquad 3.4$$

$$[B] = \frac{1}{2} \sum_{i=1}^{n} \left([Q] \cdot \left(h_i^2 - h_{i-1}^2\right)\right)$$

$$[C]=\frac{1}{3}\sum_{i=1}^{n}\left([Q]\cdot\left(h_i^3-h_{i-1}^3\right)\right)$$

Where the matrixes Q are the stiffness matrix of the materials and the [C] matrix represents the stiffness for the flexural deformation of the structure, which replaces the E·I stiffness term for monolayer structures (pls. see eq. 3.10).

The stress distribution in the beam section, resulting from an applied momentum can be calculated from the deformation of the mid-plane, as a function of the position in the section (ζ). In each layer:

$$\sigma(\zeta)=\underline{\underline{Q}}\cdot(\varepsilon^0+k^0\cdot\zeta) \qquad 3.5$$

The general description of ideal stress distribution in a single layer structure is reported in Figure 3.1. Here, the thickness coordinate is set to zero in correspondence with the neutral axis for bending of the beam, which is the barycentre of the beam in this simple case. In this model, it is clear that sensitivity of a piezoresistive cantilever increases with thinner beams, while beam length and width are not affecting the sensing properties. However, in the real structure, the stress distribution at the interface between two layers with a discontinuity in material properties is different in order to respect the equation of mechanical equilibrium, thus providing a smoother transition. In particular, a reduction of σ_{ii} for respecting the continuity is expected, and a higher σ_{ij}.

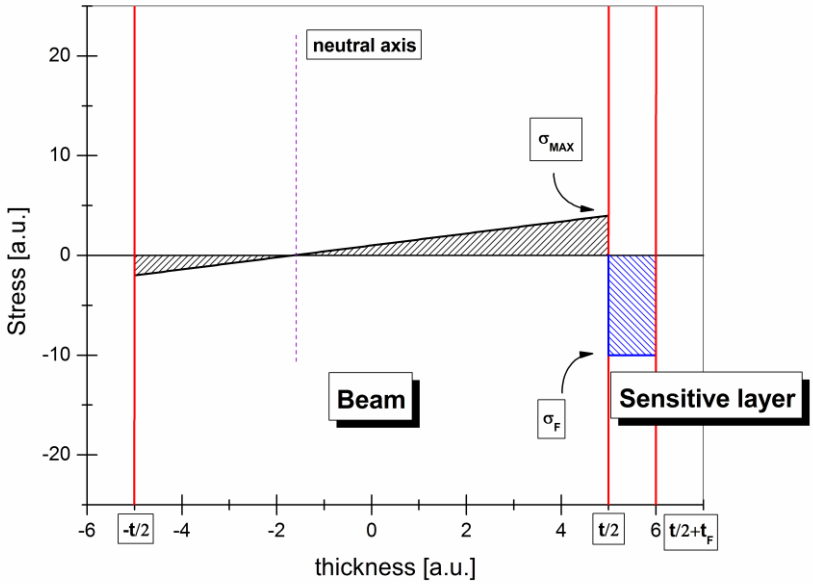

Figure 3.1. Ideal stress distribution on beam section with single layer structure: x axis: thickness of the beam, with sensitive layer (interfaces shown in red). Stress of sensitive layer (σ_F, blue hatch in the figure) results in a stress distribution over the beam section (black hatch), with maximum stress σ_{MAX} at the beam surface.

3.2. Piezoresistive read-out

Several read-out methods for the cantilever deflection have been proposed in literature, including optical methods, piezoresistive and piezoelectric reading, and electrostatic or electromagnetic based methods. The piezoresistive method is commonly used for this purpose because it can be easily implemented in a microfabrication process and then it show great advantages in term of integrability of the device. In piezoresistive cantilever detector, the sensitivity to stress largely depends on the materials used to realise the sensing elements. Here, comparison of properties for the most used materials, in particular monocrystalline silicon (both n-type and p-type, with different orientations), poly-silicon and gold [French 1988, French 2002, Gridchin 1995, Kanda 1982, Johansson 2005, Thaysen 2002] are evaluated in terms of sensitivity, integration and mechanical properties. This paragraph is particularly focused on sensitivity properties of materials to applied stresses, while further electromechanical consideration, allowing the evaluation of overall device performances, are reported in next paragraphs.

3.2.1 Monocrystalline Si

Monocrystalline Si is a well known piezoresistive material [French 1988, French 2002]; since Si resistors can be easily realised by implant on Si wafer, this approach is fully CMOS (Complementary Metal Oxide Semiconductor) compatible, even if implants with low junction depth are required for high sensitivity devices. Monocrystalline Si resistors allow a high sensitivity, with respect to both poly-Si and strain gauges. A comparison of piezoresistive coefficients π_{ij} of different materials and orientations is reported in Table 3.1, as well as the resulting relative resistance variation in unidirectional stress distribution (longitudinal and transversal with respect to resistor alignment) and in "planar" stress distribution, where the same stress is applied in both longitudinal and transversal directions. The latest distribution is similar to the ideal stress distribution on an infinite beam used in static mode, where the beam bending is caused by the adsorption of analytes on the beam surface. In this case, n-type Si provides the best sensitivity with respect to p-type Si, due to the higher symmetry of p-type Si coefficients. n-type resistors can be realised in both <110> and <100> orientations, where the latter provide advantages in "real" beams, where the stresses are not planar at the cantilever root. Further analyses of this aspect are reported in the next paragraphs. Sensitivity is dependent on both doping level and temperature [Kanda 1982] (see Figure 3.2); thus careful selection of the process parameter can provide a trade-off between sensitivity and stability vs. temperature.

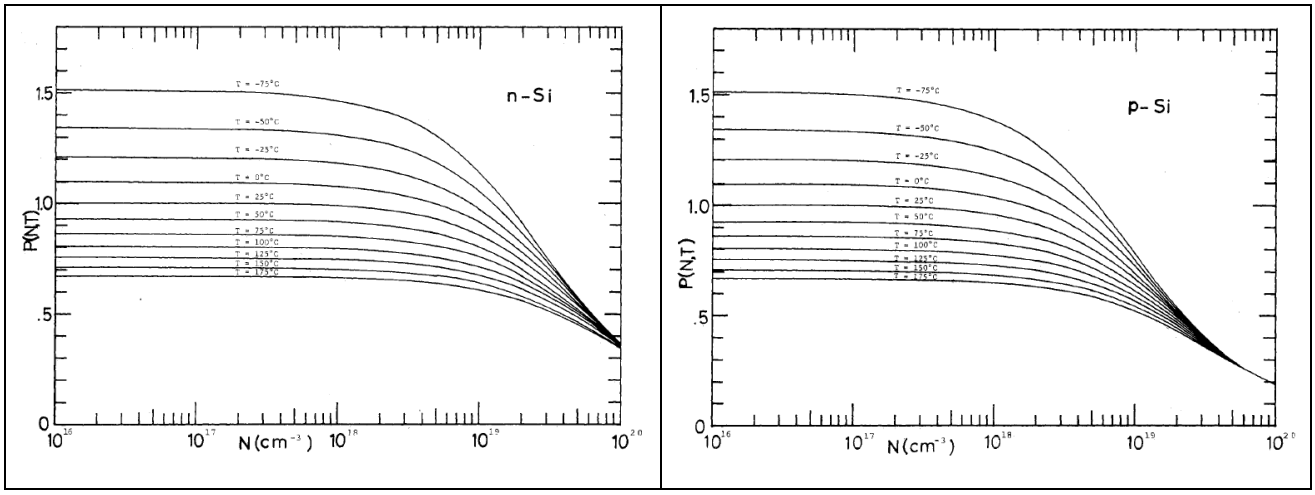

Figure 3.2. Typical piezoresitance factor of monocrystalline Si (left: n-type, right: p-type) as a function of impurity concentration and parameterised on temperature (Figure from [Kanda 1982]).

3.2.2 Polysilicon

Polysilicon is a standard material in CMOS processes, Since often poly-Si is used to realise MOSFET gates in self-aligned CMOS; therefore, this material provides high compatibility with standard processes. In commercially available processes multiple poly-Si levels are often available. Polysilicon exhibits properties similar to monocrystalline silicon, even if the random orientation of grains and the presence of the grain boundary reduce the piezoresistive effect [French 1988, French 2002, Gridchin 1995]. In order to reduce the negative effects of the presence of grain boundaries, several process parameters must be adjusted; in general, high doping and large grains provide the best performances for polysilicon. By using a LPCVD (Low Pressure Chemical Vapour Deposition) process, in the $2\div3\ 10^{19}$ cm^{-3} doping range, with deposition temperature in the range 560÷600°C, sensitivity is optimal and temperature dependence (TCR) is minimised. For poly-Si, p-type resistors are preferred, due to their higher sensitivity and linearity and lower hysteresis. Typical values are reported in Table 3.1, showing performances around 60÷80% of the monocrystalline Silicon.

3.2.3 Strain gauges

Since both implanted and poly-Si resistors are not easily integrated on polymeric devices, the most effective approach to the realisation of these devices is based on the deposition and patterning of gold resistors, which exhibit strain-gauge effect. The sensing properties, in this case are far lower than piezoresistive materials, but the evaluation of overall performances must also take into account the lower stiffness of polymeric beams (even more than 2 orders of magnitude less than Silicon) [Johansson 2005, Thaysen 2002]. Thus, evaluation of this approach has been performed even if sensing properties are quite low. Usually, gold can be deposited by evaporation.

Table 3.1. Summary of material sensing properties: πij piezoresistive coefficients, Ki relative resistivity variation per stress units (L = longitudinal stress, T = transversal stress, P = planar stress)

Material	***Orientation***	π_{11} $[10^{-11}\ Pa^{-1}]$	π_{12} $[10^{-11}\ Pa^{-1}]$	π_{44} $[10^{-11}\ Pa^{-1}]$	K_L $[10^{-11}\ Pa^{-1}]$	K_T $[10^{-11}\ Pa^{-1}]$	K_P $[10^{-11}\ Pa^{-1}]$
p-Si	<110>	6.6	-1.1	138.1	72	-66	6
n-Si	<110>	-102.2	53.4	-13.6	-31	-18	-49
	<100>	-24.5	-24.5	-155.6	-102	53	-49
poly-Si (typical)	-	-	-	-	51	-18	33
Gold	-	-	-	-	2	-2	0

Table 3.2. Summary of typical material mechanical properties.

Material	***E [GPa]***	***v***	σ_R ***[MPa]***	ρ $[Kg\ m^{-3}]$
Si	E [110] = 169 E [100] = 130 G_{xy} = 51 $G_{xz} = G_{yz}$ = 79	νxy = 0.064 νxz = νyz= 0.361	0	2329
poly-Si	150	0.17	-	2329
Au	80	0.35	155 on SiO_2	19280
SU-8	4.02	0.22	16÷19 on Si	1190
PDMS	360÷870 10^{-6}	0.5	-	970

In order to provide a simple but still useful model, the analytical analysis has been performed in a mono-dimensional beam by assuming a beam with "infinite length", thus not considering the effect of beam root. The description is effective only at a certain distance from the beam root, since in real beams with finite length, the presence of a constraint at beam root modifies the stress distribution in a region of length approximately 1÷2 times the beam width. These effects will be further described in the paragraph devoted to the FE analysis of the device.

According to the working mode, the beam deformation can be evaluated in different ways.

3.2.4 Resistor geometrical efficiency: resistor and passivation thicknesses

Since stress sensor is expected to detect σ_{MAX} at the beam surface, thickness of the piezoresistor must be as shallow as possible. Since the stress distribution along z is linear, the geometrical efficiency (η_{geom}) of the piezoresistor related to the ideal case of a resistor with null thickness can be estimated with the approximated function (where z_{SUP} is the distance between neutral axis of the beam and resistor top surface, t_R is the thickness of the piezoresistor):

$$\eta_{geom} = \frac{z_{sup} - t_R/2}{z_{sup}} = 1 - \frac{t_R/2}{z_{sup}} \qquad 3.6$$

Thus, piezoresistor must be as thin as possible. Furthermore, the thickness of the electrical insulator film over the beam modifies the neutral axis position with respect to the sensing ele-

ment position, thus reducing the z_{SUP}. Also in this case, efficiency is reduced. The formula can be used for estimating a proper trade-off between read-out efficiency and a suitable electrical insulation.

3.2.5 Thermo-mechanical and electrical noise and SNR ratio

Noise is an important parameter for piezoresistive read-out and can limit the device resolution. Different terms should be taken into account: electrical noise (Johnson and Flicker noise) and thermo-mechanical noise. The Johnson noise deals with thermal energy in the resistor and is frequency independent. The spectral power density is:

$$S_J = 4 \cdot k_B \cdot T \cdot R \qquad [V^2\ Hz^{-1}] \qquad 3.7$$

The Flicker noise can be evaluated by:

$$S_H = \frac{\alpha \cdot V_B^2}{N \cdot f} \qquad [V^2\ Hz^{-1}] \qquad 3.8$$

where V_B is the bias voltage, N is the total effective number of charge carriers in the piezoresistor, f is the frequency and α is a dimensionless parameter related to the annealing of the implanted resistor. Thus, electrical noise can be limited by devices with high doping or, if the implant dose is set by temperature or sensitivity consideration, by implant region as wide as possible and with a proper geometry to optimise the effective carrier number, which is related to the current density uniformity in the resistor.

Thermomechanical noise must be also considered, since the thermal vibrational noise that can affect the measurement results and set a limit to device resolution, especially for low thickness (and stiffness) and highly damped cantilevers, where the low energy of the vibration is easily dissipated by damping. In fact the thermo-mechanical noise is strictly related to the damping of the structure [Butt 1995]. The spectral density of the thermo-mechanical fluctuation force depends on temperature T and drag coefficient of the structure b and can be evaluated by:

$$F_{tm} = \sqrt{4k_B \cdot T \cdot b} \qquad [N\ Hz^{-1/2}] \qquad 3.9$$

This effect is lower than piezoresistive read-out noise in structures with thickness in the micron range and resistors with resistance in the kΩ range, and becomes more effective only for thinner beams.

3.3. Resonating cantilever sensors

In resonance mode, the beam vibrates at its Eigen-frequencies, resulting in a deformation and stress distribution typical for each resonance mode. At first mode, the resonance frequency

can be estimated by the simplified models reported in the literature [Madou 2002, Raiteri 2001, Baller 2000, Rasmussen 2003, Chen 1994, Chen 1995, Datskos 2004]. The structure can be considered as a simple spring-mass oscillator where the spring constant is related to physical and geometrical properties of the beam by the relationship:

$$K = \frac{3EI}{L^3} = \frac{E \cdot W \cdot t^3}{4 \cdot L^3} \qquad 3.10$$

The cantilever mass m is evaluated by the sum of the cantilever mass and the analyte adsorbed mass inducing the resonance frequency shift, and it must be corrected by using a factor n related to the device geometry (m* = n m, where n=0.24 for rectangular beams). When the structure is actuated in gas environment at atmospheric pressure a further term should be added to the mass, to take into account the gas molecules dragged by the cantilever. The addictive mass density χ (per length unit) is evaluated by:

$$\chi = \frac{\pi \cdot \rho_{gas} \cdot W^2}{2} \qquad [\text{Kg m}^{-1}] \qquad 3.11$$

For beams with thicknesses in the micron range this effect is quite low, even if it is not completely negligible. The resonance equation for the spring-mass system is:

$$\frac{d^2(z)}{dt^2} + \gamma \cdot \frac{dz}{dt} + \omega_0^2 \cdot z = 0 \quad where: \quad \gamma = \frac{b}{m^*} \quad and \quad \omega_0^2 = \frac{K}{m^*} \qquad 3.12$$

Here the damping effect has been included by means of a term proportional to the beam velocity, which is an assumption suitable for small amplitude vibrations, while for large oscillation it is proportional to the square of velocity. The parameter γ is defined as the ratio of the drag coefficient vs. the corrected linear mass density (Eq. 3.13). In first approximation the drag coefficient (b) of the beam is proportional to the cantilever width, according to the properties of a cylinder moving in a viscous flow, which is a suitable model available in literature [Buser 1994].

$$\gamma = \frac{b}{m^*} = \frac{\pi \cdot W \cdot \sqrt{2 \cdot \eta \cdot \omega \cdot \rho_{air}}}{\rho^*_{beam}} \qquad 3.13$$

Usually internal damping can be neglected in atmospheric pressure application. Finally, the solution of the equation (3.12) provides the resonance frequency for the first resonance f_0 (for the undamped oscillation):

$$f_0 = \frac{1}{2 \cdot \pi} \sqrt{\frac{K}{m^*}} = \frac{1}{2 \cdot \pi} \sqrt{\frac{E \cdot W \cdot t^3}{4 \cdot m^* \cdot L^3}} \qquad [\text{Hz}] \qquad 3.14$$

where E is the Young's modulus of Silicon, and W, t and L are width, thickness and length of the beam. The frequency shift due to damping effect can be evaluated by $\Omega^2=\omega^2-(1/2*\gamma)^2$,

where ω is referred to the undamped oscillation and Ω is the corrected value. In Chapter 4 some correction for different geometries are reported.

The sensor sensitivity can be calculated by:

$$S_m = \frac{1}{f_0}\frac{df_0}{dm} = -\frac{1}{\sum \rho \cdot t} \qquad [\mathrm{m^2\ Kg^{-1}}] \qquad 3.15$$

where the sum takes now into account the multilayer structure. Thus higher sensitivities can be achieved from thin, low density devices. Then resonance frequency depends on both mass increase and induced superficial stress. These effects have opposite sign, since a mass increase result in a lower resonance frequency and the stress stiffening effect results in a higher frequency [Chen 1995]. In general:

$$\Delta f = \frac{1}{2 \cdot \pi}\left(\sqrt{\frac{K + \delta K}{m^* + \delta m^*}} - \sqrt{\frac{K}{m^*}}\right) \qquad 3.16$$

The stiffening effect due to thin film residual stresses can be evaluated by means of FE simulations (see paragraph 4.2.3). With regard to the sensitivity of the device, both δm and δK are related to sensitive layer and analyte properties, and an experimental measurement of the analyte-sensitive material interaction is needed in order to estimate the overall beam sensitivity. The detection limit is:

$$\Delta\rho_{\min} = \frac{1}{S_m}\frac{\Delta f_{\min}}{f_0} = \frac{\sum \rho \cdot t}{f_0} \cdot \Delta f_{\min} \qquad [\mathrm{Kg\ m^{-2}}] \qquad 3.17$$

A lower detection limit can then be obtained at high resonance frequency, and hence if material properties and beam thickness are set by the fabrication process, short structures provide better resolution. A limit to the scale-down process is set by actuation and read-out methods reliability, as well as by fabrication process.

Another important parameter of resonating structures is the quality factor, which depends on the viscous damping of the cantilever. The amplitude of the sensor output for a given actuation intensity is strictly related to the quality factor, and then a Q estimation is needed in order to optimise the detection of the resonance frequency. The detection of the resonance frequency and the amplitude of the read-out for a given actuation intensity are strictly related to the quality factor. Q depends on the cantilever density per length unit (ρ_{beam}), on the drag coefficient b and on the resonance frequency:

$$Q = \frac{\omega_0 \cdot \rho_{beam}}{b} \qquad 3.18$$

Then, since both drag coefficient and linear mass density are proportional to W, in first approximation the quality factor does not depend on cantilever width, but decreases with beam

thickness at constant frequency. Then, in the resonance mode, higher sensitivities can be achieved from thin, low-density devices.

The efficiency of resonance methods is strongly affected in liquid environments, making the deflection mode more suitable for such applications. However, an improvement of the quality factor can be achieved by using a feedback system for the actuation, where the signal read from the cantilever is fed to the actuator. This has been demonstrated to improve the read-out efficiency of orders of magnitude [Vidic 2003], making this approach usable also in liquid phase, although generally deflection mode can provide better performances in liquid phase. Actuation can be performed with several approaches, including integrated and discrete piezoelectric devices, electrostatic and magnetic induction set-up [Vidic 2003, Lee 2004/2].

In resonance mode, the deformation can be roughly approximated to the one obtained by applying a force on the beam tip. In this case the momentum applied on each section of the beam is proportional to the distance from the tip, resulting in a maximum curvature and stress at the beam root. This point reflects on the optimal design of readout piezoresistors, which must be placed in the maximum stress region.

3.4. Static cantilever sensors

The bending of thin beam in response to a surface stress arising from the analyte adsorption results in an applied load equivalent to a uniform planar stress on the beam surface. It is useful to note that the effect of sensitive layer, which can be in principle unknown in the specific application, can be considered as the term $\sigma_F\ t_F$, which is proportional to the applied momentum $M_F = \sigma_F\ t_F\ t/2$, where t is the beam thickness. Then, it is not necessary to know sensitive layer thickness and stress separately. Thus, in the bending mode, the beam deformation can be obtained by integrating the curvature over the beam length (z and x longitudinal and thickness coordinates respectively, M applied momentum, EI bending stiffness of the beam):

$$\frac{d^2 z}{dx^2} \cong -\frac{M}{EI} = \chi = 1/R \qquad 3.19$$

Thus, in an ideal case, sensitivity of piezoresistive beams is not related to the beam length, since the applied load is uniformly distributed over the surface. Consequently, length is not a key design parameter, in contrast with force sensors (e.g. AFM probes) and cantilevers used as gravimetric sensors in resonance mode. In deflection-mode cantilevers, beam length is only effective in optical lever read-out methods, since the angular deflection of the beam is calculated by integrating the curvature along the beam.

Since real beams are multilayered structure, in order to allow the electrical insulation of sensing elements and to provide a suitable surface for the deposition of the sensitive layer, the de-

scription must take into account the geometrical and mechanical properties of the section. The bending can be evaluated by using equivalent loads in the equation for planar structures (eq. 3.2), where the applied loads are:

$$N_X = N_Y = \sigma_F \cdot t_F \qquad 3.20$$
$$M_X = M_Y = \sigma_F \cdot t_F \cdot t/2$$

The resulting stress on the beam can be calculated according to the eq 3.5.

Then, according to the previously described mechanical properties, the best sensitivity can be achieved from thin – low elastic modulus devices, even if the thermal vibrational noise increases by lowering the structure stiffness [Butt 1995].

3.5. Technologies for cantilever fabrication

The silicon microcantilever structures were fabricated at FBK Microfabrication facilities with a CMOS-compatible technology using post-processing micromachining steps. The activities performed in this thesis for the development of technologies mainly deals with the optimisation of implant parameters through the FE simulations of processes and evaluation and optimisation of stress balance in multilayered suspended structures. An overview of the used technology is reported for completeness in this section. Different fabrication processes will be described, where the first one is aimed to the realization of 10 µm-thick silicon microcantilevers, while the second one allows the fabrication of 2 µm-thick silicon beams developed with SOI (Silicon On Insulator) technology for enhanced sensitivity. Then, test structures and processes for optimisation of a new process for thinner beams (340nm single-crystal silicon) are presented. The processes were developed by taking into consideration the modelling and designs presented in Chapter 4, 5 and 6.

3.5.1 Fabrication process of 10 µm-thick silicon microcantilevers

The first fabrication process was based on n-type, 4-inch, 500-µm-thick, (100) oriented, double polished silicon wafer, with resistivity from 8÷12 Ω cm. The p-type piezoresistors were realised by ion implantation through a 28nm screen oxide with parameters in Table 3.3. A thermal annealing of 22 minutes at 1150ºC in N_2 was performed in order to diffuse and activate the implanted ion species and to recovery the crystal damage. Implant process was simulated by using the ATENA (Silvaco) software. Result summary of doping profile is shown in Table 3.3, according to implant process simulations. The junction depth was in the range 1.42 ÷ 1.8µm. This resulted in a correction of the read-out sensitivity to bending, according to the linear stress distribution on the beam section including a 700nm oxide-gold total thickness on the 10µm beams. In first approximation this effect can be taken into account by a coefficient

β, which can be calculated by the ratio of the distance between the piezoresistor mid-plane and the cantilever axis, and the mid-thickness of the multilayer structure. For this process, this factor can be evaluated to be near 0.7, due to the quite high implant depth. The efficiency of the read-out also depends on doping profile. In Table 3.3, the correction coefficients for piezoresistors' properties are reported, where the π-correction factor must be applied to piezoresistive coefficient previously indicated to take into account the dependence on doping concentration at room temperature, while "T dependence" shows the temperature dependence of the π_{ij} coefficients. The lower doping concentration considerably enhances the temperature stability of the device, with a low reduction of the sensitivity at room temperature.

Table 3.3: Implant parameters and simulations results.

Ion	**Energy [keV]**	**Dose [at cm^{-2}]**	**Junction depth [µm]**	**Sheet resistance [Ω/□]**	**N_A [cm^{-3}]**	**π correction factor**	**T dep. [°C^{-1}]**
BF_2	110	$2\ 10^{15}$	1.86	108	$3.5\ 10^{18}$	~ 0.9	$-4.4\ 10^{-3}$
B	70	$2\ 10^{14}$	1.66	407	$5\ 10^{17}$	~ 1	$-6.4\ 10^{-3}$
B	70	$2\ 10^{13}$	1.42	1660	$8\ 10^{16}$	1	$-6.7\ 10^{-3}$

Estimations of noise in piezoresistors for the different doping level are shown in Table 3.4.

Table 3.4: Noise estimation for different doping levels

Dose [at cm^{-2}]	**R [Ω]**	**N [cm^{-3}]**	**SJ [V^2 Hz^{-1}]**	**SH @ 1Hz [V^2]**
$2\ 10^{15}$	216	$6.4\ 10^{8}$	$3.6\ 10^{-18}$	$7.8\ 10^{-15}$
$2\ 10^{14}$	814	$8\ 10^{7}$	$13.5\ 10^{-18}$	$61.5\ 10^{-15}$
$2\ 10^{13}$	3320	$1\ 10^{7}$	$55.0\ 10^{-18}$	$449.1\ 10^{-15}$

According to results, for working frequencies in the range 100 ÷ 200 kHz flicker noise can be neglected.

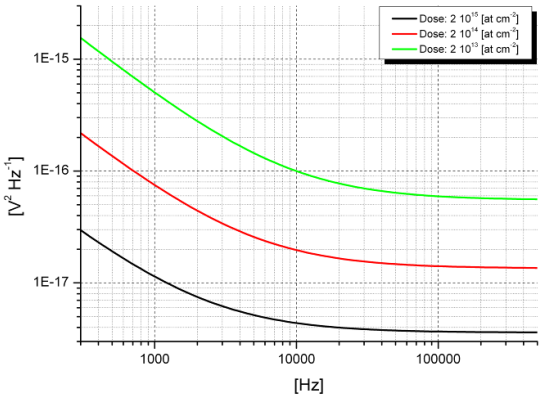

Figure 3.3: Noise power vs. frequency for different implant doses.

The thermomechanical noise was evaluated for the different beam geometries according to the equations (3.9).

Table 3.5: Evaluation of thermo-mechanical noise for different beam sizes.

Geometry	**F_{tm} [N $Hz^{-1/2}$]**
1000 x 106 x 10	$7\ 10^{-14}$
500 x 106 x10	$7\ 10^{-14}$
150 x 50 x 2	$4\ 10^{-14}$

Three different implant splitting were implemented in this step in order to test and evaluate the dependence of piezoresistive coefficients with the doping concentrations.

Table 3.6: Implant parameters summary

Implant Element	**Energy (keV)**	**Dose [at/cm^2]**
Boron	70	$2.0\ 10^{13}$
Boron	70	$2.0\ 10^{14}$
BF2	110	$2.0\ 10^{15}$

A second lithographic step was used to define the n+ regions for substrate contact realisation. Phosphorus was implanted, with energy 80 keV and dose $3\ 10^{15}$ at/cm^2. The third lithographic step allowed the definition of the contact regions of the piezoresistors, implanted with BF_2 (energy 110 keV, dose $3\ 10^{15}$ at/cm^2) in order to have an ohmic contact (p+ region) with the overhanging metal lines. The piezoresistor regions were implanted with As with a thermal annealing performed at 925ºC for 15 minutes in oxygen atmosphere to diffuse and activate the piezoresistors and n+ and the p+ implants. The hard mask for the final wet chemical etching during the bulk micromachining steps was then realised on the back of the wafer with a multilayer stack of TEOS, LPCVD silicon nitride and LTO. The forth lithographic step defined the openings in the TEOS front side layer by dry etching for the metal lines to contact the piezoresistors and the n^+ regions. The deposition of the metal multilayer (Ti/TiN/Al:Si1%/Ti) was done by sputtering technique. A fifth lithographic mask defined the metal lines, in order to lead the electric signal outside the cantilevers area to the chip pads. The metal multilayer was passivated by a layer of silicon dioxide (LTO). This deposition was performed at low temperature (430ºC), in order not to damage the aluminium layer. The sixth lithographic step was used to define the back-side bulk micromachining etching. The seventh lithographic step was used to define the openings for the pad regions through the LTO passivation film. A thin film of gold (Cr/Au, 5/100nm thickness respectively), needed for the device functionalisation, was deposited and patterned on the devices by means of electron gun evaporation. To release the microcantilevers structures, bulk silicon was then anisotropically removed from the backside by wet etching with tetramethyl ammonium hydroxide in aqueous solution (TMAH 25 wt

%) at 90ºC, until 20µm thickness was obtained. The last etching step was performed on both sides in order to release the structures.

Figure 3.4. Fabricated devices cross sections.

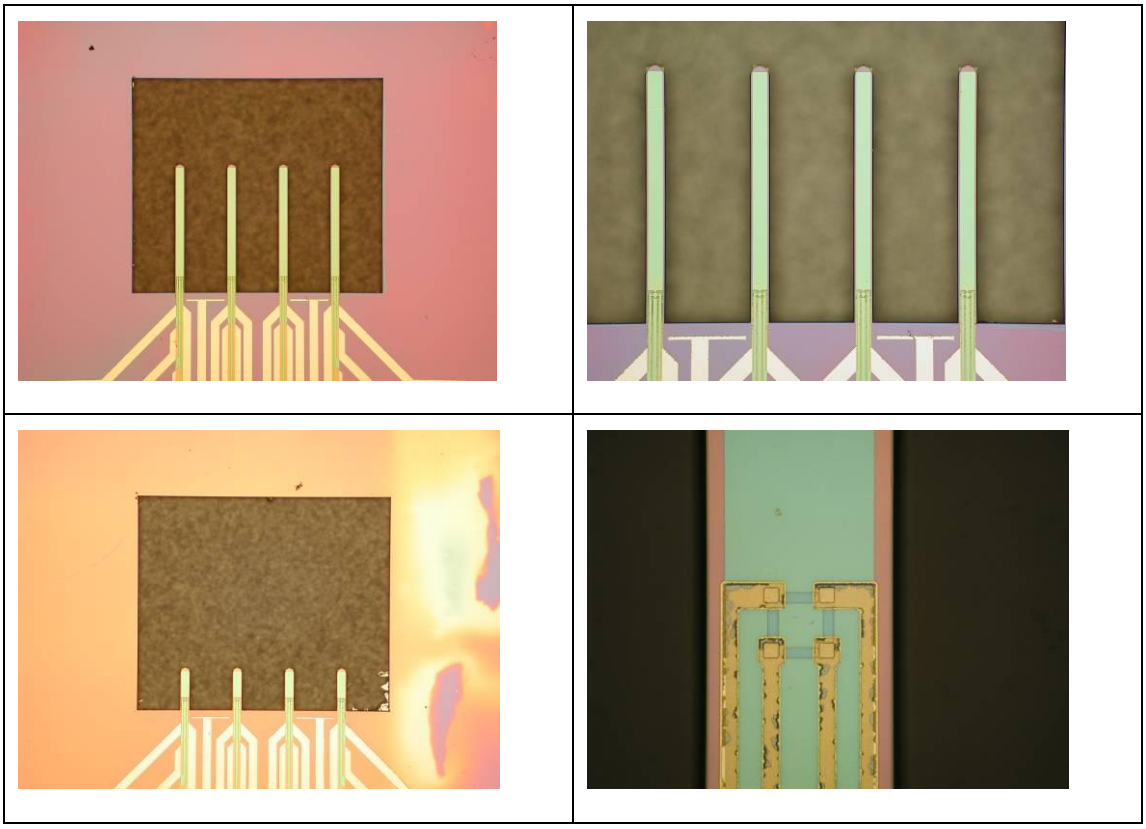

Figure 3.5. Process photograph of devices after the beam release. Clockwise from top-left: 1500μm beam array, detail of beams, detail of a Wheatstone bridge, 500μm beam array.

The process characterisation was performed on the test structures implemented on the design. Main results are reported in Table 3.7.

Table 3.7. Results of test stripes characterization (p resistor values for splittings in Table 3.6.

Layer	***Resistivity***
Aluminium wires	0.07 ± .01 Ω/□
Gold	.45 ± .01 Ω/□
p+	106 ± 10 Ω/□
p resistor	1940 ± 40 Ω/□, 390 ± 16 Ω/□, 1653 ± 100 Ω/□

3.5.2 Fabrication process of 2 µm-thick silicon microcantilevers

The second fabrication process was implemented on Silicon-on-Insulator (SOI) wafers with 2 µm-thick surface layer of silicon (usually named as device layer), an underlying 0.5 µm-thick layer of silicon dioxide (buried oxide, BOX), and a support or "handle" silicon wafer, having a thickness of 500 µm. As for the first process the wafer was n-type, 4-inch, (100) oriented, double polished, with resistivity from 8÷12 Ω cm. The BOX layer was used as an etch stop during the post processing steps of micromachining, thus allowing the fabrication of thin cantilevers with enhanced device sensitivity. Apart from piezoresistors realization, front side beams definition and post-processing micromaching steps, the fabrication process of the 2 µm-thick silicon microcantilevers was similar to the previous process. Due to the reduced-beam thickness (2 µm), implant parameters were adjusted in order not to overpass the neutral axis of the cantilever, lowering the efficiency of the piezoresistive transduction.

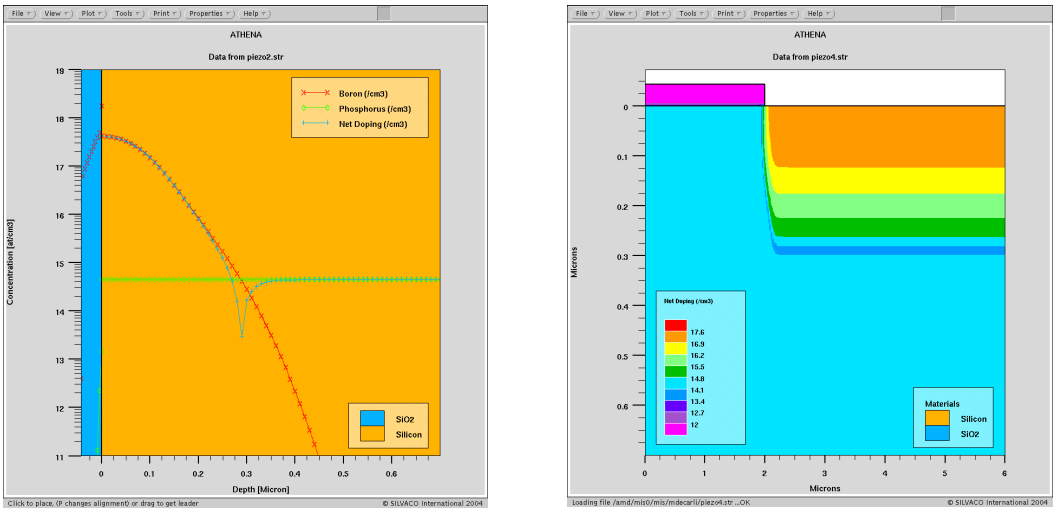

Figure 3.6. Simulation of piezoresistor doping profile and net doping. (Athena Silvaco simulation software).

Based on implant simulations made with ATHENA (Silvaco) software, BF_2 implant with dose 5 10^{12} at/cm^2 and energy 80 keV was selected. The thermal annealing was performed at 975°C for 20 minutes in nitrogen atmosphere. The values of the simulated implant depth and sheet resistance were respectively 288 nm and 7383 Ω/sq. In the new process, due to the relative low thickness of the beams, the definition of the beam structures was realised from the front side with a standard dry etching step, restricting the number of the micromachining steps to one single back side wet etching of the handle layer, using the BOX layer as an etch stop. The BOX was removed with a wet etching of the silicon dioxide.

Figure 3.7. Cross-sections of 2 µm-thick beams.

Table 3.8. Results of test stripes characterization.

Layer	***Resistivity***
Aluminium wires	0.061 ± .007 Ω/□
p+	62 ± 1 Ω/□
p resistor	18000 ± 6000 Ω/□

3.5.3 Development of 340nm beams

In order to realise static cantilevers for biosensor applications the device thickness must be below 1µm due to the strict application requirements. A further reduction of beam thickness is then needed. SOI wafers with suitable properties were purchased from SOITEC (Table 3.9).

Table 3.9. SOI wafers specifications

Parameter	***Value***	***Unit***
Wafer diameter	4	inch
Doping type (device layer)	P type (B)	-
Orientation	(100)	-
Resistivity (device layer)	14 ÷ 22	Ω cm
Thickness (device layer)	296 ÷ 384	nm
BOX thickness	392 ÷ 407	nm

The critical points for the realisation of piezoresistors on thin structures are the residual stresses balance for the realisation of flat structures, the release procedure of mechanical structures and the receipts for piezoresistor implantation. In order to evaluate the better technological approaches and to optimise the technological steps, performed tests are reported in the following paragraphs.

3.5.3.1. Characterisation of residual stresses of materials

Based on standard wafers, depositions of different stacks of thin film materials for the realisation of gold layers on cantilever devices were performed and residual stresses were evaluated by means of the Stoney's formula after each deposition, in order to evaluate the differential contribution of each layer:

$$\frac{1}{R} = 6\frac{(1-\upsilon)\cdot L^2}{ET^2}(\Delta\sigma_t - \Delta\sigma_b) \qquad 3.21$$

The selected thicknesses and sequence of layer and measured residual stresses are reported for each wafer in Table 3.10 and Figure 3.7.

Table 3.10. Test of residual stresses: selected thicknesses and sequence of layers.

wafer	*first layer (PECVD Si oxide)*		*second layer (Cr-Au)*		*both layers*		
						before anneal	*after anneal*
	thickness [nm]	*stress [MPa]*	*thickness [nm]*	*stress [MPa]*	*thickness [nm]*	*stress [MPa]*	*stress [MPa]*
POC1T/1	10.0	-350.4	23	441.6	33.0	317.0	152.3
POC1T/2	13.7	-402.1	23	241.7	36.7	85.0	67.4
POC1T/3	18.5	-395.7	23	349.5	41.5	49.1	91.9
POC1T/4	24.0	-444.8	23	457.7	47.0	-205.3	-35.6

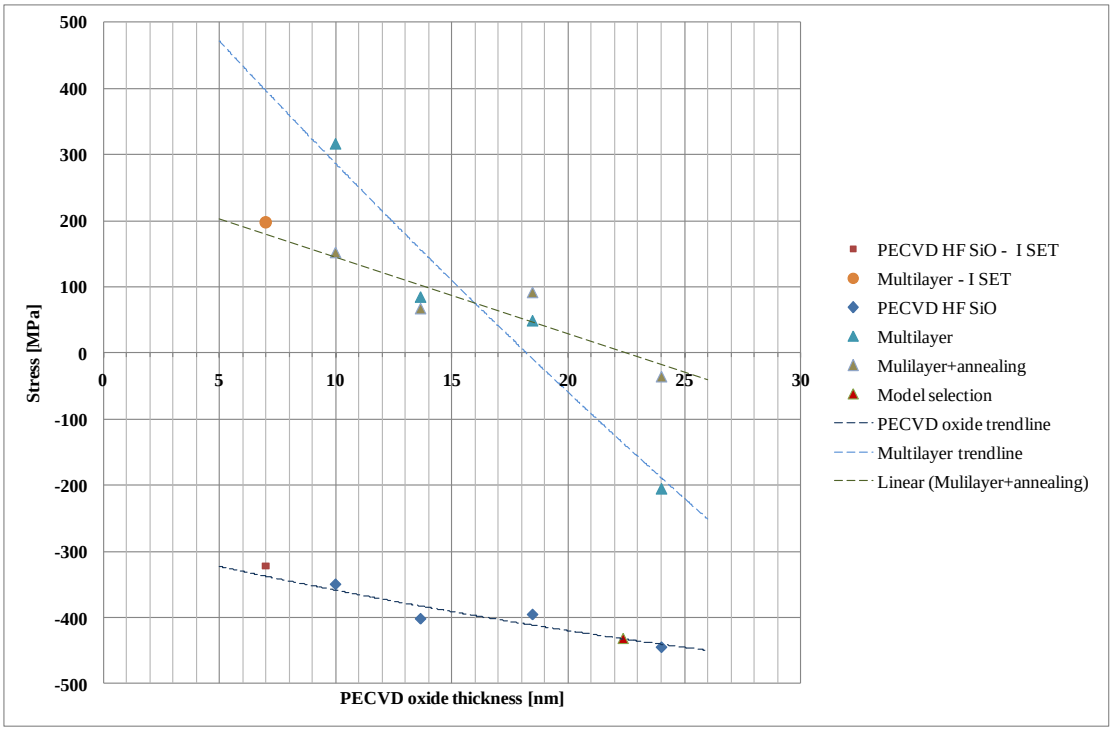

Figure 3.7. Overview of residual stresses of oxide and overall multilayer structure as a function of the Si oxide layer [nm]. Effect of gold annealing is also reported.

On the basis of the results, the multilayer structure for the test devices has been defined to two possible implementations, later used for the test structure fabrication. The Cr/Au layers have been fixed to 23nm total thickness and oxide to 16 and 20nm in order to find the best stress compensation.

3.5.3.2. Test structures

One test process has been focused on the steps for the definition and the release of suspended structure, as well as the study of mechanical properties of beams with different geometries. Thus, no readout has been included in the test structures. The process is based on Silicon-on-Insulator (SOI) wafers similar to the one expected to be used for the final devices. This process has provided test structures for the optimisation of the device functionalisation and the refinement of release techniques for the thin structures. The process uses three design layers (namely FRONT, BACK and GOLD) for the definition of the front side of cantilever arrays on the device layer, of the back side etching for cantilever release and of the gold adhesion layer on beams respectively.

Table 3.11. Mask-set of the process

Mask name	***Mask polarity***	***Align on***
FRONT	Dark field	Alignment Mask
BACK	Dark field	FRONT
GOLD	Dark field	FRONT

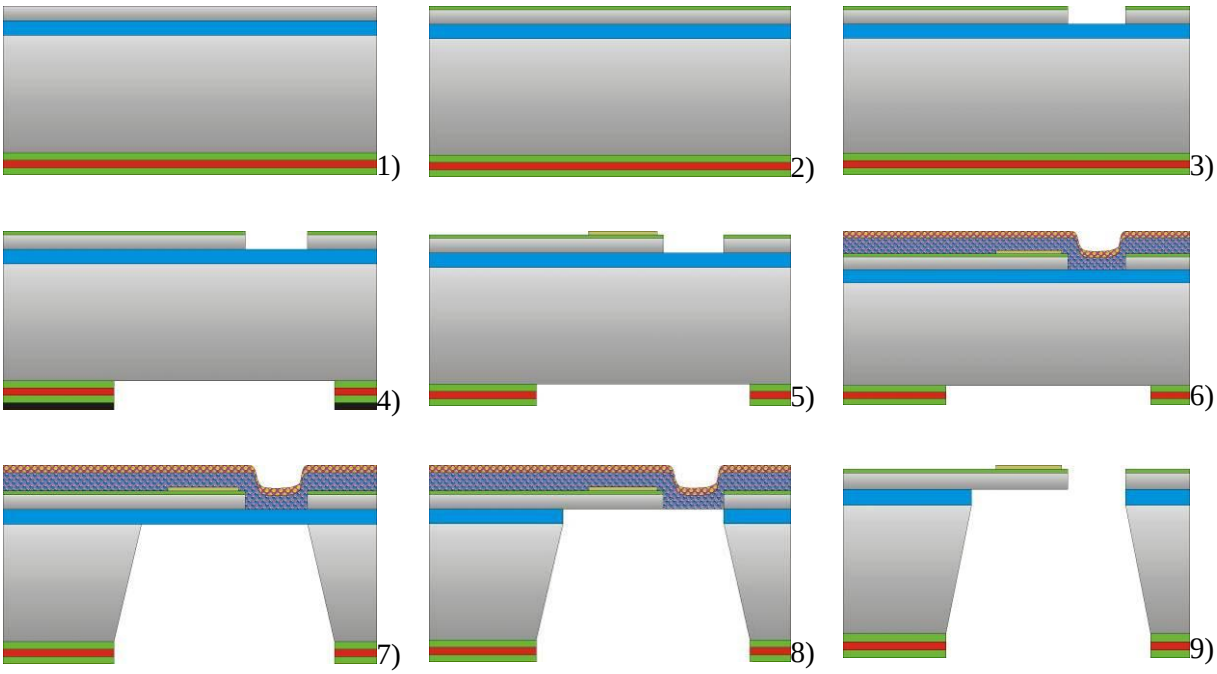

Figure 3.8. Process flow: 1.Deposition of a multilayer stack (TEOS/ LPCVD nitride / TEOS) on the back side. 2. Deposition of a thin PECVD oxide layer on the front side 3. Lithographic definition of FRONT mask and front side etching of suspended structure in the device layer. 4. Lithographic definition of BACK mask and hard mask etching. 5. Lithographic definition of the GOLD mask, Cr/Au deposition and lift-off. 6. Front side coating with protective layer. 7. Back side etch and pre-dicing of wafers. 8. Oxide (BOX) removal. 9. Coating removal and structure release.

A multilayer stack (TEOS/ LPCVD nitride / TEOS) is deposited on the back side for the realisation of the back side hard mask, while a thin PECVD oxide layer is used for gold adhesion on the beam. A technological splitting has been implemented (16 and 20nm thickness respectively) for evaluating the stress compensation of the structure, on the basis of the test process for stresses (POC1T). The FRONT mask is used to define the front side etching of suspended structure in the device layer, followed by the lithographic definition of BACK mask and hard mask etching. The GOLD mask is then used to define the Cr/Au layer on beams by means of a lift-off process. A protective coating is used to protect the suspended structure during the TMAH wet etching process of handle layer from the backside and BOX removal. The process flow is reported in Figure 3.8.

A set of array geometries were designed, for the realisation of preliminary structures and functional tests. In Figure 3.9 and 3.10, the complete design on the wafer and alignment markers are reported, also showing the correspondence of colour codes with process layers.

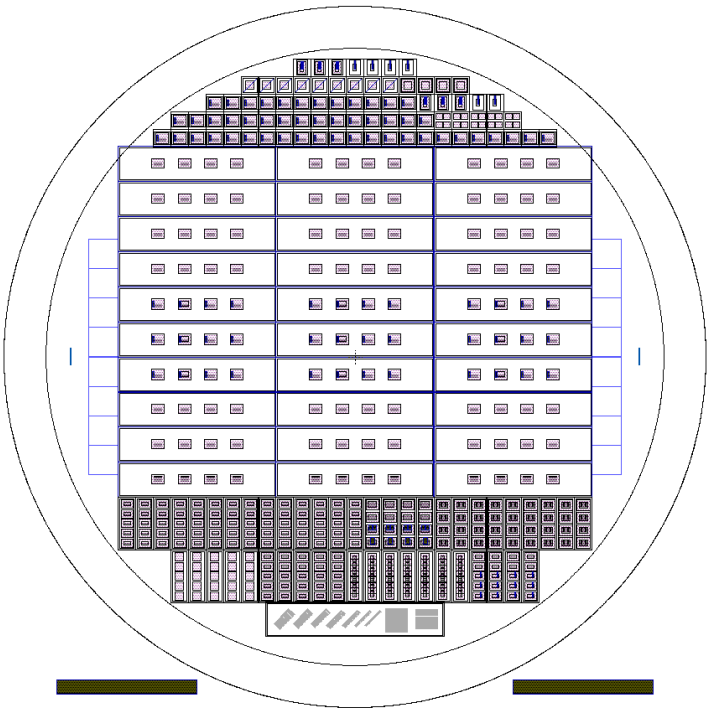

Figure 3.9. Top view of the whole wafer design for the test process "POC1", showing the contour of the 4" wafer and useful area for devices (black circles). Details of the included devices are reported in the next Figures.

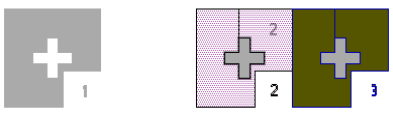

Figure 3.10. Alignment marker for masks layers (1 front-etch, 2 back-etch, 3 gold adhesion layer)

Different length, dimensions, array configuration have been designed in order to evaluate the best design for final devices. A review of main geometries is reported below.

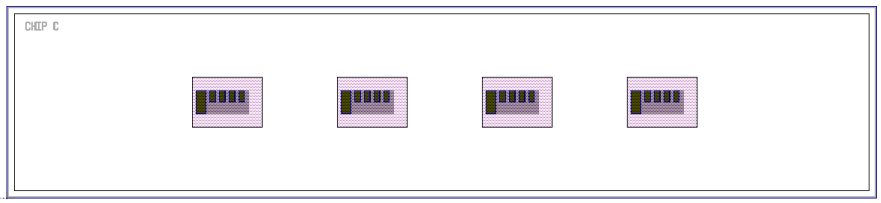

Figure 3.11. Main devices for sensitivity tests, compliant with Protiveris™ instrumentation for evaluation of beam deflection. Overall chip dimensions: 22400 x 5000 μm^2. Configuration: 4 wells with 4 beams (300 x 150 μm^2 each).

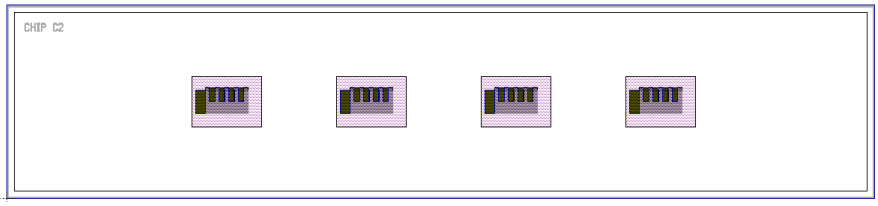

Figure 3.12. Same device as in previous figure, with a different etching design.

Figure 3.13. "Vector type" devices with beams in one row, used to evaluate reproducibility of beams over long rows. Overall chip dimensions: 7500 x 2500 μm^2. Configuration: single well with 28 beams (300 x 60 μm^2 each).

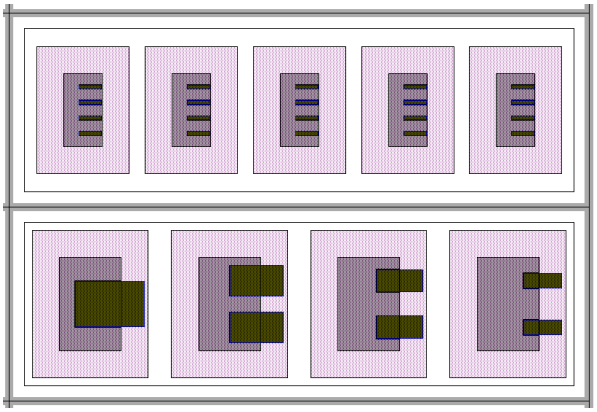

Figure 3.14. Two different "matrix type" devices with different beam dimensions. Overall chip dimensions: 7500 x 2500 μm^2. Configuration: upper design: 5 well with 4 beams (300 x 60 μm^2 each), lower design 4 wells with different beam dimensions (600 x 600, 400 x 400, 300 x 300, 200 x 200 μm^2 respectively).

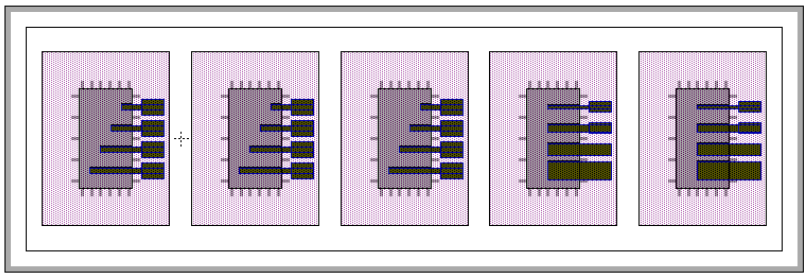

Figure 3.15. Arrays with beam length increase (wells 1 to 3: beams 100, 200, 300, 400 x 60 μm^2 each) and increasing width (wells 4 and 5: beams 300 x 40, 80, 120, 180 μm^2 each). Overall chip dimensions: 7500 x 2500 μm^2. Configuration: 5 well with 4 beams each. Extensions of gold pattern outside the beams have been introduced in order to evaluate single-drop functionalisation of surfaces, driven by gold wettability.

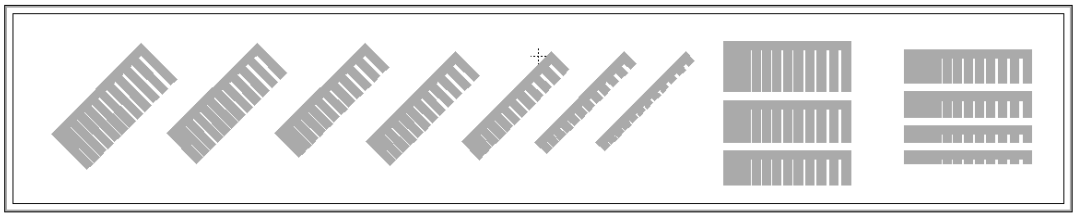

Figure 3.16. Structures for front-etch test.

Other implemented structures, strictly devoted to technological tests, are not reported here.

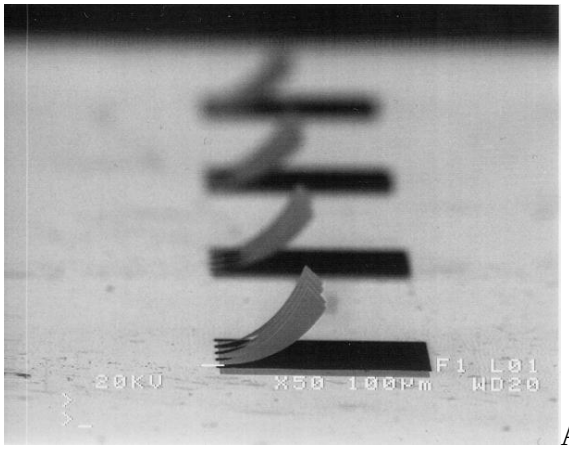

A)

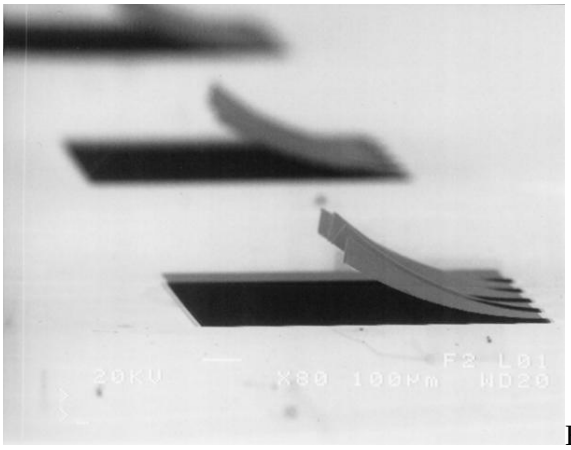

B)

Figure 3.17. SEM micrographs of realised devices. A): wafer 1 with 16nm PECVD oxide. B) Wafer 6 with 20nm PECVD oxide.

A SEM micrograph of realised devices is reported in Figure 3.17 for wafers with different oxide thicknesses. In particular, wafer with lower PECVD oxide thickness showed higher upward bending (wafer 1). The non perfect balancing of stress in the structure can be due to the slightly different thermal processing during the process with respect to the test process for

stresses. The process also allowed the optimisation of release procedure, involving both wet and dry etching steps.

3.5.3.3. Test of piezoresistor implant process

A second test process for the investigation and optimization of critical fabrication steps was set up with technological splitting in Table 3.12, especially for the evaluation of the better approach for the realisation of implanted piezoresistors with suitable sensing performances.

Table 3.12. Summary of technological steps for implant test process

STEP		Wafers			
		POC2T/2	**POC2T/3**	**POC2T/5**	**POC2T/6**
1	Implant BF2 E=60 keV - Dose = 1 1013 - Frontside	X	X		
2	Implant B E=60 keV - Dose = 5 1012 - Frontside			X	X
3	Diffusion - T = 1150°C - t = 30 min (N_2)	X	X		
4	Diffusion - T = 1000°C - t = 20 min (N_2)			X	X
5	Implant As E=40 keV - Dose = 1 1014 - Frontside	X	X	X	X
6	Diffusion - T = 890°C - t = 20 min - (N_2)	X	X	X	X

A correction of the substrate doping by means of a BF_2 implant allowed a reduction of the junction depth, thus increasing the geometrical efficiency of the piezoresistors. Due to lower diffusivity, As was the dopant of choice for the realisation of n-type piezoresistors. The implant doses and energies were chosen on the basis of preliminary process simulations realised with Athena Silvaco^{TM} software. Main results are reported in Figure 3.18. Experimental characterisation of results was performed by means of TOF-SIMS measurement of element concentration in the wafer section, in order to provide a validation of the doping profiles achieved with the selected implant receipt. The TOF-SIMS analysis on test wafers provided, for the B-implanted wafers, a substrate p-type doping of about 110^{17} at/cm^3, with implanted n-type resistors with doping about 8 10^{18} at/cm^3 and junction depth about 75nm (Figure 3.19). This splitting was preferred because of the higher reproducibility of implanted profiles and higher resistor doping. The sheet resistance measurements over the wafer provide results similar to the simulated and acceptable uniformity over the wafer (pls. cfr. Figure 3.18 C and D).

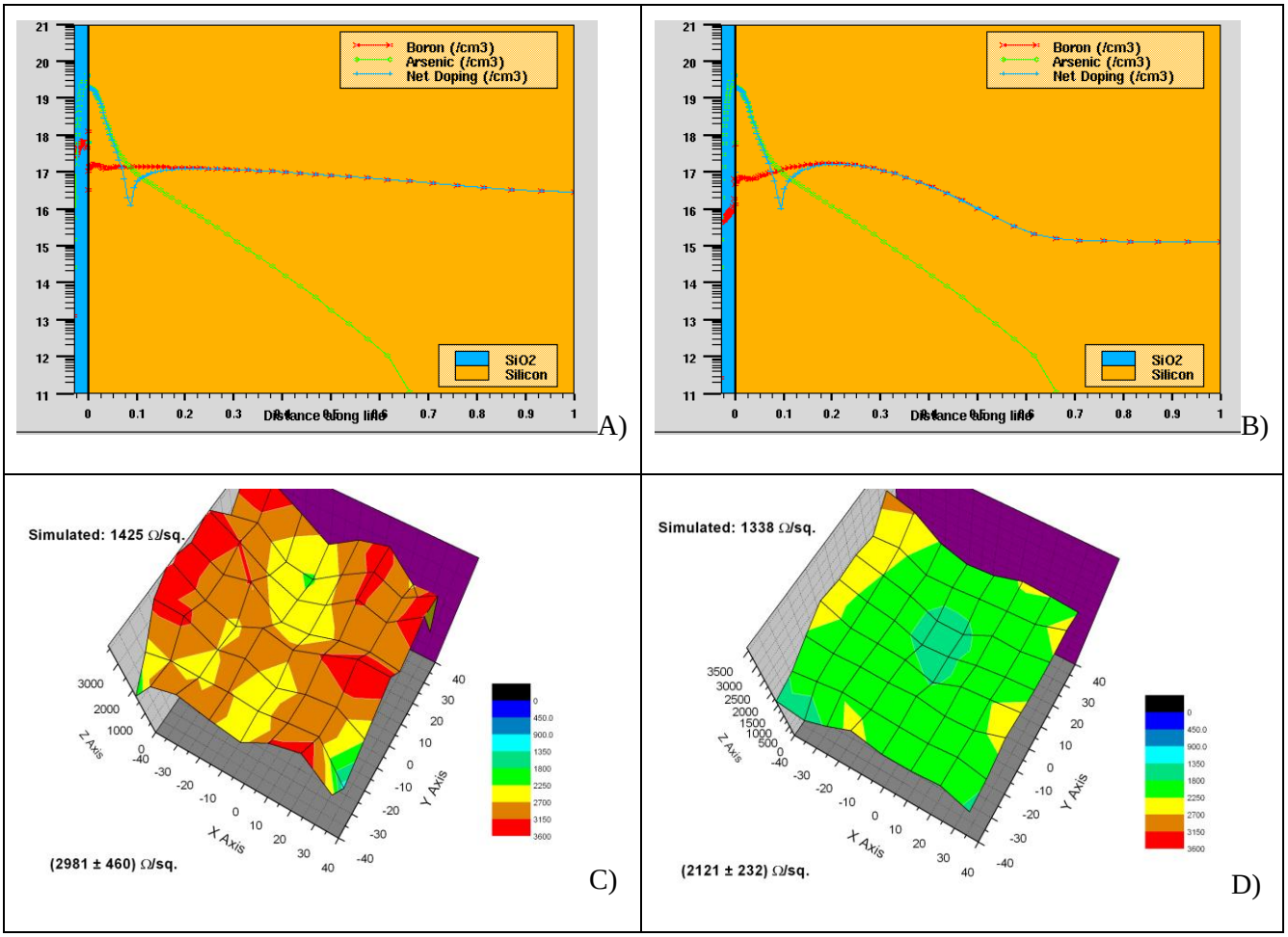

Figure 3.18. Simulated doping profiles for wafer 3 (A) and wafer 5 (B), showing a junction depth below 100nm, and 4-probes measurement of sheet resistance over the wafer 3 (C) and wafer 5 (D), compared to simulated sheet resistance.

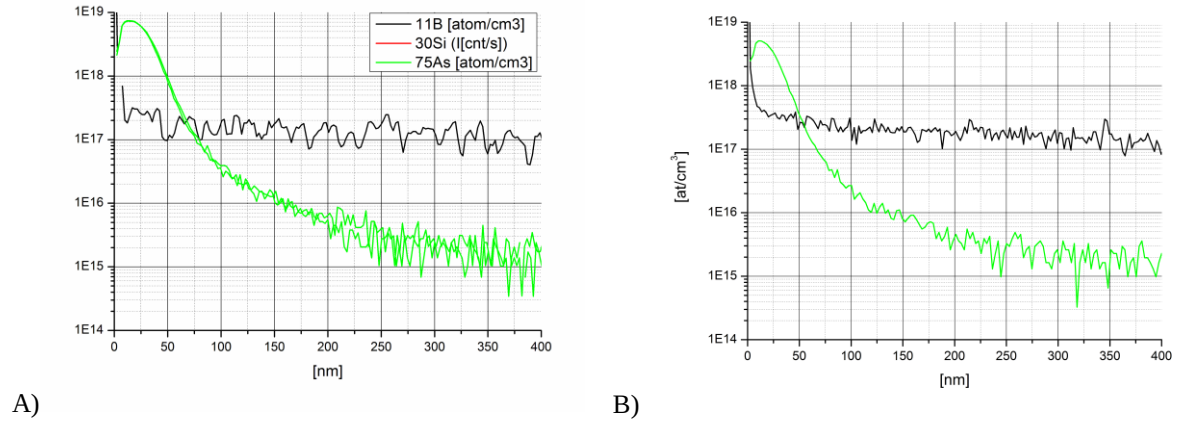

Figure 3.19. A) TOF-SIMS analysis of wafer 6 (B doping). B) wafer 3 (BF_2 doping)

Chapter 4

4. Development of microcantilever detectors for gravimetric sensing

The development of microcantilever for gravimetric sensing was carried out starting from the evaluation of best geometries and sensing properties by means of analytic and numerical modelling. The first model was implemented with a simple spring-mass model, properly implemented to evaluate resonance properties and some beam issues such as the multilayer structure and damping-related effects. Sensitivity and resolution of the sensor calculated with this methods are presented in this chapter. Finally, finite elements (FE) models were developed to take into account geometrical effects, meanly related to the beam root region, and effects of residual stresses on device properties. FE analysis was also used to verify the analytical result and to optimise the design of the devices. Then, testing of fabricated devices in terms of electromechanical properties and sensitivity have also been performed in order to evaluate the proper design and implementation of the sensors.

4.1. Analytical modelling

Analytical modelling was performed using the procedures described in Chapter 3 for the calculation of mechanical properties of multilayer structures and the simplified mass-spring model, also taking into account damping in resonance equations. On the basis of the technologies available at FBK clean room and described in Chapter 3, two different technological processes were taken into consideration for the realisation of the devices. In the first process, based on standard wet bulk micromachining steps to release the suspended structure, the layer sequence of the structure was defined as Si/TEOS/LTO/Au, with respective thicknesses 10/0.4/0.2/0.1μm. In the second fabrication process, based on Silicon-on-Insulator (SOI) wafers, the layer sequence was 2/0.2/0.1/0.1μm. Moreover, for the latter process, the effect of multilayer thickness on device performances was investigated with the set of calculations performed with a layer sequence 2/0.4/0.2/0.1 μm. These results are marked as "thick oxide" in Table 4.1. Materials properties were set to values in Table 4.5, where residual stresses are data obtained during the technological process characterisation and Young's modulus and density are estimated according to data available in literature. Properties of crystalline silicon are well-known and analysis results show low dependence on properties of thin film deposited on the Si beam, due to their low thickness. On the basis of analytical modelling and technological and design constrains, a first selection of beam geometries was performed in order to match the resonance frequency with the properties of the external piezoelectric actuator. In table 4.1 resonance properties for different geometries are shown, also including the evaluation of damping effect on resonance frequency.

Table 4.1: Effect of gas density and damping on resonance frequency for different device geometries.

Geometry (L, W, t) [μm]	*χ [Kg m-1]*	*f_0 [kHz]*	*f_0 (with χ correction)*	*f_0 (with γ correction)*	*Q*
1500 x 106 x 10	$2.281\ 10^{-8}$	6.039	6.015	6.014	23.1
1000 x 106 x 10	$2.281\ 10^{-8}$	13.589	13.534	13.533	34.7
500 x 106 x 10	$2.281\ 10^{-8}$	54.355	54.136	54.134	69.4
300 x 106 x 2 (thick ox.)	$2.281\ 10^{-8}$	31.919	31.493	31.478	16.1
300 x 106 x 2	$2.281\ 10^{-8}$	28.944	28.524	28.506	14.0
200 x 50 x 2	$5.075\ 10^{-9}$	65.124	64.673	64.654	20.8
150 x 50 x 2	$5.075\ 10^{-9}$	115.777	114.974	114.956	27.7

In Table 4.2 the estimated sensitivity and resolution are summarized for different geometries, where the mass resolution is calculated as function of the frequency resolution of the measurement set-up.

Table 4.2: Calculated sensitivity to mass and mass resolution for different beam geometry.

Geometry (L, W, t) [μm]	*f_0 [kHz]*	*S_m [$cm^2\ g^{-1}$]*	*$\Delta\rho$min [$g\ cm^{-2}\ Hz^{-1}$]*
1500 x 106 x 10	6.014	-373.8	$4.4\ 10^{-7}$
1000 x 106 x 10	13.533	-373.8	$2.0\ 10^{-7}$
500 x 106 x 10	54.134	-373.8	$5.2\ 10^{-8}$
300 x 106 x 2 (thick ox.)	31.478	-1231	$2.6\ 10^{-8}$
300 x 106 x 2	28.506	-1340	$2.6\ 10^{-8}$
200 x 50 x 2	64.654	-1361	$1.1\ 10^{-8}$
150 x 50 x 2	114.956	-1361	$6.4\ 10^{-9}$

In order to evaluate the sensitivity of the piezoresistive read-out, a preliminary evaluation of resistors efficiency was performed. According to the maximum efficiency of piezoresistive properties of monocrystalline Silicon, p-type resistor on n-doped substrate were preferred, with [110] crystallographic orientation.

Table 4.3: Typical piezoresistive properties of Silicon.

Material (Si)	*π_{11} [Pa^{-1}]*	*π_{12} [Pa^{-1}]*	*π_{44} [Pa^{-1}]*
p-type, 7.8 Ω cm	6.6 10-11	-1.1 10-11	138.1 10-11
n-type, 11.7 Ω cm	-102.2 10-11	53.4 10-11	-13.6 10-11

According to literature [Kanda 1982], piezoresistive coefficients π_{ij} are expected to have the maximum values shown in Table 4.3 for low doping concentration in the [100] orientation, resulting in the properties in the [110] direction and its perpendicular direction (p-type silicon):

$$\pi_l = \frac{\pi_{11} + \pi_{12} + \pi_{44}}{2} = 71.8 \cdot 10^{-11} \qquad [\mathrm{Pa}^{-1}] \qquad 4.1$$

$$\pi_t = \frac{\pi_{11} + \pi_{12} - \pi_{44}}{2} = -66.31^{-11} \qquad [\mathrm{Pa}^{-1}]$$

An important issue about piezoresistors is the dependence of parameters on temperature and doping. As reported in [Kanda 1982], these effects are correlated and maximum read-out sensitivity and temperature dependence are obtained for low doping. Using higher doping dose the dependence on temperature can be strongly reduced, but in this case also piezoresistive properties are reduced, resulting in lower read-out sensitivity. Different doping levels were evaluated for the fabrication process, in order to select the best set of process parameters. Process parameter and doping levels are reported in paragraph 3.5.

4.1.1.1. Actuation

An external commercial piezoelectric device was chosen for the device actuation, due to the ready availability of commercial devices. Selected component was a PL033.20 device by PI Ceramics, with the specifications in Table 4.4.

Table 4.4: Specification of the piezoelectric device.

Code	*Dimensions [mm]*	*Mass [g]*	*f0 [kHz]*	*C [nF]*	*Displacement @ 100V [μm]*
PL033.20	3 x 3 x 2	0.14	> 300	100	2.2

Starting from actuator performances, it is possible to evaluate the "inertial" actuation of the beams. The force at the beam barycentre for a sinusoidal actuator displacement of modulus z_0 is:

$$F = m \cdot z'' = -m \cdot z_0 \cdot (2\pi f_0)^2 \sin(2\pi f_0 t) \qquad 4.2$$

where m is the corrected beam mass and f_0 and z_0 are the actuation frequency and amplitude respectively.

The maximum working frequency in operative condition of the actuator must be corrected by considering a spring-mass model where the device mass is added to the chip mass, which can be considered as a "load mass". The effective maximum frequency is then approximately 200 kHz and it sets the upper limit for the design value of the resonance frequency of the devices. The displacement should be considered at a voltage lower than the maximum allowed for the device in order to reduce the device heating, which is the 2% of the bias power at low voltages, but can reach the 15% at 100V. The efficiency increases with the beam mass and the square of the actuation frequency. Typical resonance behaviour, including actuation and damping, is shown in Figure 4.1.

A feed-back system for actuation, where the signal read from the cantilever is fed to the actuator, was used for high resolution frequency measurements, as reported in paragraph 4.5.2. This approach allowed an increase of Q factor of the resonance of some order of magnitude.

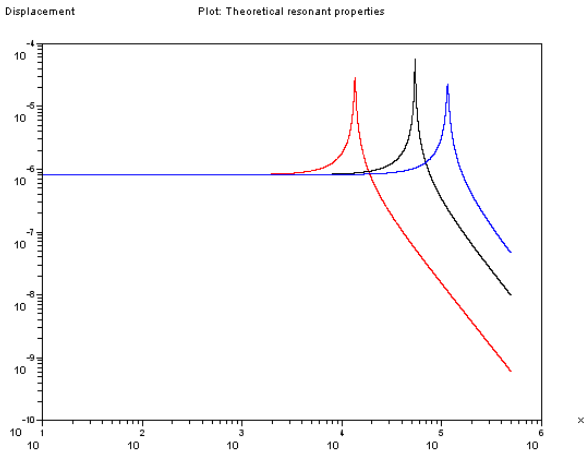

Figure 4.1: Analytical calculation of resonance properties of cantilever for 3 V actuation voltage of the piezoelectric actuator. Tip displacement [m] vs. frequency [Hz]. The resonance displacement is in the ten μm range. (Beam geometry: 1000x106x10 μm (red), 500x106x10 μm (black), 150x50x2μm (blue))

4.2. Finite Element (FE) modelling

The simulation of the device behaviour was performed by means of the ANSYS™ simulation software. At first static models were implemented in order to preliminarily estimate the spring constant K of the beam for the spring-mass analytical model, also for a comparison with theoretical equations. Then FE modal analyses were implemented to investigate the dynamic properties of devices. The effect of residual stresses in the multi-layered structure was taken into account in a preliminary static simulation by applying an equivalent thermal load and proper thermal expansion coefficients in order to evaluate the pre-stress condition for the modal analysis. In a second set of FE simulations initial stresses where directly implemented in multilayered shells. Effects on the properties of the device of process parameters such as beam root definition by means of silicon wet etching or residual stresses were also evaluated by numerical methods. In particular the target resonance frequency was estimated in order to match the specifications of the piezoelectric device used for actuation. The structure sensitivity to mass adsorption was evaluated by means of modal analyses.

4.2.1 Static analysis

In order to implement the FE model, an approach based on shell elements was chosen to easily implement the multilayer section by using a small element number. The element of choice was the SHELL181, since it allows mechanical and modal analysis with a multilayer structure. Defined structure is summarized in Table 4.5 for 10 micron thickness beams, also reporting material properties. Thin films were modelled as isotropic materials, whereas silicon has been modelled according with an orthotropic material. Thicknesses were defined according to the fabrication process, residual stresses have been measured during the equipment tuning, while Young's modulus (E), Poisson ratio (υ) and density (ρ) were selected from lit-

erature data. This can result in an error of estimation of device properties, in particular with regard to the properties of the thin film properties, but this error was neglected due to the low thickness of these layers. Different geometries, previously evaluated with the analytical model (Table 4.1), were implemented for simulation.

Table 4.5: Material properties and layer sequence.

Material	***Thickness [μm]***	***E [GPa]***	***v***	***σ_R [MPa]***	***ρ [Kg m^{-3}]***
Au	0.100	80	0.35	155	19280
LTO	0.200	70	0.25	153	2200
TEOS	0.400	70	0.25	-51	2200
Si	10.000	E [110] = 169 E [100] = 130 Gxy = 51 Gxz = Gyz = 79	υxy = 0.064 υxz=υyz= 0.361	0	2329

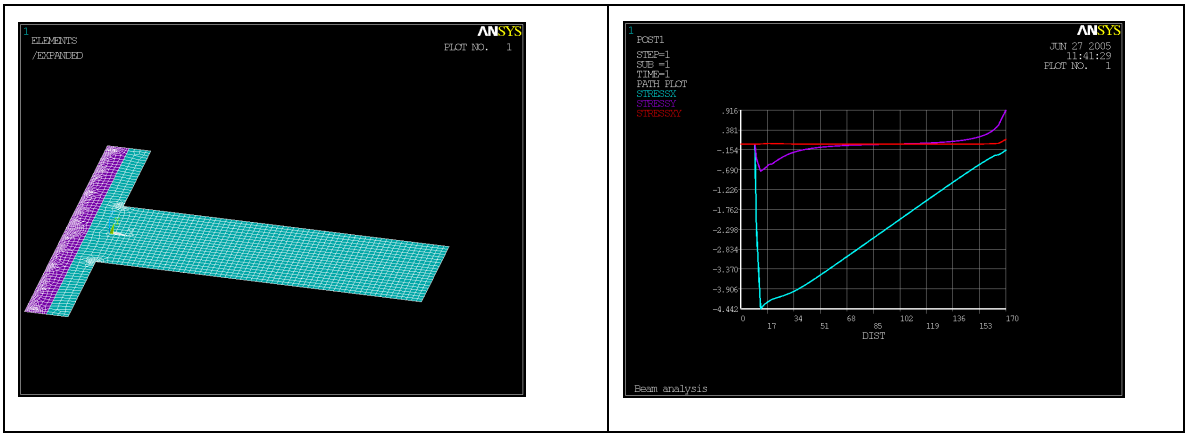

Figure 4.2: A) Static model of beam, length 150μm, width 50μm, Silicon thickness 2μm. Multilayer structure has been included in the shell section definition, bulk substrate (violet region) and underetch have been included. B): Stress distribution for the static tip-load model, 20μm underetch is included.

Only half of the cantilever was included in the model, by using the structure symmetry in order to reduce the element number. Boundary conditions were set to zero displacement at beam root and symmetry condition at beam axis. In the static analysis a tip load of 1μN has been set at the tip. Model and results are shown in Figure 4.2.

4.2.2 Modal analysis

The same geometries and meshes used for static analysis were also used for modal analysis, with the same boundary conditions and mesh. The selected solution method was the Block Lanczos method available in ANSYS solver. A static analysis was performed as a preliminary step to include residual stress effect, by means of an equivalent thermal load. Stresses on nodes calculated during the preliminary step has been saved to an external file and loaded in the modal analysis as pre-stress conditions before solving the

model. A result summary for some device geometries is reported in Table 4.6, where resonance frequencies are presented for model not including stresses (f_0), with stress (f_0 + stress) and including a dummy mass to model the sensitive layer (f_0 + stress and s. layer). Results for non stressed beams are compatible with analytical results. An overview of modal analysis results is presented in Figure 4.3 for a beam with 150 μm length and 2 μm thickness.

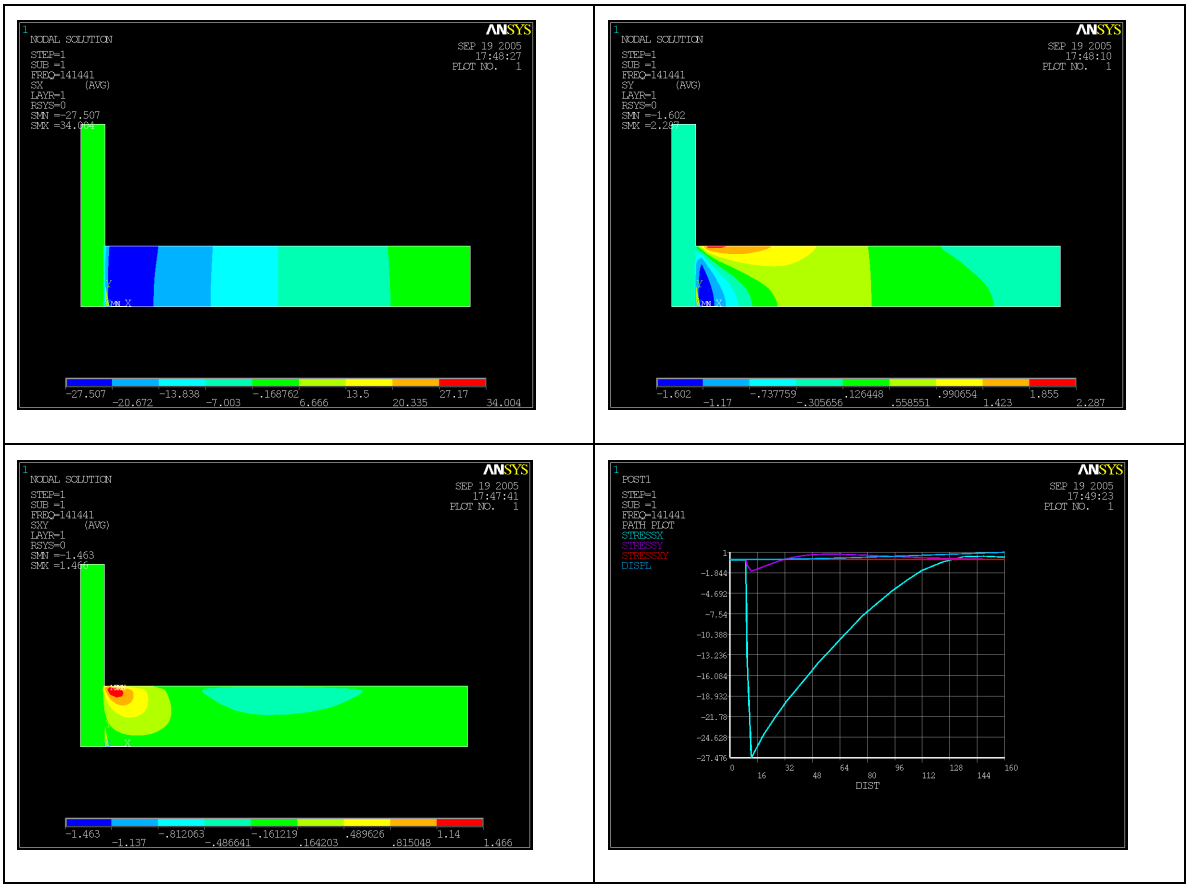

Figure 4.3: (Clockwise from top left) A) Modal analysis, σ_X stress distribution. B) Modal analysis, σ_Y stress distribution. C) Modal analysis, stress distribution on cantilever axis. D) Modal analysis, τ_{XY} stress distribution

Table 4.6: Comparison of resonance frequency [kHz] evaluated by FE for some of the devices.

Geometry	***f_0***	***f_0 + stress***	***f_0 + stress and s. layer***
1000x106x10	13.542	15.617	15.559
500x106x10	54.148	56.372	56.161
150x50x2	114.941	143.379	141.441
120x40x2	179.534	209.407	206.577
100x40x2	258.557	289.300	285.392

Torsional resonance modes of the structure are also present and they cannot be evaluated by using the symmetrical model. Tthese modes were investigated by means of a model including the complete structure (see Figure 4.4). These resonance modes are present at frequencies higher than first mode resonance.

In general the first torsional mode occurs as third mode for selected geometries, and then can be neglected in this analysis.

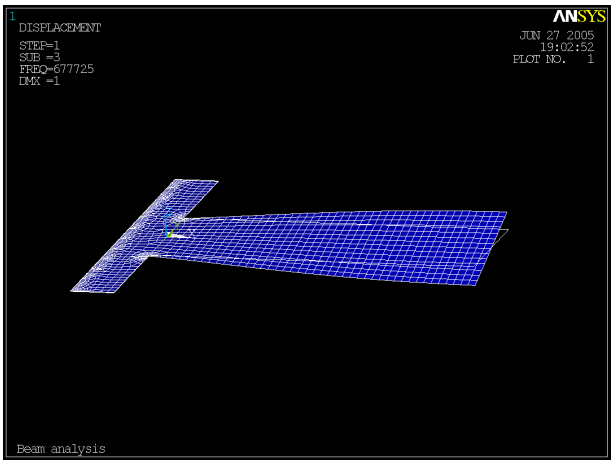

Figure 4.4: Deformed shape for a torsional resonance mode, at 677 kHz (Beam 150μm length).

4.2.3 Stress-stiffening

The investigation of the mechanical behaviour of the system was also aimed to the evaluation of the effect of residual stresses on the frequency. Effect of thin film residual stresses on resonance properties has been included in the simulation by means of an equivalent thermal load in preliminary static analyses. Results are shown in Figure 4.5 A) and B), showing the deformation of a device working at 3rd resonance mode and the resonance frequencies vs. the residual stress of the top PECVD nitride insulation film. Since this deposition techniques allows the tuning of material properties by using high, low or mixed frequency deposition, the process parameters of the layer was then tuned in order to obtain a residual stress of the nitride in the range 10÷100MPa, providing three resonance modes below 200kHz.

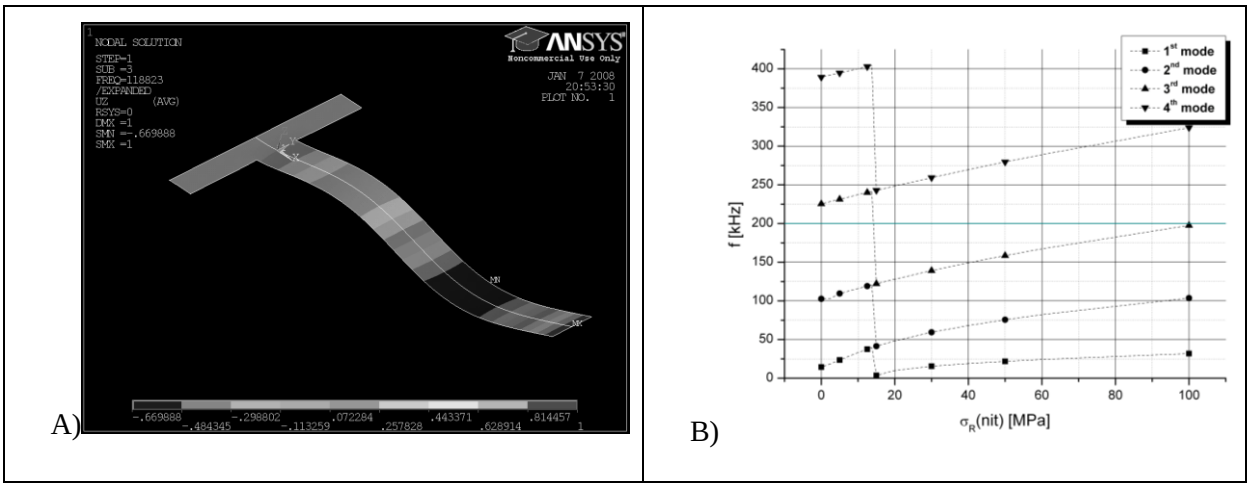

Figure 4.5: FE modelling: A) displacement at third mode, B) effect of residual stresses.

4.2.4 Under-etch effect

The effect of under-etch on resonance properties was investigated in order to estimate the effect of this issue related to the fabrication process. Since the release of the mechanical structure is performed by means of bulk wet etching, alignment inaccuracies between the mask and the crystal and variations of anisotropic etching ratio (Ra) may result in a under-etch at the beam root. Resonance frequency is lower for larger under-etch regions, due to the different mechanical properties of the beam.

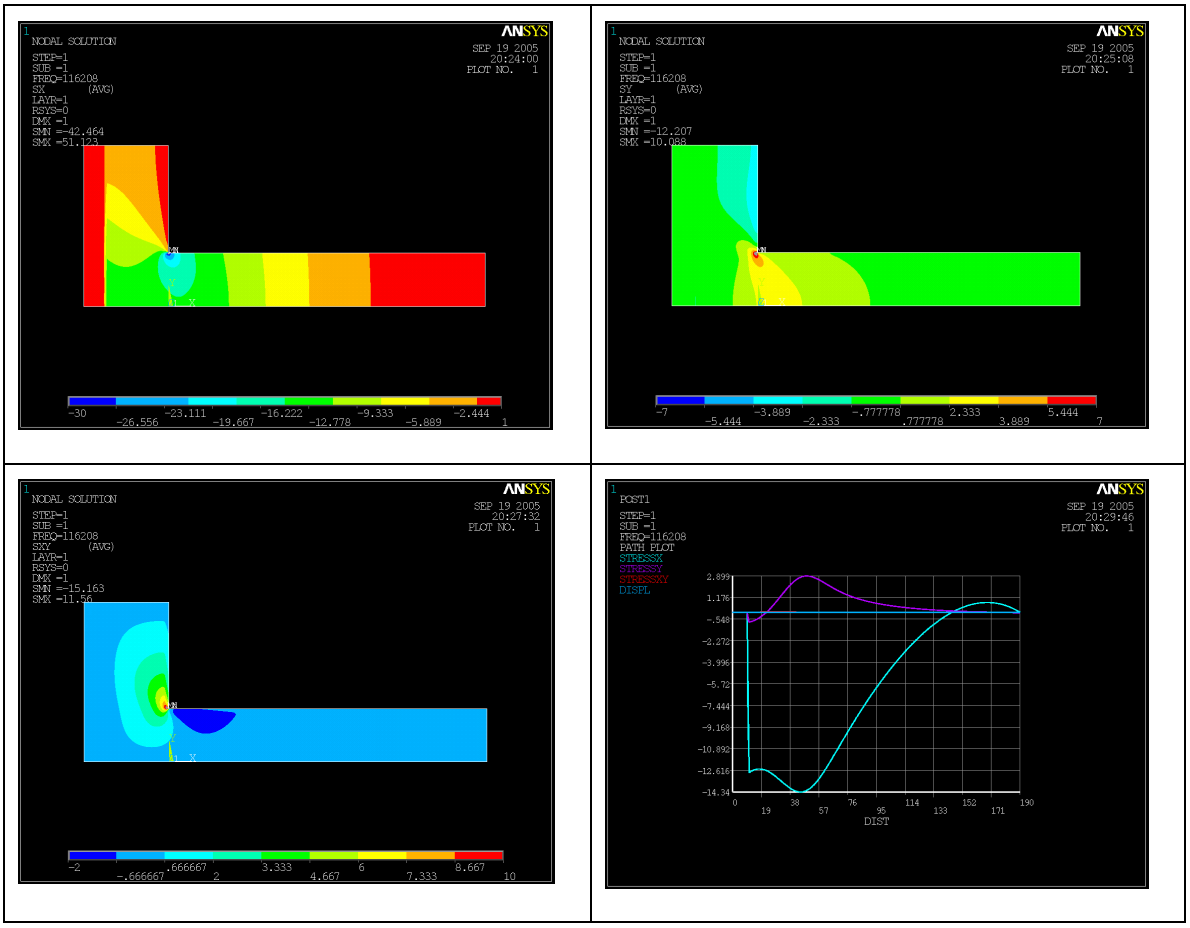

Figure 4.6: Modal analysis, stress distribution on cantilever, with 30μm underetch and 10μm bulk.

The beam compliance can be approximated by the series of the beam and under-etch region compliances, while the total mass is substituted to the beam mass. According to the simplified spring-mass model, it can be evaluated as:

$$f_0^{'} = \varphi \cdot f_0 \quad where: \quad \varphi = \left[\left(1 + \frac{W_b}{W_u} \frac{L_u^3}{L_b^3} \right) \cdot \left(1 + \frac{W_u \cdot L_u}{W_b \cdot L_b} \right) \right]^{-1/2} \qquad 4.3$$

The first term in the square root takes into account the K variation ($1/K=1/K_b+1/K_u$), while the second considers the mass variation. This expression fits the simulated Δf_0 for a $W_u = 2 \div 3\ W_b$, which is a rough

estimation of the width of the under-etch region affected by the stresses. In Table 4.7 comparison of simulated and calculated under-etch effects is presented for the 150 μm x 50 μm x 2 μm beam.

Table 4.7: Summary of underetch effect (Beam 150 μm length , Wu/Wb = 3).

Underetch [μm]	f0 [kHz] – (approx. expr.)	f0 [kHz] - FE
0	(143.379)	143.379
10	131	130.433
20	121	122.150
30	113	116.208

The stress behaviour in the beam region is quite similar to the results of the model without under-etch, but at cantilever root significant variations of stresses distributions occur. This effect is further discussed in the next paragraph, dealing with the read-out optimization.

4.2.5 Read-out optimization

The position of the piezoresistive read-out was evaluated for each beam geometry, in order to optimise its efficiency. Piezoresistive effect was evaluated by applying the π_{ij} coefficients to stress distribution obtained by FE modal simulations. The extracted parameter is the distance of the read-out from the cantilever root. A summary of results is shown in Table 5.8, and a sample graphs of the analysis are reported in Figures 4.7-4.9.

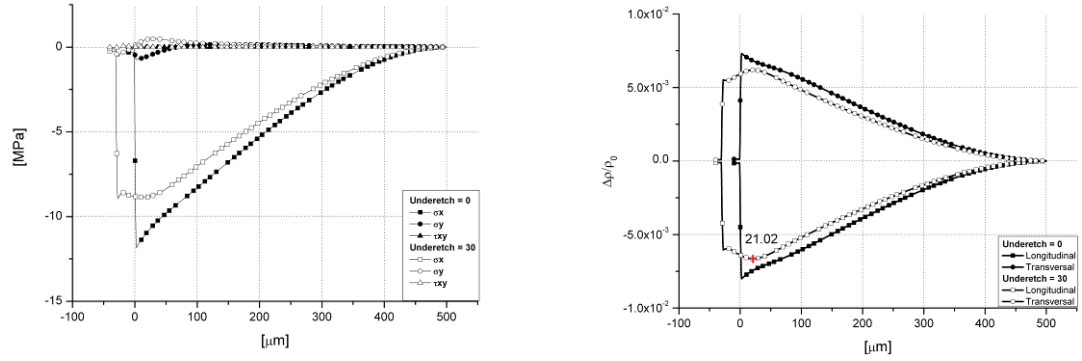

Figure 4.7: Stress distribution at Si surface and respective resistivity variations calculated by means of modal analysis for 500x106x10 μm beams.

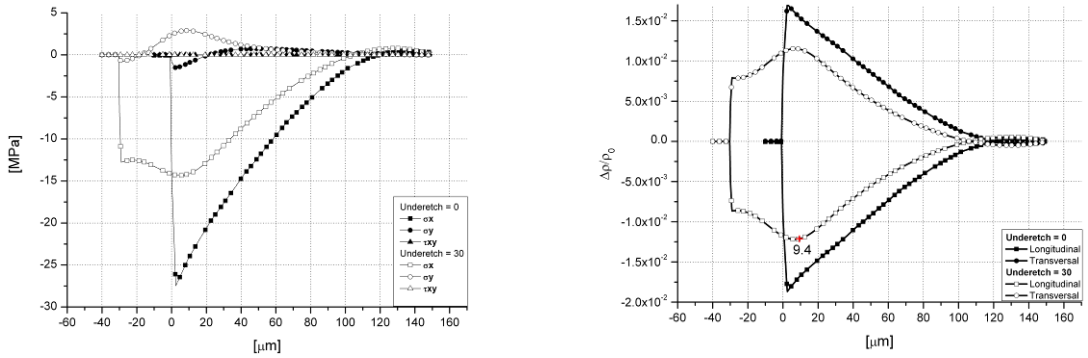

Figure 4.8: Stress distribution at Si surface and respective resistivity variations calculated by means of modal analysis for 150x50x2μm beams.

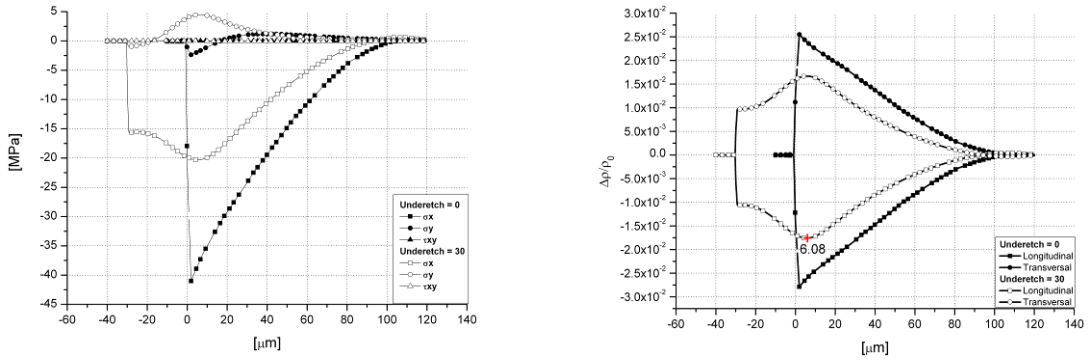

Figure 4.9: Stress distribution at Si surface and respective resistivity variations calculated by means of modal analysis for 120x40x2μm beams.

Stresses were considered at the silicon surface, and then the efficiency factor β must be included to take into account the piezoresistor thickness. The presence of under-etch also modify the stress distribution on the structure and then optimal position of the read-out has been calculated for different under-etch values.

Table 4.8. Optimal position of the read-out.

Geometry [μm]	***Optimal position of read-out [μm]***
500 x 106 x10	21
150 x 50 x 2	9
120 x 50 x 2	6

Due to the narrow width of devices with length 150 μm or less, a piezoresistor bridge cannot be implemented on beams. In these devices a configuration with a single resistor should be selected, with an optimal length of longitudinal branches calculated according to the $\Delta R/R_0$ parameter.

$$\frac{\Delta R}{R_0} = \frac{1}{L}\int_L \frac{\Delta\rho}{\rho_0}\cdot dl \qquad 4.4$$

Sample results are shown in Figure 4.10. for beam with length 150 and 120 μm.

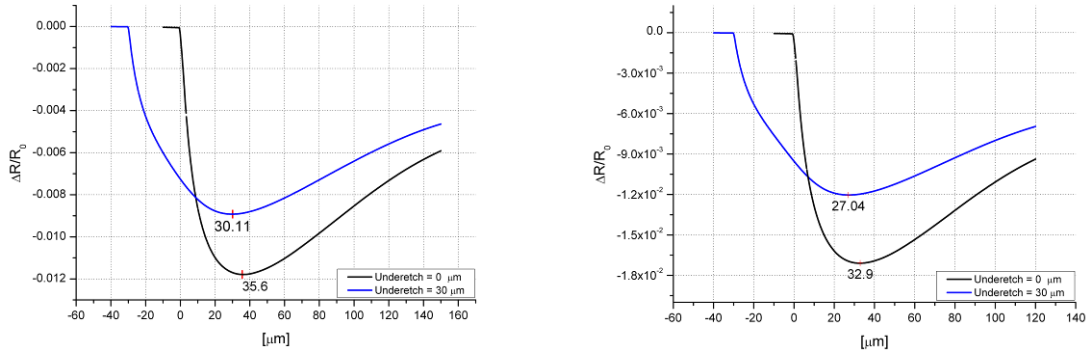

A) B)

Figure 4.10: Configuration of piezoresistor for narrow beams, and results of calculation on simulated stress for beam length 150 (A) and 120μm (B).

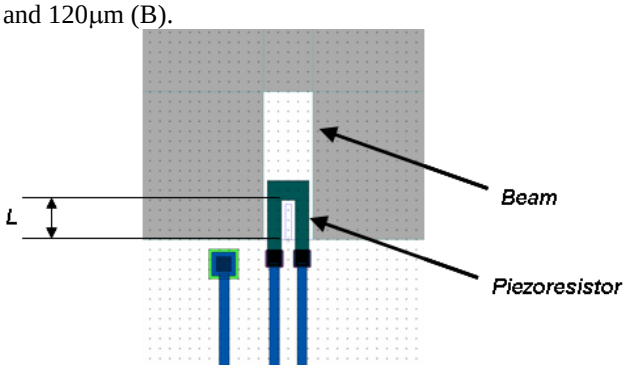

Figure 4.10: C) Configuration of piezoresistor for narrow beams.

4.2.6 Mass sensitivity and resolution

In order to investigate the mass sensitivity of the device and to verify the results obtained by analytical calculations, a dummy layer was added to the multilayer structure to simulate the sensitive layer properties. Thickness has been set to 200nm, according to the typical thickness of the deposited layers, and density has been set to 1000 [Kg m^{-3}], which could be a reasonable value for an organic compound. The resonance frequency was of course lower than for the beam without dummy layer and also sensitivity is affected, due to the increase of the cantilever mass.

Shift of resonance frequency correlated to the analyte adsorption onto the sensitive layer was simulated by varying the material density. Results are shown in Table 4.9, where the density increase has been converted to surface mass density increase for the given film thickness.

Table 4.9. Calculated resolution and sensitivity to mass increase for different beam geometry.

Geometry (L, W, t) [μm]	S_m [$cm^2\ g^{-1}$]	$\Delta\rho_{min}$ [$g\ cm^{-2}\ Hz^{-1}$]
1000 x 106 x 10	-214	$3.0\ 10^{-7}$
500 x 106 x 10	-190	$9.4\ 10^{-8}$
150 x 50 x 2	-669	$1.1\ 10^{-8}$
120 x 40 x 2	-671	$7.2\ 10^{-9}$
100 x 40 x 2	-670	$5.2\ 10^{-9}$

FE results fit quite well (Figure 4.11) with the analytical model including the sensitive layer mass, where the Δf/f variation derived from the mass spring model has been calculated by:

$$\frac{\Delta f}{f} = \sqrt{\frac{\rho_{Beam}}{\rho_{Beam} + \Delta\rho_{Sup}}} \qquad 4.5$$

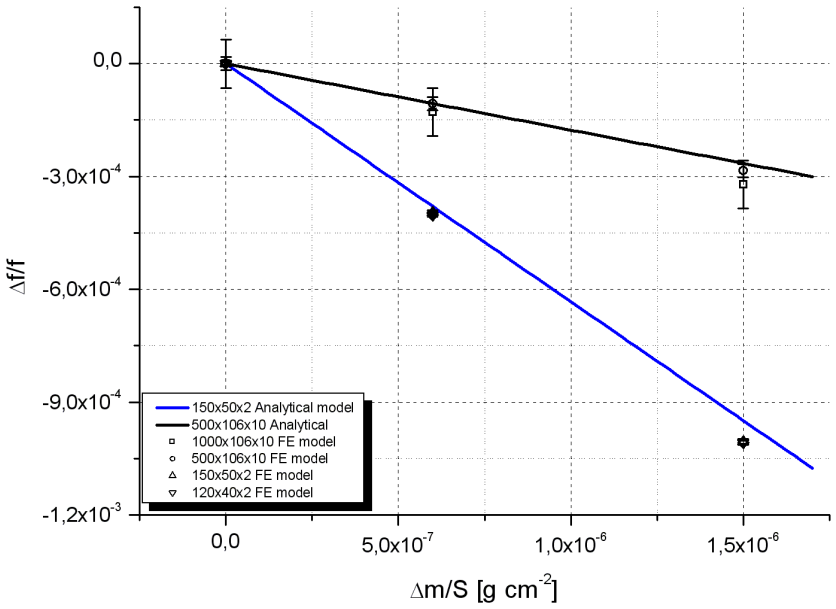

Figure 4.11: Comparison between calculated and simulated sensitivity (graph slope) for different geometries, using 200nm sensitive layer thickness. Lines refer to the analytical model model described in Chapter 3.

These results should be considered as "substrate performances" for mass increase detection and need to be integrated with the adsorbing material performances in order to evaluate the overall sensitivity of the sensor to specific analytes.

According to data in literature [Datskos 1999] for different gravimetric devices such as Surface Acoustic Wave devices (SAW) and Quartz Microbalances (QMB), the described cantilever devices provide better sensitivities and comparable mass resolution. The comparison between data in the cited reference and proposed simulation results is shown in Table 5.10. The minimum detection limit has been calculated by applying the relationship $\Delta f_{min}/f_0 = 10^{-6}$, which is reported in literature to estimate the frequency resolution [Madou 2002, Datskos 1999]. The used value (10^{-6}) can be considered as a "worst case value" with respect to the value 10^{-7} reported in the cited references.

Table 4.10: Review of mass sensitivity and resolution of cantilever devices, compared with results of different gravimetric devices in literature. (* Data from [Datskos 1999])

Gravimetric sensor	f_0 *[MHz]*	*Thickness [μm]*	S_m *[cm² g⁻¹]*	$\Delta\rho_{min}$ *[ng cm⁻²]*
Cantilevers	0.013 - 0.258	10 - 2	214 – 670	30 – 0.5
SAW*	30-300	760	151	1.2
QMB*	5	500	14	10

The real sensor efficiency must also consider the properties and the adsorption performance of the sensitive materials, expressed in terms of [g cm^{-2} / $ppm_{gas\ phase}$], which will be discussed in Section 4.6. Starting from these data, the frequency shift Δf vs. the analyte concentration in the gas sample will be also discussed.

4.3. Cantilever design

4.3.1 Design of 10μm devices

An overview of the mask set of the 10μm-thick process is reported in Table 4.15. Several different devices were implemented using this technology. The beam thickness in this process is 10μm, and design was based on results of modelling previously described. Both single beam and beam array chips were implemented. Arrays have length 500, 1000 and 1500 μm with chip dimensions 9844μm x 6924μm. Single beams with different configurations of gold surface have length 1000μm and chip dimensions 9344μm x 4646μm. Corner compensation for the cantilever tip was not included in the design to avoid the presence of stressed mask patterned that can interfere with the deposition of the sensitive layers.

Table 4.15: Layer sequence for the process.

Layer	GDSII number	Polarity	Type	Align on	Purpose
PBODY	1	dark	str.		Piezoresistor definition
NDIODE	2	dark	str.	PBODY	Substrate contacts
PDIODE	3	dark	str.	PBODY	P-Diode definition
BACK	4	dark	str.	PBODY	Etch window definition
CONHO	5	dark	str.	PDIODE	Contacts to p-diode
METAL	6	light	str.	CONHO	Metal definition
VIA	7	dark	str.	METAL	Via's to metal
MASS	8	light	str.	METAL	Proof mass definition
FRONT	9	dark	str.	METAL	Etch window definition

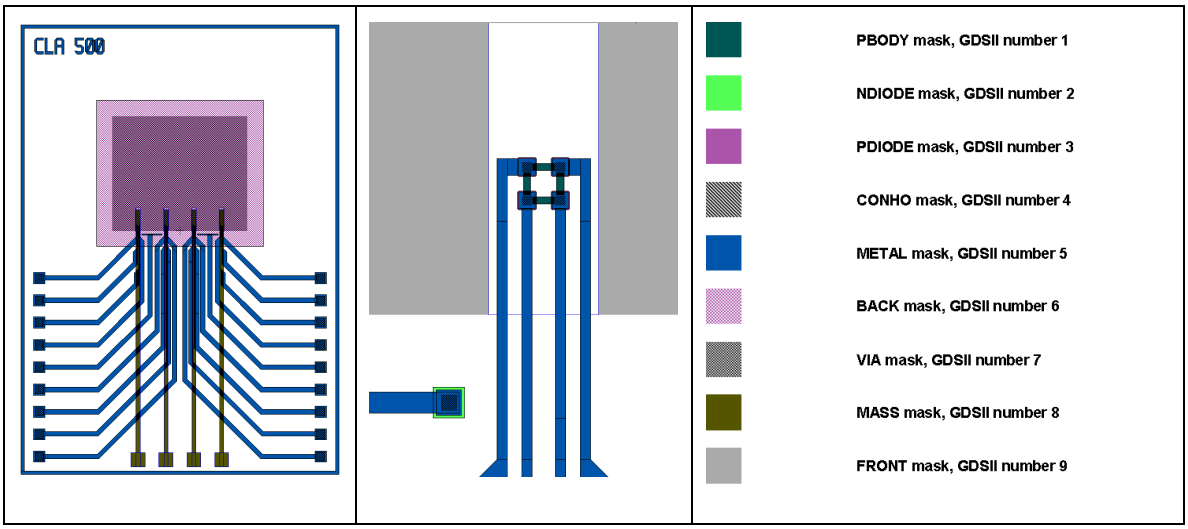

Figure 5.16. A) Cantilever array design, beam length 500μm. B) Detail of the piezoresistive bridge. Here Gold (MASS mask) is not shown.

In order to reduce the temperature dependence and achieve a higher device response, a Wheatstone bridge configuration for the piezoresistive read-out was chosen. According to the design rules, which set minimum dimensions for contacts, sensitive elements and wires, the minimum beam width is 106 µm. Piezoresistors have dimensions 7x14 µm and resistances in the order of 1kohm, depending on the implant dose. Position of the read-out on the beam has been set according to the FE modelling and optimization results.

Gold film was patterned on the beam surface to provide suitable properties for the sensitive layer deposition. In the array chips, the gold layer of each beam has a separate contact to allow electro-deposition of different sensitive materials. Some devices with interdigitated wires on the beam were implemented to couple mass detection and electrical detection. Wires have 12 µm width and 10 µm spacing. Other devices were designed with gold electrodes on half of the beam length or completely covered (Figure 4.17).

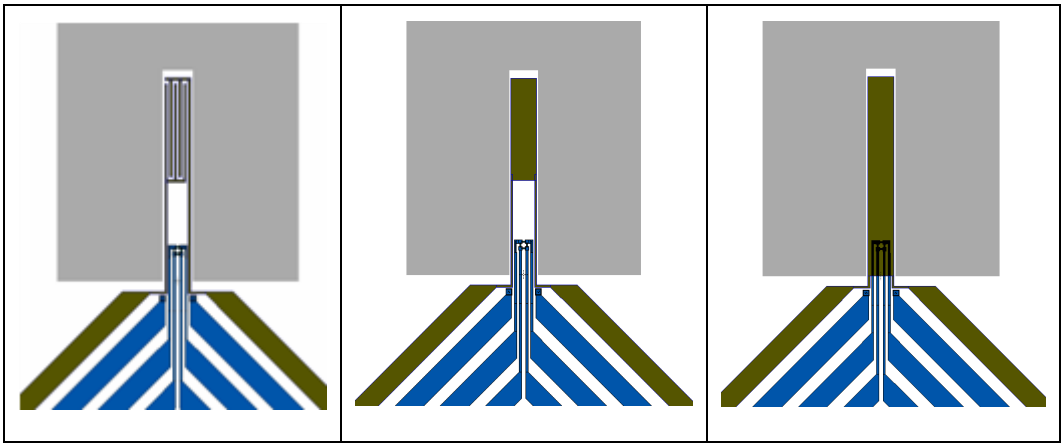

Figure 4.17. A) Single beam with interdigitated contacts. B) Single beam with tip gold electrode. C) Single beam with complete gold electrode.

4.3.2 Design of 2µm devices

The design of 2µm devices was developed for the implementation with the process described in Chapter 4, and taking into account the results of modelling. The device configuration was similar to devices of the previous process, thus using a Wheatstone bridge configuration of p-type piezoresistors located near the beam root, apart from device "150", on which small dimensions only admit the implementation of a single resistor. Position of readout was selected according to FE modelling results. Different geometries were implemented in the design, the main being devices "150", "M2" and "M3" showed in Figure 4.18. Dimensions were selected in order to test the performances of devices working at first, second and third resonance mode, with working frequencies as high as allowed by the piezoelectric actuator. A diode for temperature measurement was implemented in all devices.

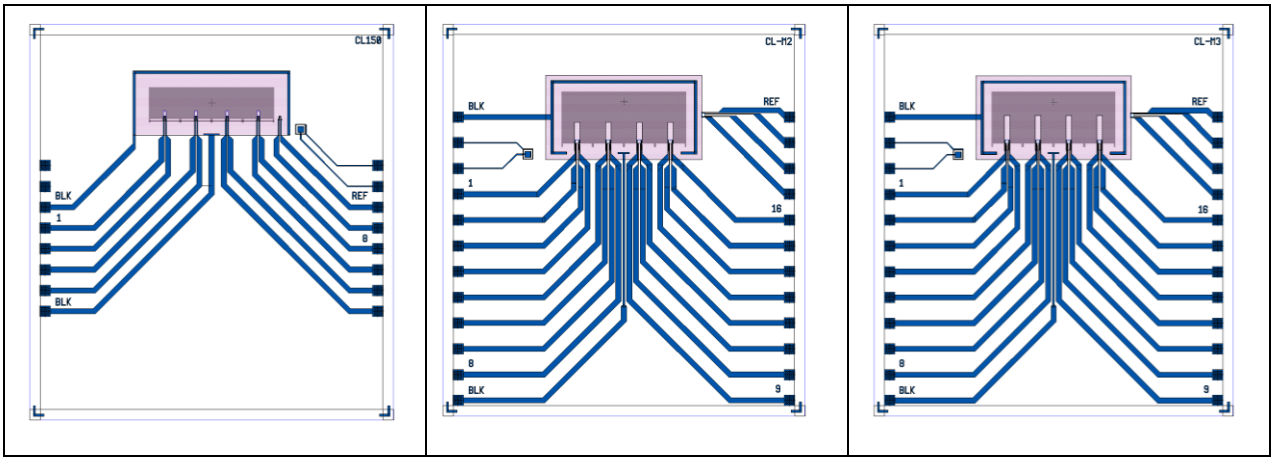

Figure 4.18. Design of 2µm devices. From left to right devices "150", "M2" and "M3".

An overview of geometries and configurations are reported in Table 4.16.

Table 4.16. Overview of geometries and configurations of devices "150" (first mode device), "M2" (second mode device) and "M3" (third mode device).

Device	***150***	***M2***	***M3***
Die dimensions [mm^2]	7000 x 7600	7000 x 7600	7000 x 7600
Front opening [mm^2]	2400 x 600	2400 x 1000	2400 x 1000
Beam geometry [mm^3]	150 x 50 x 2	383 x 106 x 2	630 x 106 x 2
Read-out	1 resistor / beam + 1 reference on bulk	1 Wheatstone bridge / beam + 1 reference on bulk	1 Wheatstone bridge / beam + 1 reference on bulk
T sensing	1 diode on bulk	1 diode on bulk	1 diode on bulk
Instances per wafer	12	5	4

4.4. Electro-mechanical characterisation of devices

Preliminary characterisation of the fabricated devices was performed in order to test the dynamic behaviour of the cantilevers, the read-out efficiency and to validate a packaging strategy for the devices.

The piezoelectric device and the chip under testing were clamped to a steel substrate by means of a silicon rubber gasket and a screw manipulator. The chip pads have been bonded to secondary pads on the substrate. A schematic of the system and the equivalent electrical circuit are shown in Figure 4.19.

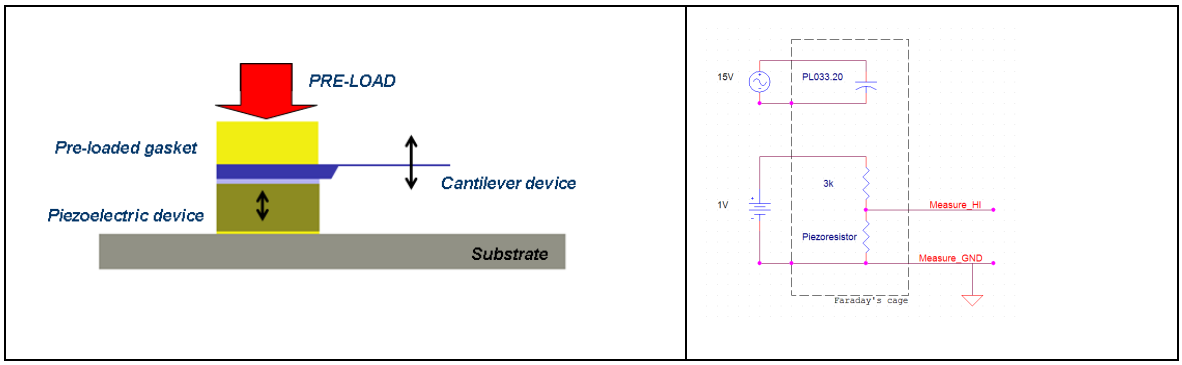

Figure 4.19. A) Schematic of the packaging strategy, B) Equivalent electrical circuit.

At first, a static characterisation was performed in order to evaluate the displacement sensitivity of the piezoresistive read-out. The resistance of each piezoresistor of the Wheatstone bridge was measured at different tip displacements, applied by means of a micromanipulator. Results are shown in Figure 4.20 and in Table 4.17.

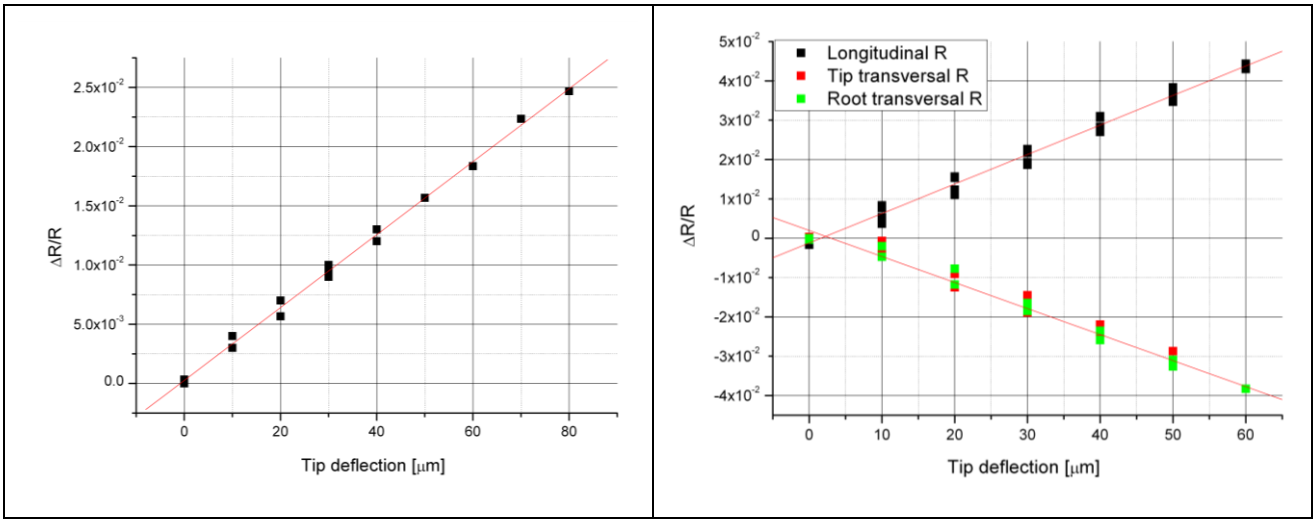

Figure 4.20. A) 1500μm-length device, relative resistance variation vs. tip displacement of longitudinal resistor. B) 1000μm-length device, relative resistance variation vs. tip displacement of longitudinal and transversal resistors.

Table 4.17. Overview of tip displacement sensitivity of fabricated devices.

	R	$\Delta R/R\ [\mu m^{-1}]$
1000μm device	Longitudinal	$7.5\ 10^{-4}$
	Transversal	$-6.6\ 10^{-4}$
1500μm device	Longitudinal	$4.5\ 10^{-4}$
	Transversal	-

The results show an opposite behaviour of longitudinal and transversal resistor, as predicted by the simulation results. This leads to an increased efficiency of the bridge read-out, which can be evaluated in a factor 2.5 improvement of the read-out response with respect to the single resistor.

After the preliminary characterisation of the read-out sensitivity, the dynamic behaviour was investigated. The piezoactuator was polarised with a sinusoidal potential (5 to 20V peak-to-peak amplitude, frequency in the 1÷300kHz range) provided by a function generator. The piezoactuator impedance showed a phase shift in the 180-200kHz frequency range, due to the expected upper frequency limit of the device with this system configuration.

The optical inspection of the chip during the frequency shift clearly highlighted the cantilever resonance, as a different light reflection on the moving beam (pls. see dark zones on beams in Figure 4.21).

A) 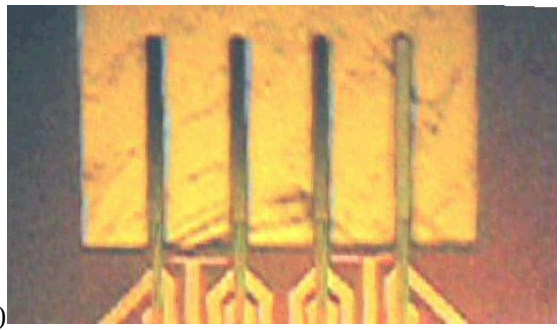 B) 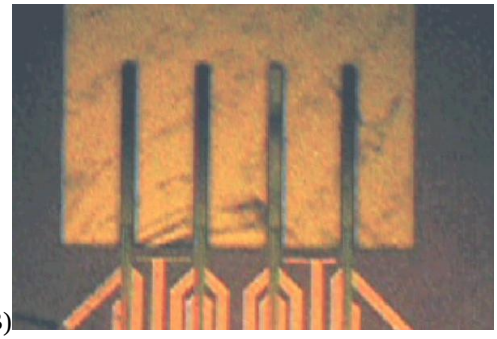

Figure 4.21. A) 1500μm length device, first mode resonance (4th beam from left). B) 1500μm length device, third mode resonance (3rd beam from left).

Then dynamic behaviour was tested by using the integrated read-out, by measuring the Wheatstone bridge potential with an oscilloscope. Results are summarised in Figure 4.22, where the amplitude of peaks in the frequency domain are plotted vs. the actuation frequency.

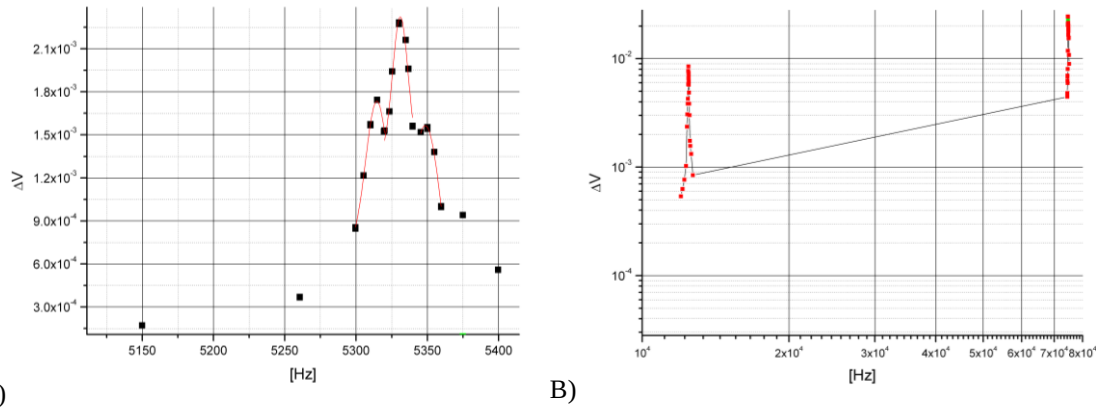

A) B)

Figure 4.22. A) ΔV vs. actuation frequency characteristic of 1500μm length device, showing first mode resonance peak. B) ΔV vs. actuation frequency characteristic of 1000μm length device, showing first and second resonance mode peaks.

In Table 4.18 simulation results are compared to the experimental results. The simulation results have been obtained for devices without the gold layer (as the real devices were) and considering some fabrication parameters (0 ÷ 30 µm underetch and 8 ÷ 10 µm thickness). The experimental result error is related to a scattering of the resonance frequencies of the different beams on the chip, probably due to slightly different thicknesses across the array. In general the results fit with the expected values.

	f [kHz]	***1st mode***	***2nd mode***	***3rd mode***
1000μm device	Simulated	11.1 ÷ 14.2	67.1 ÷ 87.2	186.9 ÷ 243.7
	Experimental	12.2 ± 0.2	73.9 ± 0.7	-
1500μm device	Simulated	4.8 ÷ 6.4	30.1 ÷ 38.9	84.2 ÷ 108.44
	Experimental	5.2 ± 0.5	-	90 ± 5

Table 4.18. Overview of simulated and experimental resonance frequencies.

Preliminary tests for the investigation of the actuation and read-out performances were also performed on 2µm non functionalised devices and compared to the results of FE modelling, in order to validate obtained results. According to chip dimensions and required pin number, the package configuration has been implemented with a ceramic Dual In Line (DIL) package with 40 pins (NTK, IDK40F1-642ZAL), by using a PZT ceramic piezoelectric actuator (PL033 made by PI, C=80nF, displacement = 2.2µm @ 100V) placed at the bottom of the chip. Actuation is provided by function generator (Tektronix AFG 3102), allowing to provide the piezoactuator with a sinusoidal signal. Read-out amplitude has been measured with an oscilloscope (LeCroy 9354L) on a half Weathstone bridge with 5V bias potential. Result summary for one of the new realised devices (CL-M3, dimensions 610 x 106 x 2 μm^3) is reported in Figure 4.23.

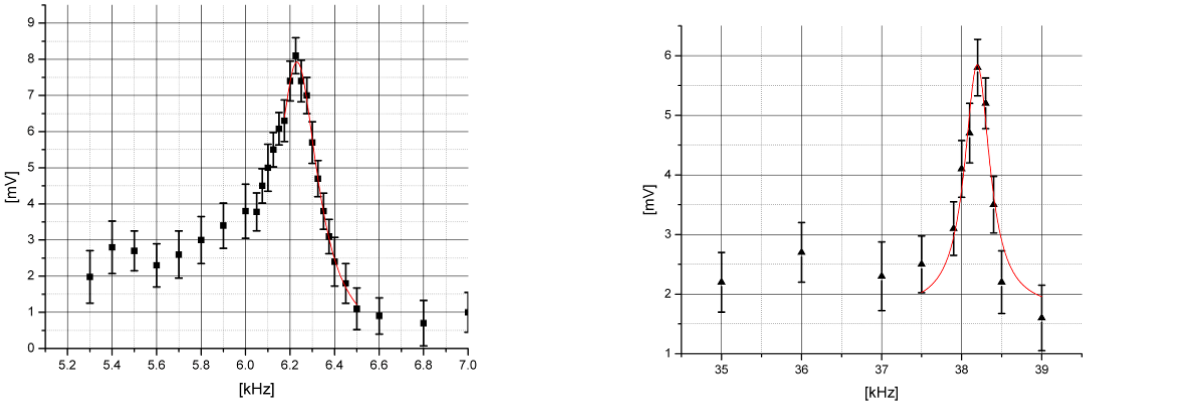

A) B)

Figure 4.23: Electromechanical characterisation of a CL-M3 device, output response vs. actuation frequency for first and second resonance modes.

The first and second mode resonance frequencies have been measured (first mode: 6.2 kHz, second mode: 38.2 kHz) and compared to the FE simulation results, by taking into account the scattering of process parameters, such as the underetch of the realised mechanical structure and residual stress. FE results (7.1 kHz, 42.4 kHz, 118.8 kHz for first, second and third mode) are compatible with experimental results. Differences between experimental data and modelling can be due to damping effects and deviations of elastic moduli of the deposited thin films from estimated values. By using an analytical model, the frequency shift due to the damping, which has not been included in the FE model, has been evaluated to be in the 100 Hz order of magnitude. Furthermore, the experimental resonance quality factor in air at 1bar pressure, which is 20 for the first mode and 119 for the second mode, is also in the calculated range.

Table 4.19. Comparison of experimental resonance properties and calculated sensitivities and resolution of devices fabricated with the two technologies.

Geometry (L, W, t) [μm]	***f [kHz]***	***S_m [$cm^2\ g^{-1}$]***	***$\Delta\rho_{min}$ [$g\ cm^{-2}\ Hz^{-1}$]***	***Q ($Q=1/(\Delta\omega\ t_0)$)***
1000 x 106 x 10	f_0: 12.4 f_1: 74.7	-214 -214	$3.0\ 10^{-7}$ $6\ 10^{-8}$	147 152
500 x 106 x 10	f_0: 56.16	-190	$9.4\ 10^{-8}$	286
150 x 50 x 2	f_0: 141.4	-936	$8.8\ 10^{-9}$	-
630 x 106 x 2	f_0: 6.6 f_1: 40.9 f_2: 115	-890 -933 -933	$1.7\ 10^{-7}$ $2.5\ 10^{-8}$ $9.1\ 10^{-9}$	22 82 96

As shown in Table 4.19, the thinner devices show an increase of sensitivity and a decrease of the quality factor, as expected for lighter structures at room pressure. Interestingly, working at higher resonance mode allows an increase of quality factor of a factor 4 or better, as expected from results in the literature,

thus leading to performances comparable to thicker devices. Of course a higher Q allows a better frequency resolution and finally a better detection limit.

The characterisation of frequency response of functionalised devices has also been performed, in order to compare the resonance performances of devices with and without sensitive layers. Results are reported in Figure 4.24 for CL-M3 devices.

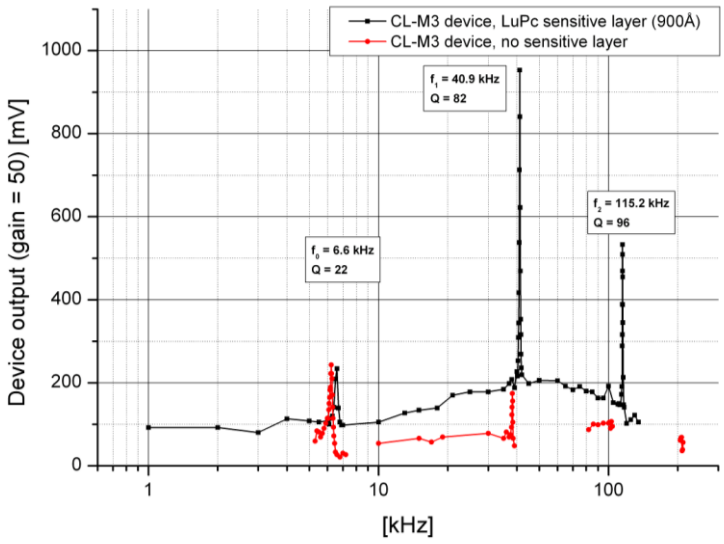

Figure 4.24: Electromechanical characterisation of a functionalised CL-M3 device (device number 11), output response (1.5V bridge bias, gain 50) vs. actuation frequency, compared with a non-functionalised device.

4.5. Device sensitivity

The selection and deposition of sensitive material on cantilevers were performed by the University of Valladolid in the framework of the GOODFOOD Project. Here, a summary of deposition techniques and materials is reported for completeness. Phthalocyanines were the materials of choice, because they are able to interact with a variety of volatiles and they are well known sensitive materials for resistive gas sensors. A range of phthalocyanines, including monophthalocyanine (MPc) derivatives and sandwich type bisphthalocyanines ($LnPc_2$), were deposited by ultrahigh vacuum evaporation and casting and used in the experimental activities. Figure 4.25 shows the SEM image of a monophthalocyanine film (ZnPc), deposited onto the silicon cantilevers. The evaporated films of Phthalocyanine molecules obtained are made up of micro-crystallites with sizes depending on deposition parameters.

In order to investigate the specifications required for cantilever sensor design, preliminary test on sensitive materials performances were performed by means of quartz microbalance (QMB)-based characterisation setup. The method of the piezogravimetry sorption based on quartz piezoresonators can be considered as an effective method to evaluate the mass adsorption properties of sensitive layers. A set of different materials were tested with ammonia, dimethyl-amine (DMA) and trimethyl-amine (TMA), as a

set of analytes for the tests. Water vapours response has also been considered. All the measurements have been performed in collaboration with the BioMEMS group at the N.S. Kournakov Institute of Common and Inorganic Chemistry RAS in Moscow (Russia), in collaboration with the group of the Prof. Vladimir G. Sevastyanov. The sensors prepared for this work are listed in Table 4.20.

Table 4.20: List of QMB devices for preliminary tests.

	Material	Deposition technique	Layer structure
LU6	LuPc2	Casting	disordered
Lu+C	LuPc2 + Multi-Wall Carbon NanoTubes	Casting	disordered
C	Multi-Wall Carbon NanoTubes	Casting	disordered
Zn4	ZnPc	UHV	microcrystalline
Zn8	ZnPc	UHV	microcrystalline
Zn4M	ZnPc	UHV	microcrystalline

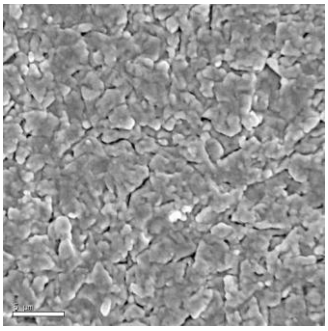

Figure 4.25: SEM image of a PcZn deposited by UHV Evaporation onto the Ag electrode of a QMC

Piezoresonators were standard crystal of AT-cut with silver electrodes using a working frequency of 8-15 MHz. The tests of functionalised QMB sensors were carried out using express method with impulse input of gas sample into micro-chamber (volume 14 ml) without the application of sample accumulation. To get results close to real conditions of sensor operation, the measurements were carried out in the flow of humid laboratory air. Vapour analytes at known concentration were injected in a stream of the gas-carrier and passed through the cell with the gauge with a sample volume of 1-20 ml. Required concentrations of the analyte were prepared by a method of multiple dilution of saturated vapour by an injection of air in syringes of various capacities. Samples of gases also contained a certain amount of water vapour, thus the sensitivity of QMB sensors to water was also evaluated, and a compensation of the water response was applied during the data treatment. The sensor response was evaluated by monitoring the resonance frequency shift of the quartz piezoresonator covered by the adsorbent layers. The frequency changes were measured with a frequencymeter Y3- with ±1Hz resolution.

Water vapour contents of different injected solution were evaluated by considering the environmental laboratory conditions listed in Table 4.21.

Table 4.21: Room conditions for measurements

Temperature [°C]	25
Laboratory air relative humidity	~ 0.5
Laboratory CO2 content [ppm]	300
Pressure [kPa]	107.5

Water partial vapour pressure at room conditions can be evaluated by:

$$\log_{10}(P[bar]) = 5.40221 - \frac{1838.675}{T[K] - 31.737} \qquad 4.6$$

Then the saturated vapour has a moisture content about 32000 ppm. This allows evaluating room and injected samples water concentrations (Table 4.22).

Table 4.22: Analytes properties.

Property	***Ammonia***	***Dimethylamine (DMA)***	***Trimethylamine (TMA).***	***Water***	***Air***	***Dry air***
Molecular weight	17	45	59	18	-	-
Boiling point[°C]	-33	7	3	100	-	-
Melting point [°C]	-78	-92	-120	0	-	-
CO2 [ppm]	-	-	-	-	300	300
H2O [ppm]	-	-	-	-	15000 ÷ 16000	0

Water solutions of ammonia, DMA and TMA were used as sources for injected samples. Solutions are summarized in Table 4.23. Species concentrations in the vapour in equilibrium with solutions were evaluated, by assuming moisture content constant for pure water and amine solutions. Concentrations for ammonia solution are quite accurate, while concentrations for DMA and TMA solutions should be considered as a rough estimation due to non-ideal properties of these solutions and require further analyses.

Table 4.23: Analyte concentrations in solution and vapour phase.

	Solution in water [w%]	***Vapour concentration [ppm]***	***H_2O vapour concentration [ppm]***
NH_3	10.8	100000	32000
DMA	31.4	250000	32000
TMA	23.6	200000	32000
H2O	-	-	32000

Response to the real target analytes was evaluated in the 0-100 ppm range by considering an adsorbed analyte dependence on partial pressure in gas phase p:

$$a = k\frac{b \cdot p}{1 + b \cdot p} \qquad 4.7$$

where b and k are coefficients.

In order to evaluate the detection resolution of cantilever sensors using the described sensitive layers, the adsorption properties of materials at different analyte concentrations must be extracted from QMB tests.

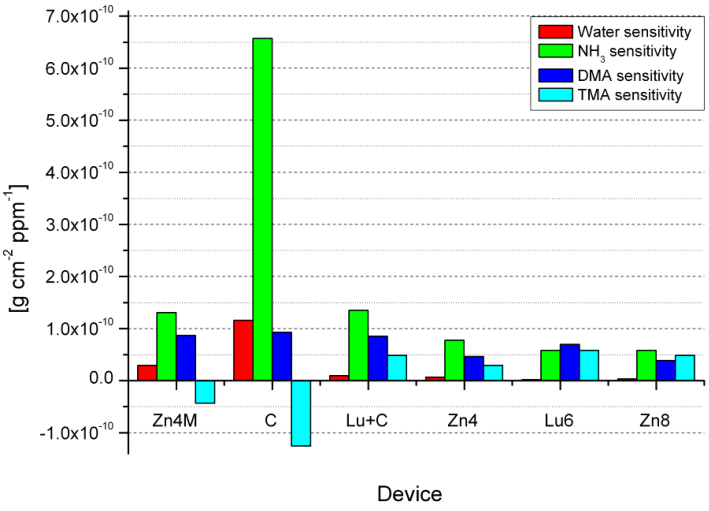

Figure 4.26: Adsorption performaces of different materials in the analyte concentration range 1 ÷ 100 ppm for ammonia, DMA and TMA and in the 15200 ÷ 15800 ppm range for water.

The mass adsorption is proportional to the frequency shift of the QMB and can be evaluated by using the expression:

$$\Delta f[Hz] = -2.3 \cdot 10^{6} \cdot f_0^2[MHz] \frac{\Delta m}{S}[g \cdot cm^{-2}] \qquad 4.8$$

Then the material adsorption expressed as adsorbed mass for unit of surface at a given analyte concentration in vapour phase can be easily calculated by using the eq. (4.8). Results are shown in Table 4.24 and in Figure 4.26.

Table 4.24: Analyte adsorption [g cm^{-2} ppm^{-1}] for the different sensitive materials.

Material	***Water sensitivity***	***NH_3 sensitivity***	***DMA sensitivity***	***TMA sensitivity***
1	2.90 10^{-11}	1.30 10^{-10}	8.70 10^{-11}	-4.35 10^{-11}
2	2.90 10^{-11}	7.73 10^{-11}	-7.73 10^{-12}	-1.93 10^{-11}
3	1.16 10^{-10}	6.57 10^{-10}	9.28 10^{-11}	-1.26 10^{-10}
4	9.66 10^{-12}	1.35 10^{-10}	8.50 10^{-11}	4.83 10^{-11}
5	6.44 10^{-12}	7.73 10^{-11}	4.64 10^{-11}	2.90 10^{-11}
6	3.22 10^{-12}	5.80 10^{-11}	6.96 10^{-11}	5.80 10^{-11}
7	3.22 10^{-12}	5.80 10^{-11}	3.86 10^{-11}	4.83 10^{-11}
8	2.17 10^{-11}	9.66 10^{-12}	5.22 10^{-11}	2.17 10^{-11}
9	2.90 10^{-11}	1.30 10^{-10}	8.70 10^{-11}	-4.35 10^{-11}

Furthermore, a normalisation of adsorption on layer mass was performed. Results are shown in Figure 4.27 for the different materials. The best performances have been achieved by Lu6 layer, because of its low thickness compared to the other films.

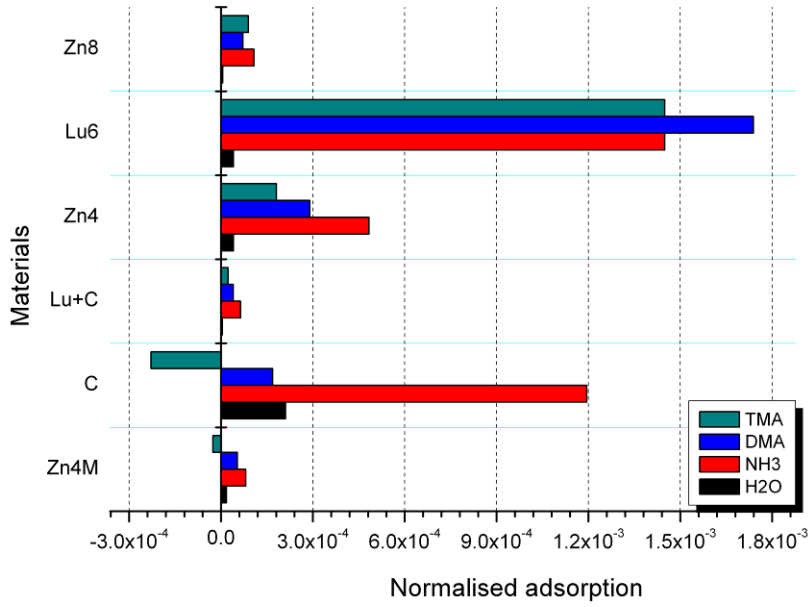

Figure 4.27: Normalised adsorption for the materials: adsorbed mass per square centimetre per gram of sensitive layer at 1ppm analyte concentration in gas phase.

4.5.1 Estimation of cantilever performances

By using the non-normalised adsorption properties, cantilever device sensitivities (Sc) with respect to analyte concentration in the gas sample (c) can be estimated by using the mass sensitivity S_m for the beams, calculated in the modelling section, and the sensitive layer adsorption A [g cm^{-2} ppm^{-1}].

$$S_c = \frac{1}{f_0}\frac{df_0}{dc} = \frac{1}{f_0}\frac{df_0}{dm}\cdot\frac{dm}{dc} = S_m \cdot A \qquad \text{[ppm-1]} \qquad 4.9$$

Then the cantilever frequency shift for a given concentration change in the vapour phase is:

$$\frac{\Delta f}{\Delta c} = S_c \cdot f_0 \qquad \text{[Hz ppm-1]} \qquad 4.10$$

This parameter was evaluated for two different geometries, the first being beams with 500µm length, 106µm width, 10µm thickness and the second 150µm length, 50µm width, 2µm thickness. Results are plotted for the different material in Figure 4.28.

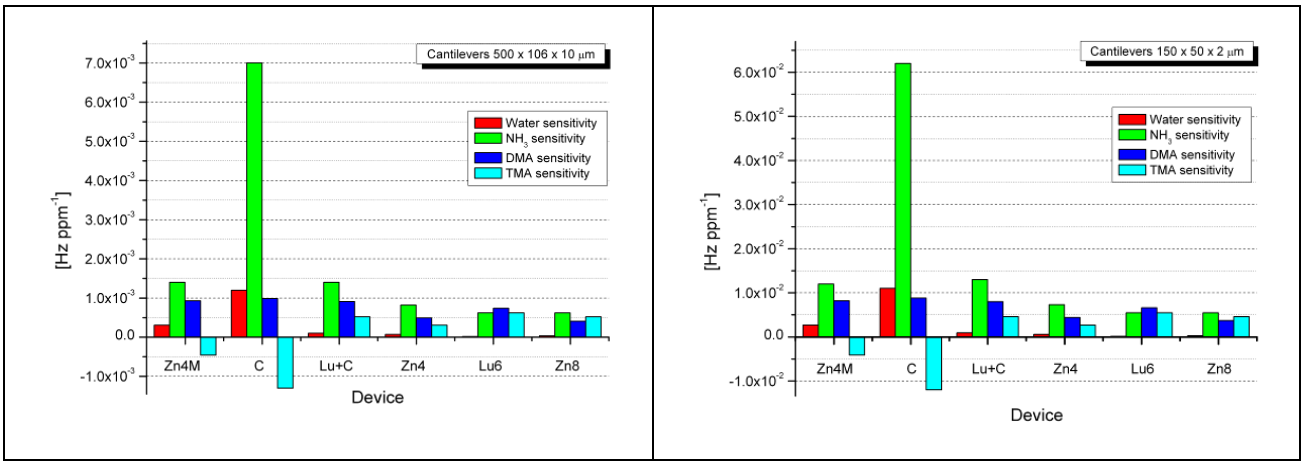

Figure 4.28: Estimation of beam properties on the basis of material testing results. Calculated frequency shift for 1ppm analyte concentration.

Results of sensor resolution also depend on frequency resolution, which could be preliminary estimated in the (0.01 ÷ 0.1 Hz) range for devices resonating at 100 ÷ 200 kHz.

4.5.2 Sensitivity tests

In order to test the module sensitivity to amines, preliminary measurements of the response to Ammonia were performed at different concentrations in steady flow, using the previously described device. Starting from NH_3 solution in water at different concentrations, the corresponding vapour pressure can be found in literature (Table 4.25).

Table 4.25 Calculation of NH_3 concentrations in the gas phase.

$[NH_3]_l$ [w%]	$[NH_3]_g$ [ppm]
0	0
1.25	10171
2.50	20861

The device has been mounted in a chamber of small volume. Dry nitrogen has been used as carrier gas with 20sccm flow. Several steps of analyte and carrier gas have been fluxed in the chamber (30 min analyte flow and 30 min carrier flow for sensor recovery).

Device actuation and readout were performed by using an interface board ad hoc developed by the SOI Research Unit of FBK. Summarising its main properties, the system is composed by an analog part, which realise the cantilever interface, and a digital part which allows measuring the resonant frequency of the cantilever. In the analog section, a fixed 1.5 V potential is applied to the piezoelectric Wheatstone bridge realised on the sensing device. The unbalanced signal, which corresponds to

the oscillation movement of the cantilever, is amplified with a low noise instrumentation operational amplifier and squared before the connection to the PLL. The PLL is opportunely dimensioned in order to guarantee the lock condition in the frequency range correspondent to the resonant frequency variation of the used device. The output digital signal of the PLL is employed as input signal for the piezo microactuator driver, which output is connected to the piezoactuator. The introduction of a piezo microactuator driver into the control circuit to drive is needed in order to cope with the high capacitance of the piezoactuator (80 nF). With this configuration, the closed-loop control circuit maintains the cantilever oscillation at the resonant frequency. The readout circuit is interfaced to a PC through an FPGA, driven by a Front Panel developed in the LabVIEW ambient. The FPGA is not included into the feedback loop, in order to guarantee a faster response of the readout circuit to frequency variations. The digital output signal of the readout circuit is obtained by buffering the output signal of the PLL. The signal is sent to the FPGA in order to measure the frequency by means of a counting system and store the data. The operating mode is set by a LabVIEW Front Panel, which allow monitoring the measurement results and storing the measured data on a PC in text format. The $(2\ \Delta f)/(f_0)$ ratio of the system, which account for the frequency detection resolution of the system, varies from 118 10^{-6} to 1.2 10^{-6} at the different sample rates.

The results of sensitivity tests to NH_3 are shown in Figure 4.29. The 0 w% step has been used for the compensation of the water content in the delivered gas samples.

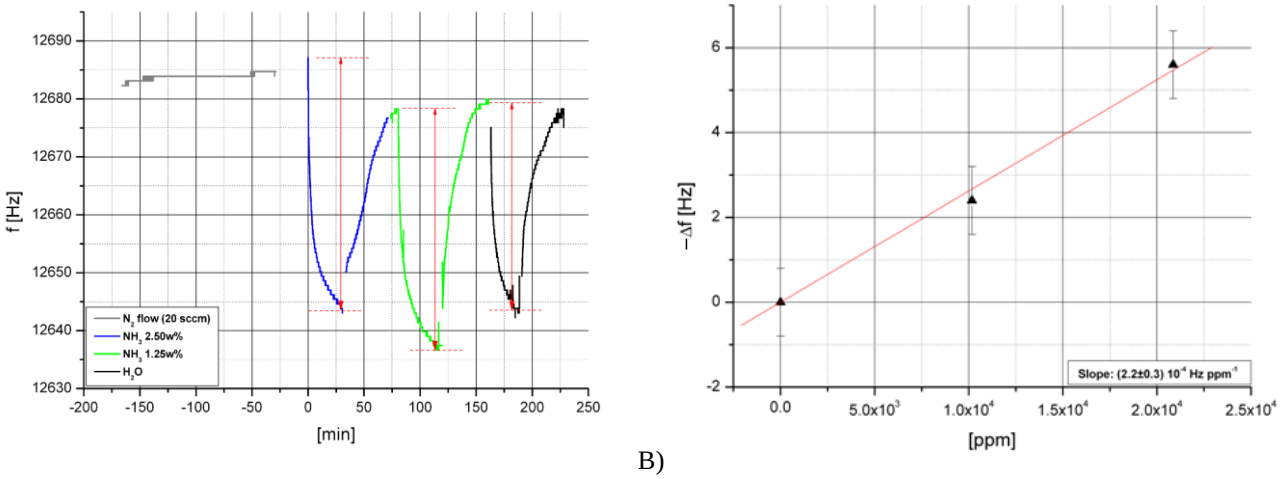

A) B)

Figure 4.29: A) Dynamical responses to different NH_3 concentrations. B) Frequency shift after the compensation of water content.

Experimental sensitivity results have been compared with the estimations previously reported. The comparison is reported in Table 4.26.

Table 4.26. Comparison of measured sensitivity and estimated sensitivity.

Device: CL1000, LuPc	***Experimental***	***Estimated***
NH_3 sensitivity [Hz/ppm]	2.2 (±0.3) 10^{-4}	(1.4 ÷ 1.9) 10^{-4}

The preliminary obtained results validate the modelling performed in order to evaluate the device performances. With these devices and also taking into account the frequency resolution of the electronic board (0.008 Hz), the expected detection limit is 45 ppm. By extending results to fabricated devices with 2μm thickness, a significant increase of the performances is expected, with a resolution in the ppm range.

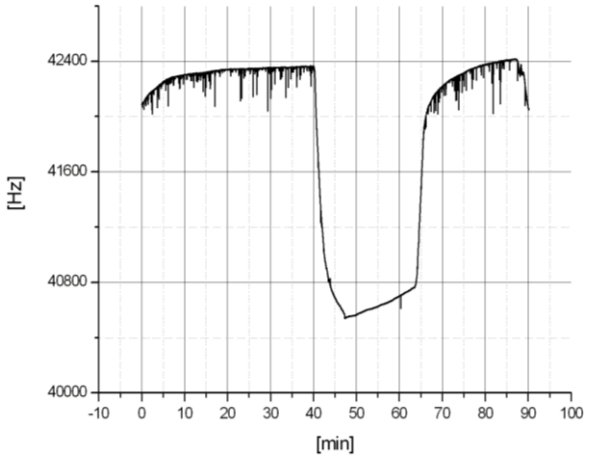

Figure 4.30: Response to water vapour of CL-M3 operated at the second resonance mode.

The obtained results of CL-M3 devices operated at the second resonance mode indicate a sensitivity improvement of about one order of magnitude with respect to preliminary devices, leading to a detection limit in the ppm range. Sensitivity performances of the devices are still under testing.

4.6. Discussion

The development of cantilever-based sensors was presented, in order to design the device with optimum performances in terms of mass sensitivity and resolution of the substrates. In particular, devices were implemented with two different technological processes, allowing the realisation of beams with respectively 10 and 2 μm thickness. In the first case sensitivity has been evaluated in about -190 [$cm^2\ g^{-1}$] and resolution about 9.4 10^{-8} [$g\ cm^{-2}\ Hz^{-1}$], while the thinner beams provide better performances, in the order of -669 [$cm^2\ g^{-1}$] for sensitivity and 1.1 10^{-8} [$g\ cm^{-2}\ Hz^{-1}$] for resolution. Here resolution is expressed in terms of mass resolution per Hz of resolution of the resonance frequency measurement. According to data in literature for different gravimetric devices such as Surface Acoustic Wave devices (SAW) and Quartz Microbalances (QMB), the described cantilever devices provide better sensitivities and comparable mass

resolution. The resolution and sensitivity of cantilever sensors for ammines were estimated by using the adsorption properties of the phthalocyanines layers. The calculated resolution for devices realised by the first process (thicker structure) is in the order of 10-100 ppm for NH_3, DMA e TMA, by using the properties of sensitive materials without thickness normalisation. Preliminary experimental characterisation validate the modelling results. For devices designed for the second process instead, the estimated resolution is in the order of 1-10 ppm.

Chapter 5

5. Development of microcantilever detectors for stress sensing

In this Chapter, the development of piezoresistive microcantilever arrays for stress sensing is presented, especially focused to the realisation of DNA sensors for biomedical applications. In particular, the presented activities deal with the modelling of sensors in order to select the most suitable geometries and technologies for optimised performances. Starting from the literature, analytical models of DNA sensors were implemented for different technological option and results were further refined with FE analysis in order to investigate the best configuration and to achieve the optimal performances. Then, the design of test structures for process optimisation was implemented, as well as the design of final cantilevers arrays.

According to the mechanical properties of beams, bending and deflection methods differ in design, technologies and approaches for the optimization of the performances. Usually stiff and light structures are preferred in resonance mode, while compliant structures are better suited for the deflection mode. In fact, high stiffness provide high quality factor of resonance, i.e. a higher resolution in frequency measurement, and a lower deflection for stress-based applications. The ratio between adsorbed mass and beam density is proportional to sensitivity in resonance mode, while is indifferent in deflection mode. This aspect must be taken into account when selecting the materials and technologies to realize a cantilever structure. Different implementation using sensing elements made of different materials and different structural materials were evaluated. Different aspects were considered; starting from material properties, technology suitability, achievable sensitivity, stress distribution and the possibility to integrate the detector module in portable systems.

5.1. Analytical modelling and technology comparison

On the basis of the physical description of the detector previously reported, an analytical model of the detector was implemented, in order to evaluate the performances of the detector for different fabrication technologies and design. Three main technological approaches were investigated: monocrystalline Si beams with implanted piezoresistors, thin film cantilever with poly-Si piezoresistors and polymeric beams with gold strain gauges. Different integration strategies can be implemented by using different materials; implanted resistors on single-crystal silicon and polysilicon elements are fully compatible and easily implemented in CMOS processes, while gold strain gauges are suitable for the integration of sensing elements on polymeric devices [Thaysen 2002], allowing low realisation costs and beam stiffness. Furthermore, polymeric materials theoretically allow a reduction of beam stiffness, and thus an increase of sensitivity, because of their low elastic modulus. For deflection mode, recently polymeric beam (thus with Young's modulus orders of magnitude lower then silicon-based materials such as crystalline Si, silicon

oxide and nitride) have been realized [Calleja 2005], featuring gold strain-gauges elements for deflection detection [Johansson 2005, Thaysen 2002]. Nevertheless, due to the low sensitivity of strain gauges, with respect to piezoresistive read-outs, the overall advantage of using polymeric beams with low material stiffness must be investigated, as well as the device stability in operative conditions. Furthermore, the integration of polymer-based technologies with standard technologies and CMOS readout is less easily implemented with respect to other approaches.

The model included material properties and geometry of the real section of different fabrication processes for the evaluation of the section properties, as well as the resonance evaluation and thermo-mechanical and electrical noise evaluation, in order to evaluate the response and signal-to-noise ratio related to DNA hybridisation. In particular, the differential response to hybridisation of strands with a single nucleotide mismatch was evaluated. In order to set a simple model of the beam-DNA interaction, the mechanical model was adapted to the devices used in [Fritz 2000], in order to evaluate the differential momentum arising from DNA hybridisation for the DNA concentration and probe length in the reference (Pls. see Table 5.1).

Table 5.1. Summary of condition of experimental results in [Fritz] and extracted differential momentum arising from DNA hybridisation

Paper: Fritz, Science 2000	
Beam material	Silicon
Beam geometry (L, W, t) [μm^3]	500 x 100 x 1
Beam spring constant [N m^{-1}]	0.02
DNA concentration and probe length	400nM in HB; 12-mer
Response (tip deflection [nm])	around 60
Differential response to single mismatch in a 12-mer strand (tip deflection [nm])	10
Model	
Calculated spring constant [N m^{-1}]	0.02
Differential deflection [nM]	10
Calculated (σ_F t_F) term [Pa m]	2 10^{-3}

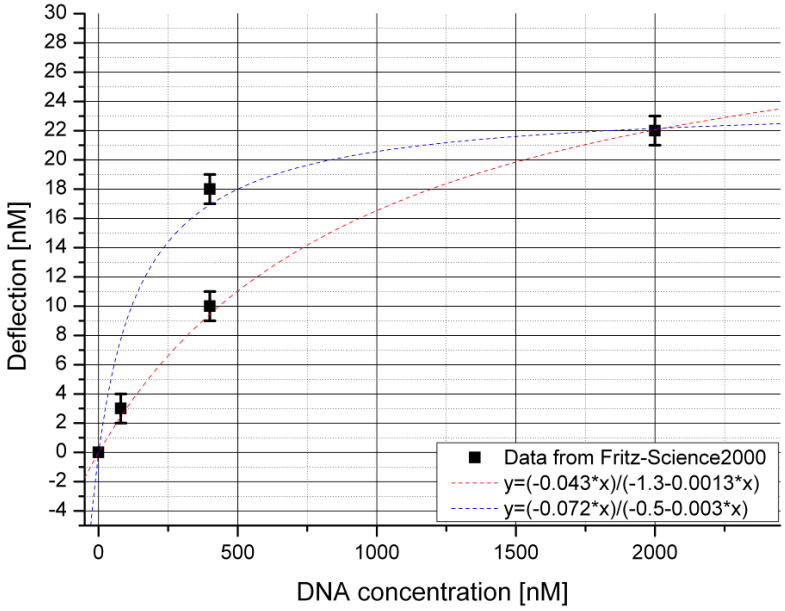

Figure 5.1. Variation of cantilever differential deflection in response to 12-mer probe hybridisation with single nucleotide mismatch at different DNA concentration, with a fitting function in red. Data extracted from [Fritz 2000]

Table 5.2. Summary of condition of experimental results in [Mukhopadhyay 2005], based on Cantion™ devices, and comparison with model results

data from [Mukhopadhyay 2005]	
Beam materials and thicknesses	Silicon nitride + poly-Si resistors (total 450nm) Gold 30nm
Beam geometry (L, W, t) [μm^3]	120 x 50 x 0.480
Beam spring constant [N m^{-1}]	0.139
Resonance frequency [kHz]	43
Bias of the bridge read-out configuration [V]	2.5
DNA concentration and probe length	1000nM in HB; 12-mer, 29-mer (12-mer probe + 17-mer non-matching extension)
Response (electrical readout [µV])	12.5 (12-mer), 28 (29-mer)
Model: 350nm Si_3N_4, 50 nm poly-Si, 50nm Si_3N_4, 30 nm Au	
Calculated spring constant [N m^{-1}]	0.150
Calculated resonance frequency [kHz]	42
Calculated half bridge response and resistivity variation	ΔV = 12.5 [µV] ($\Delta R/R$=10 [ppm]) (12-mer probe)

Since sensor response is dependent on DNA concentration [Fritz 2000], an evaluation of the response at different concentration can be estimated on the basis of the data in Figure 5.1. For instance, an increase of DNA concentration from 400nm to 1µM corresponds to an increase by a factor 1.2÷1.6 of the beam deflection, which is in turn proportional to the $\sigma_F\ t_F$ term. Thus, DNA-induced stress at 1µM concentration has been calculated as:

(DNA-induced stress @ 1µM) = (data from [Fritz] @ 400nM) * 1.6 5.1

A preliminary cross validation of the model was obtained by evaluating the response of beams in [Mukhopadhyay 2005] with the DNA-induced stress extracted from [Fritz] and compared with the real experimental data in the reference. By implementing a structure with patterned piezoresistor and also including a passivation in Si_3N_4, response is about 12.5µV for p-type poly-Si (pls. see Table 4 for structure details). Due to the spread of material properties, the limited description of the device implementation in [Mukhopadhyay 2005] and the strength of DNA interaction with the surface (e.g. depending on buffer solution, probe and target length, etc.), the fitting can be considered enough accurate, at least for evaluating and comparing different technologies.

After the preliminary validation of the model, different technologies were evaluated by adjusting the model in terms of section geometry, material properties and sensitivity of piezoresistors. A review of cross-sections is reported in Figure 5.2. Responses to 400nM concentration are reported, on the basis of the typical DNA hybridisation interaction previously calculated.

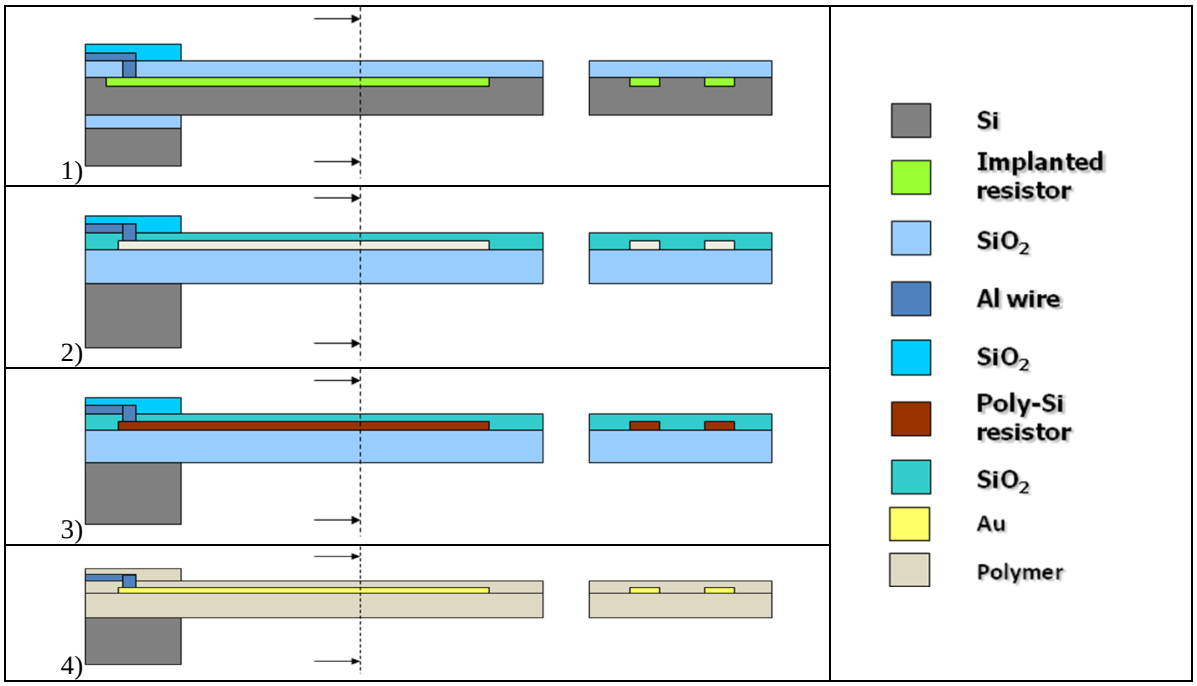

Figure 5.2. Schematic sections for the three different fabrication processes evaluated with the analytical model

5.1.1.1. Approach 1: SOI-based approach:

This approach is based on SOI (*Silicon-On-Insulator*) wafers (device layer 340nm) for the realization of thin mono-crystalline Si beams. The structure is defined by dry and wet bulk micromachining techniques, while the piezoresistors are directly implanted on the Si beam. n-type and p-type resistors have been evaluated, with a typical junction depth of 100nm, which is a reasonable trade-off between suitable process parameters and resistor geometries. In the first approach, a 200nm SiO_2 passivation layer is considered. In a more "extreme" implementation, a multilayered passivation layer in SiO_2 / Si_3N_4 is considered over the resistors (implant depth 80nm), with typical thickness (30 + 30) nm. In this case, a higher efficiency of the read-out can be obtained. In the tables below, a summary of main results is reported for n-type Silicon, while p-type is not performing well in planar stress conditions, as already described in the material section.

Table 5.3. Main properties and modeling results of SOI-based cantilevers with n-type resistors (Type 1)

Beam materials and thicknesses	Silicon 340nm+ implanted n-type resistors (100nm) +200nm oxide + Gold 30nm
Beam geometry (L, W, t) [μm^3]	200 x 200 x 0.540
Beam spring constant [N m^{-1}]	0.140
Resonance frequency [kHz]	15.0
Bias of the bridge read-out configuration [V]	3.3
DNA concentration and probe length	400nM in HB; 12-mer (from [Fritz 2000])
Calculated half bridge response and resistivity variation	ΔV = 9.6 [μV] ($\Delta R/R$=5.8 [ppm])
SNR	15.6

Table 5.4. Main properties and modeling results of SOI-based cantilevers with n-type resistors (Type "extreme")

Beam materials and thicknesses	Silicon 340nm+ implanted n-type resistors (80nm) +60nm oxide + 30nm nitride + Gold 20nm
Beam geometry (L, W, t) [μm^3]	200 x 200 x 0.540
Beam spring constant [N m^{-1}]	0.09
Resonance frequency [kHz]	13
Bias of the bridge read-out configuration [V]	3.3
DNA concentration and probe length	400nM in HB; 12-mer (from [Fritz 2000])
Calculated half bridge response and resistivity variation	ΔV = 12 [μV] ($\Delta R/R$=7.5 [ppm])
SNR	18

A further structure, based on SOI beams with poly-Si resistors and 2 passivation (oxide between substrate and resistors, nitride over resistors, has been considered. The double passivation layer and the reduced poly-Si sensitivity make this approach performing worse than implanted resistors.

Table 5.5. Main properties and modeling results of SOI-based cantilever with poly-Si resistors

Beam materials and thicknesses	Silicon 340nm+ 100nm oxide + p-type poly-Si resistors (80nm) +100nm nitride + Gold 20nm
Beam geometry (L, W, t) [μm^3]	200 x 200 x 0.540
Beam spring constant [N m^{-1}]	0.28
Resonance frequency [kHz]	20
Bias of the bridge read-out configuration [V]	3.3
DNA concentration and probe length	400nM in HB; 12-mer (from [Fritz 2000])
Calculated half bridge response and resistivity varia-	ΔV = 6.9 [μV] ($\Delta R/R$=4.2 [ppm])
SNR	10

5.1.1.2. Approach 2: SiO_2 approach with single-crystal Si piezoresistors:

This approach is based on SOI wafer as well, and uses dry and wet etching micromachining techniques for the realization of SiO_2 beams from the BOX layer of the wafers. Mono-crystalline piezoresistors are realised by etching the device layer of the wafer, after a preliminary thinning to reduce the piezoresistor thickness to 80nm. In a first run, thickness of SiO_2 passivation layers is fixed to 100nm (on beam). The thickness of the SiO_2 beam is chosen in order to optimise device sensitivity in both cases.

Table 5.6. Main properties and modeling results of BOX-based cantilevers with n-type resistors

Beam materials and thicknesses	400nm oxide + n-Si resistors (80nm) +100nm nitride + Gold 20nm
Beam geometry (L, W, t) [μm^3]	200 x 200 x 0.540
Beam spring constant [N m^{-1}]	0.17
Resonance frequency [kHz]	16.6
Bias of the bridge read-out configuration [V]	3.3
DNA concentration and probe length	400nM in HB; 12-mer (from [Fritz 2000])
Calculated half bridge response and resistivity variation	ΔV = 8.6 [μV] ($\Delta R/R$=5.2 [ppm])
SNR	12.7

5.1.1.3. Approach 3: SiO_2 approach with poly-Si piezoresistors:

This approach is based on Si wafer, used as substrate for the realisation of beams from a deposited thin SiO_2 layer. Poly-Si piezoresistors with thickness 80nm and passivation (Si_3N_4 layer: 100nm) are also deposited. The thickness of the SiO_2 beam is chosen in order to optimise device sensitivity (optimal for 400nm thickness). Beam release is performed by wet and dry micromachining techniques.

Table 5.7. Main properties and modeling results of BOX-based cantilevers with p-type poly-Si resistors

Beam materials and thicknesses	400nm oxide + p-type poly-Si resistors (80nm) +100nm nitride + Gold 20nm
Beam geometry (L, W, t) [μm^3]	200 x 200 x 0.540
Beam spring constant [N m^{-1}]	0.17
Resonance frequency [kHz]	16.6
Bias of the bridge read-out configuration [V]	3.3
DNA concentration and probe length	400nM in HB; 12-mer (from [Fritz 2000])
Calculated half bridge response and resistivity variation	ΔV = 6.2 [μV] ($\Delta R/R$=3.8 [ppm])
SNR	9.2

5.1.1.4. Approach 4: polymeric beams with gold strain gauges as sensing elements:

This approach is based on Si wafer, used as substrate for the realisation of beams from a deposited polymeric layer (e.g. SU-8). Gold strain gauges with thickness 100nm and passivation (polymeric layer: 200nm) are also deposited.

Table 5.8. Main properties and modeling results of SU-8 cantilevers with gold strain gauges.

Beam materials and thicknesses	800nm SU-8 + gold strain gauge (100nm) +200nm SU-8 + Gold 20nm
Beam geometry (L, W, t) [μm^3]	200 x 200 x 0.540
Beam spring constant [N m^{-1}]	0.085
Resonance frequency [kHz]	10
Bias of the bridge read-out configuration [V]	3.3
DNA concentration and probe length	400nM in HB; 12-mer (from [Fritz 2000])
Calculated half bridge response and resistivity variation	ΔV = 2.4 [μV] ($\Delta R/R$=1.5 [ppm])

For both cases, the thickness of the polymeric beam has been evaluated in order to optimise the device sensitivity. Beam release is performed by wet and dry micromachining techniques. In this case, since planar stress cannot be efficiently detected by strain gauges, planar stress is considered as an ideal case where short beam are realised. Although this is a "strong" assumption, leading to an overestimation of the response, the performances achievable with this approach are still low with respect with other approaches.

5.1.1.5. Result discussion and selection of the technological approach

As reported in the respective tables, the approach leading to the highest sensitivity is the SOI-based approach, despite lower stiffness of SiO_2 and polymeric beams. The major issue in this case is the lower mechanical efficiency of the structure, due to the low beam stiffness and relatively high stiffness of Si, poly-Si resistors and strain gauges, resulting in a shift of the neutral axis of deflection toward the resistor. The shift of the neutral axis requires a higher thickness of the beam in order to produce a sufficient stress on the piezoresistor, reducing the advantage of materials with low stiffness. This issue, in addition to the lower stress sensitivity of strain gauges, makes almost worthless the stiffness reduction, especially in polymeric materials. Furthermore, polymeric materials usually present stability issues when exposed to liquid solutions, which can pose some practical issues in the specific application. By the evaluation of results coming from the analytical model, the polymeric beams have been removed from the technological options, while further investigations have been especially focused on the SOI-based approach using n-type resistors.

Another consideration regards the choice of sensing elements, pushing toward the selection of n-type resistors, which are more efficient in conditions where the stress is uniform in the plane direction, rather than p-type, which is usually preferred for mono-axial stress detection (e.g. in cantilever used in resonance mode, force detectors, etc…). More consideration will be reported in the next paragraph, dealing with FE modelling.

The response level, estimated in the ppm range, leads to consideration that high sensitivity readout of piezoresistors is required. Typically, in order to avoid the interference of lead wires (which are typically in the Ohm range for Al:1%Si wires) and increase the resolution, a Weathstone bridge configuration between four resistors can be used. Temperature effects are also compensated with this configuration.

5.2. FE modelling

Due to the beam root presence, the stress distribution in the area near to the substrate is different from the "ideal" condition in analytical models. For analysing these aspects, finite element (FE) analysis with ANSYS™ were performed. On the basis of results of the analytical model of the device, reported in previous paragraph, the best technological approaches for the application are n-Si and poly-Si, especially when planar stress is applied. p-type Si has also been considered, while polymeric beams with gold strain

gauges have been excluded from the set of FE, due to their poor sensitivity and the general considerations reported in the previous paragraph.

Beams were modelled as multilayered shells (SHELL181), in order to reduce the computational resources and efficiently model the structure with high aspect ratio (thickness in hundreds of nm, beam dimensions in hundreds of µm). Material properties and stresses coming from DNA hybridisation were the same reported in the analytic model. Results of FE modelling provide a good coherence with analytical model, especially with regard to beam deformation and total displacement (Figure 6).

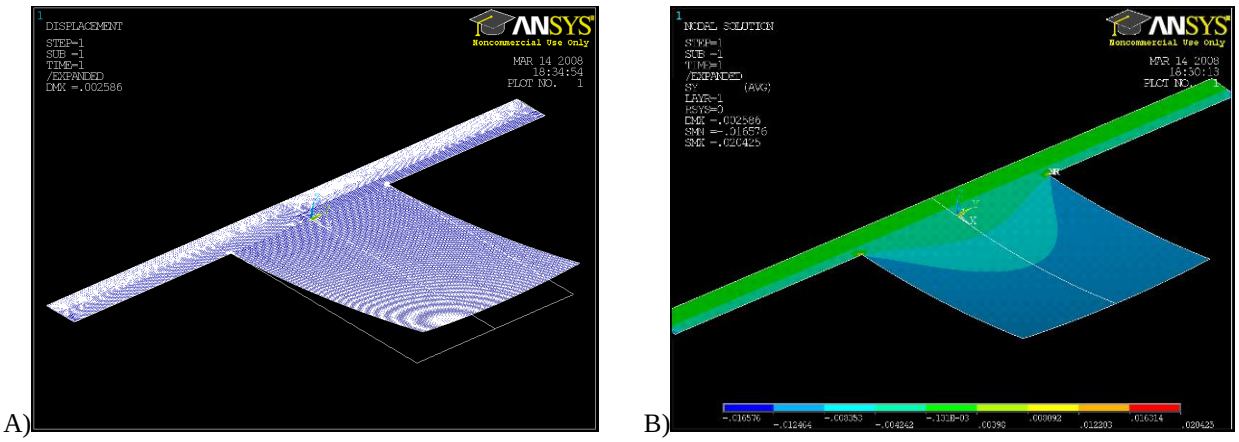

Figure 5.3. A) Deformed shape @ 400 nM DNA; B) Transversal stress @ 400nM DNA (thickness 340nm, length=width=100µm).

Results of FE modelling of stresses on readout are coherent with results of the analytical modelling, as shown in Figure 5.4 for different type of readout elements.

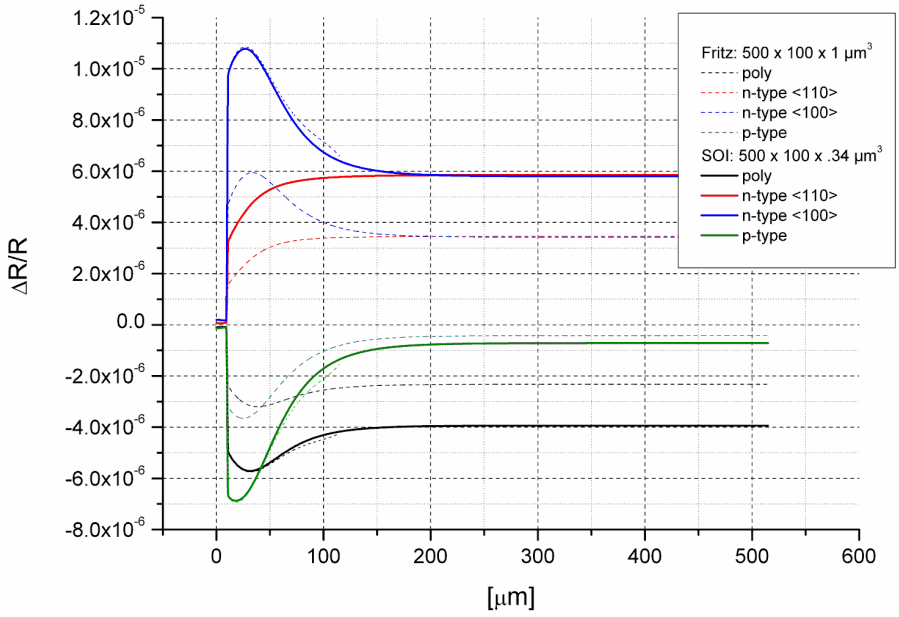

Figure 5.4. Comparison of response to 400nM DNA hybridisation for different sensible materials and orientation and with two different geometries. "Fritz" data refer to [Fritz 2000], SOI to the SOI-based approach proposed

A few considerations can be reported here:

- p-type Si has a very low performance with respect to n-type, especially for long beams, where stress distribution is almost by-axial. p-type becomes competitive in root region, although still with lower response than n-type <100>.
- orientation of resistors with respect to crystallographic planes is not influent for "long beams", while in the root region n-type <100> orientation provide an advantage in terms of sensitivity. <100> n-Si provides a response with integral average $\Delta R/R=8.1$ppm over the region with length L=W=200μm, which represent a 1.47 increase of the response with respect to "long beam" region.
- poly-Si has a response roughly about 2/3 with respect to n-Si, although the different section (here not considered), in which resistors are offset from the Si beam, is reducing the disadvantages of this approach.

Although the deflection is the same as the analytical model, the stress on Si surface is reduced, due to the "real" stress distribution at the Si-SiO_2 interface. The geometrical efficiency of resistors must be also taken into account, thus reducing the readout response of a factor 0.5÷0.7, according to passivation thickness and implant depth.

5.3. Design

Summarising the results of technological feasibility and modelling of performances, the most attractive solution, showing highest sensitivity to DNA hybridisation is based on SOI wafer, with device layer 340nm and n-type piezoresistors. The device configuration will be based on arrays up to 16 elements composed by 2 beams (1 reference beam and 1 measurement), in a Weathstone bridge configuration. The use of the reference beam can provide, apart from the compensation of thermal effects and higher resolution in resistance measurements, also the compensation of possible microfluidic forces generated on the structures by the solutions in the measurement chamber and the rejection of biochemical "common" signals not related to specific DNA hybridisation with single nucleotide mismatch.

In the worst case, (4n + 1) contacts are required for n elements arrays, which can be reduced by using common contacts for bridge polarisation. A vector implementation may provide a reduced number of pads with respect to square arrays, since some contacts may be put to common pads. A draft design is reported in Figure 5.5.

Main device specifications	
Array dimensions	16 beam couples
Element dimensions	300 ÷ 1000 μm^2
Chip dimensions	16100 x 6120 μm^2
Number of pads	54

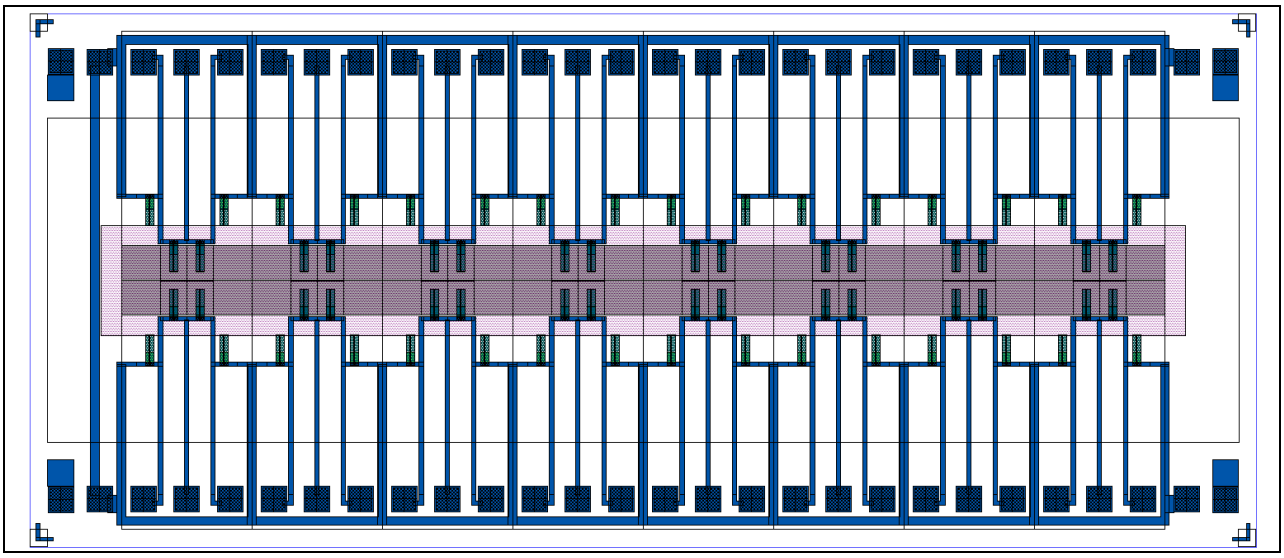

Figure 5.5. Draft chip design and main specifications

Typical expected specifications for the devices are:

- the typical capacity between device layer and handle wafer (Si 500µm, floating) is $9.96e^{-17}$ F/µm^2, which implies 10nF total capacitance with current chip dimensions
- wires are expected to have a square resistance of 0.07 Ω/sq., with a parasitic capacitance lower than 0.4 fF/µm^2 toward the substrate. Wiring to pads is expected to have typical resistance 2÷5Ω, and capacity lower than 40pF
- internal wires of the Weathstone bridges with typical resistance about 1Ω, and capacity lower than 14pF
- n-type piezoresistors with square resistance 2kΩ/sq., for a typical bridge element about 5÷30kΩ and capacity lower than 54pF. With this values, a maximum dissipation on the bridge of 1mW is reached above 5V bridge bias.
- For 12-bases oligonucleotides with concentration 400nM in HB, the differential response to DNA sequences with a single-base mismatch is expected about ΔV = 9.6 [µV] @3.3V bias (ΔR/R=5.8 [ppm]), while the absolute response to 12-bases oligonucleotides is expected to be 1 order of magnitude higher
- The required measurement resolution must be lower than 1µV (ΔV) or 0.5ppm (ΔR/R)
- Bridge resistors are expected to have a process spread of resistances in the order of some %, which reflects on the initial bridge unbalance.

5.4. Discussion

Summarising, in depth evaluation of performances achievable with different technological options were considered for the selection of best DNA cantilever sensors. In particular, best sensitivity and SNR can be achieved with single crystal silicon beams, using implanted n-type piezoresistors and SOI wafer for suspended structure realisation. This is due to high sensitivity of single crystal piezoresistors with respect to other options (poly-silicon resistors, strain gauges), which is overcoming the advantages of other approaches, such as the use of high compliance beams made of polymeric materials. The realised design configuration is based on arrays with up to 16 elements composed by 2 beams each (1 reference beam and 1 measurement), in a Weathstone bridge configuration. The use of the reference beam can provide the rejection of several "common" signals not related to specific DNA hybridisation with single nucleotide mismatch. Detection of SNPs is expected, with differential signals in the order of tens μV. Devices are expected to be fabricated in the next period for experimental testing.

Chapter 6

6. Material characterisation with micro cantilever detectors

The measurement of mechanical parameters such as Young's modulus and residual stresses of materials by means of microcantilever structures offers a reliable and accurate alternative to traditional methods, especially when dealing with thin films, which are extensively used in microfabrication technology and nanotechnology. The use of piezoresistive cantilever array can also allow the on-line measurement of film stresses during the deposition.

As a case study, MEMS-based piezoresistive cantilevers were realized and used for the determination of Young's modulus and residual stress of thin titanium dioxide (TiO_2). During the last decade titanium dioxide (TiO_2) has drawn attention as versatile material in several different applications due to its excellent physical properties. It is used in optical coatings due to its high refractive and optical transmittance in the visible range [Zhang 2007], in microelectronics as insulation layer because of its high dielectric constant [Fukuda 2002], in bio-medical coatings thanks to its excellent biocompatibility [Carbone 2006], and due to its photocatalytic effect it can decompose and remove pollutants from its surface and can be used in renewable hydrogen production [Zhang 2004]. Dedicated silicon microcantilevers were designed through an optimization of geometrical parameters with the development of analytical as well as numerical models. Young's modulus and residual stress of sputtered TiO_2 films, deposited from a TiO_2 target using an RF plasma discharge, were assessed by using both mechanical characterization based on scanning profilometers and piezoresistive sensing elements integrated in the silicon cantilevers.

In this chapter, the method and results of extraction of both TiO_2 stiffness and residual stress on dedicated MEMS-based cantilevers is reported, allowing an evaluation of Young's modulus, residual stress during the growth of TiO_2 thin films at thicknesses ranging from a few nanometers to hundreds. Two different techniques are used: with the first one residual stresses and Young's modulus were measured by scanning beams with a stylus profilometer, while with the second one residual stresses were measured with integrated piezoresistors. The procedure for the data extraction was also optimized in order to increase the measurement accuracy and robustness and in order to overcome some practical issues.

In order to implement a MEMS-based platform for material characterization and proceed with the characterization of TiO_2 thin films, Si-based beams with reduced dimensions (length 500÷1500 μm, width 20÷60 μm, thickness down to 2.3 μm) were developed, allowing high resolution measurements of stiffness and bending variation.

6.1. Modelling and design of structures for material characterisation

The design of the microcantilevers array was done taking into account the typical residual stress of the materials to be characterized. The static as well dynamic mechanical features of the microcantilevers were studied by means of analytical and numerical models, allowing the optimization of both beam geometry and technological parameters for the realization of the piezoresistors. In particular, ANSYS® simulations were used for the evaluation of mechanical properties and sensitivity, while numerical simulations of ion implant and diffusion steps for the read-out optimization have been performed with ATHENA® (SILVACO®) simulation software.

Devices were designed for the characterization of stiffness of materials with a stylus profilometer and of electrical measurements of residual stress; they include a beam structure, and two bridge structures with different shape for further mechanical tests. The selected geometry and method can be easily implemented with high density arrays of beams, allowing the analysis of materials with high parallelism, also allowing a combinatorial approach to material characterization [Ludwig 2005]. Devices were designed for the realisation with a technological process based on a Silicon On Insulator (*SOI*) approach for the realisation of the suspended structures with low thickness and high dimensional control. The lower thickness allows an improved sensitivity to both stresses and Young modulus. The realised geometries were designed for the use with the "revolver" sample holder use for the film deposition. Two different devices were designed, including a beam structure, and two bridge structures with different shape for further mechanical tests. An overview of designed structures is reported in Figure 6.1 and Table 6.1.

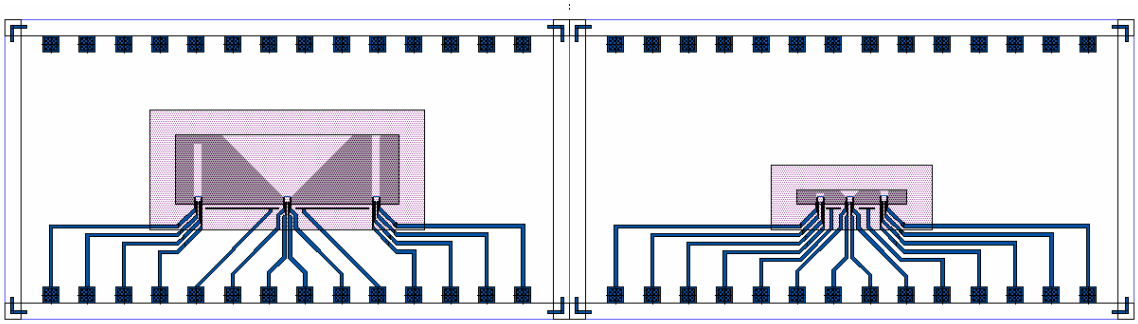

Figure 6.1. Device design of structure with different dimensions. A) Device Strint-1. B) Structures Strint-2.

***Table 6.1*:** Overview of geometrical dimensions of the devices for single tests.

Device	**Strint-1**	**Strint-2**
Die dimensions [µm^2]	7000 x 3696	7000 x 3696
Front opening [µm^2]	2780 x 854	1367 x 169
Beam geometry [µm^3]	752 x 106 x 2	138 x 106 x 2
Bridge geometry [µm^3]	854 x 106 x 2	169 x 106 x 2
Geometrical intensification factor	15.09	2.52
Read-out	1 Wheatstone bridge / structure	1 Wheatstone bridge / structure

The main purpose of the device Strint-1 was the characterisation of mechanical properties of combinatorial materials with a stylus profilometer, for which a longer scanning length allows an increase of the measurement resolution. The shorter structures on the device Strint-2 were focused on electrical-only measurements of residual stress, for which a long structure is not required.

The triangular stress-intensifier structures were designed in order to circumvent an issue of the selected technology. Being the piezoresistors p-type, the best sensitivity is achieved for mono-axial stress distributions rather than bi-axial uniform stress distributions, which are found for stress sensing purposes. Thus, on suspended beams, piezoresistive stress sensing is not favourable in region far from the beam root, since they approach the ideal unconstrained condition leading to an uniform bi-axial stress distribution. As a result, p-type piezoresistors are only effective in beam root regions. By using a bridge structure instead of a bridge, the structure deflection is prevented, resulting in a uniform stress distribution across the beam section in the beam direction, rather than the triangular stress distribution described in Chapter 3. For thin beams this stress configuration become of advantage, due to the reduced lever arm and bending momentum applied by the film in traditional bending detection, and the higher mean stress in the section in "longitudinal sensing" mode. The stress distribution is, however, still bi-axial in regions far from the beam root. In order to increase the asymmetry of stress distribution in the two directions, a triangular-shaped bridge has been implemented, showing an increase of sensitivity in FE models implemented.

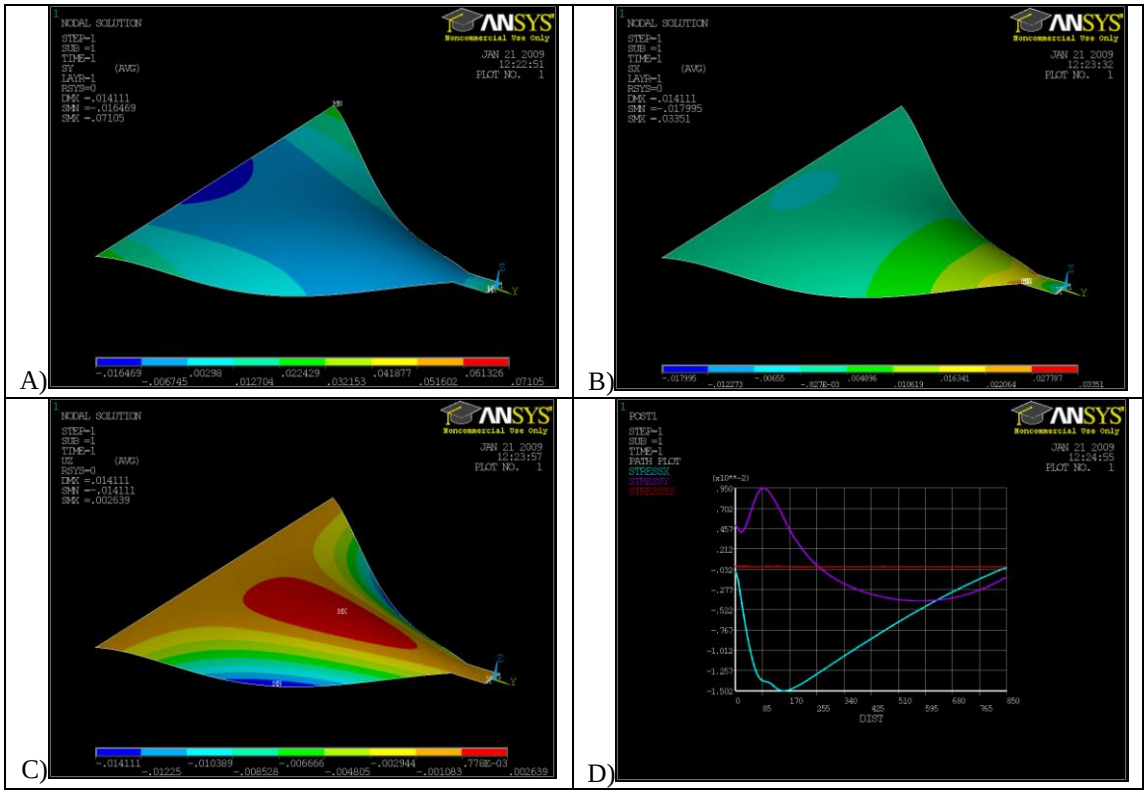

Figure 6.2. Simulation of stress intensifier structures, with thickness 340nm and 203kPa, 10nm applied film. A) longitudinal stress σ_y. B) transversal stress σ_x. C) vertical displacement. D) Stress distribution over the central symmetry axis.

Results of FE modelling are shown in Figure 6.2, 6.3 and 6.4 for thin beams (340nm Si structures, in accordance with process described in Chapter 3), with an applied 203kPa stress on a 10nm layer. The increase of performances of p-type resistors is quite evident in the graph.

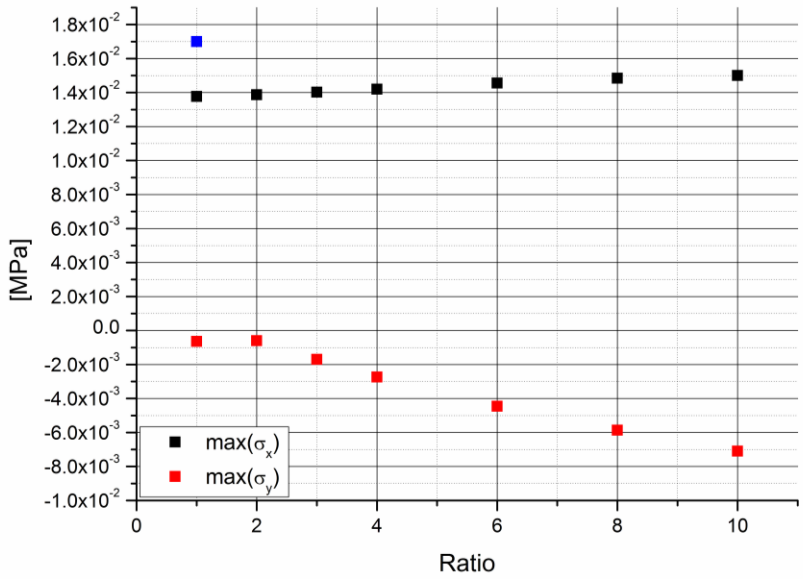

Figure 6.3. Comparison of FE results: maximum stress on longitudinal (σ_Y) and transverse (σ_X) directions. Ratio 1 denotes straight bridge structures. Blue point refers to both σ_X and σ_Y for beam structures in the same conditions.

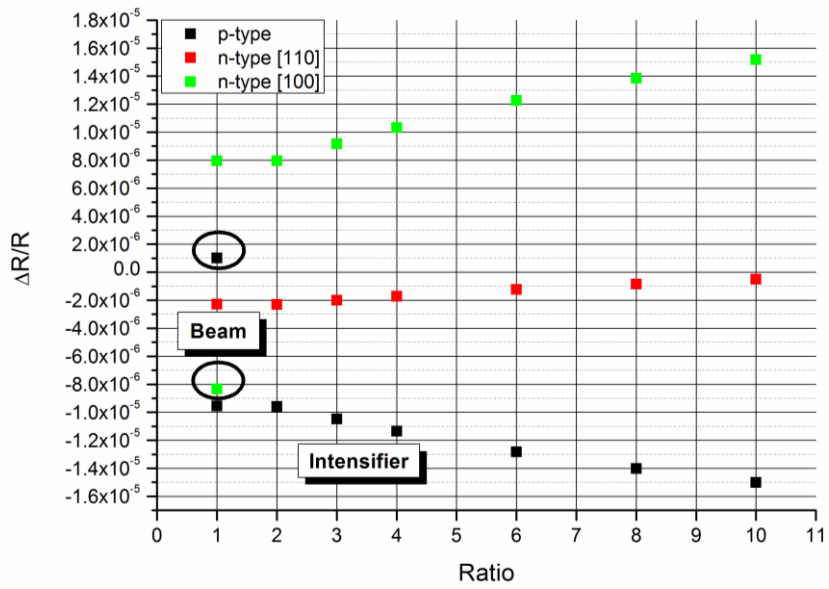

Figure 6.4. Comparison of calculated relative variation of resistance for p-type and n-type piezoresistors on intensifier as function of ratio width of readout beam vs. triangle maximum width. Conditions are same as previous Figure. Ratio 1 denotes straight bridge structures. Circled points refer to beam structures in the same conditions.

In addition to the described designs, two more geometries with an array approach were implemented. Five beams with piezoresistive read-out were included in the first one, while the second features five beams

with integrated microheaters. The geometry summary of these devices is reported in Figure 6.5 and Table 6.2.

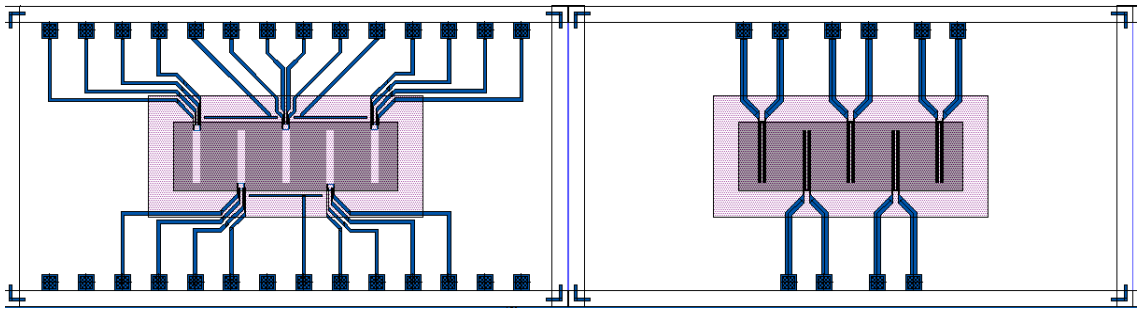

Figure 6.5. Device design of structure with different dimensions. A) Cantilever array with integrated piezoresistive read-out. B) Cantilever array with integrated microheaters.

***Table 6.2*:** Overview of geometrical dimensions of the array devices.

Device	**uCOMBI-array**	**uCOMBI-array-T**
Die dimensions [µm^2]	7000 x 3896	7000 x 3896
Front opening [µm^2]	2780 x 854	2780 x 854
Beam geometry [µm^3]	752 x 106 x 2	752 x 106 x 2
Read-out	1 Wheatstone bridge / beam	-
Notes	-	1 Al resistor / beam
Instances per wafer	3	4

The microcantilevers arrays were realised with the previously described technologies, using p-type resistor on n-doped substrate with [110] crystallographic orientation. p-type silicon resistors are expected to have the maximum piezoresistive coefficients $\boldsymbol{\pi_{ij}}$ values for low doping concentration in the [110] orientation (6.6, -1.1, 138.1 [10^{-11} Pa^{-1}] for π_{11}, π_{12} and π_{44} coefficients respectively). Coefficients for longitudinal and transversal stress with respect to the resistor orientation are 71.8 10^{-11} Pa^{-1} for stress longitudinal with respect to the piezoresistor and -66.31 10^{-11} Pa^{-1} in the transversal direction. High doping of resistors can reduce the dependence on temperature, but in this case also piezoresistive properties are reduced, resulting in lower read-out sensitivity [Kanda 1982].

6.2. Measurement method

By scanning the surface with a stylus profilometer, with a load F, the displacement at a distance x from the beam root is:

$$\delta(x,F)=\frac{F}{K(x)}+\delta_0(x)=\frac{F\cdot x^3}{3\cdot W\cdot C}+\delta_0(x) \qquad 6.1$$

Then, scanning the device with two different loads, the deformation at zero load and the device stiffness can be calculated for each position coordinate x:

$$\delta_0(x)=\frac{F_2\cdot\delta(x,F_1)-F_1\cdot\delta(x,F_2)}{F_2-F_1} \qquad 6.2$$

$$K^{-1}(x)=\frac{\delta(x,F_1)-\delta(x,F_2)}{F_2-F_1} \qquad 6.3$$

By performing the measurement of the stiffness before and after the deposition, it is possible to extract the Young's modulus of the material from the stiffness increase related to the additional layer deposited:

$$\Delta C=\frac{\Delta K(x)}{3}\cdot x^3=\frac{E_{layer}\cdot W\cdot\left(h_{\sup}^3-h_{\inf}^3\right)}{3}\cdot x^3 \qquad 6.4$$

h_{sup} and h_{inf} are the distance of the upper and lower surfaces of the deposited film from the neutral plane for bending (1.33µm in the realized devices).

The residual stress of the deposited film induces a beam deflection. By supposing a constant stress along the structure, the displacement is:

$$\delta(x)=\frac{\sigma_{film}t_{film}h_{film}}{2\cdot C}\cdot x^2 \qquad 6.5$$

By using the displacement variation before and after the deposition, it is possible to calculate the related film stress. The stress sensitivity is then increasing for thinner beams.

Ideally, the determination of the Young's modulus is not directly affected by the residual stresses of materials. In fact, the Young's modulus is calculated from the increase of beam stiffness, which is in turn calculated from the differential measurement of deflection at different loads, thus compensating the curvature of the beam. However, minor effects may be related to stress-stiffening of the structure, which can be found for high thicknesses and residual stresses of the film resulting in large displacements of the structure. Since this condition is not verified for considered TiO_2 films, this effect can be neglected.

6.3. TiO_2 films

The deposition and characterisation with laboratory equipments of the titanium dioxide films were performed by the "Plasma and Advanced Materials" (PAM) group of the FBK. Here, a short description of the techniques and results is reported for completeness.

The deposition of the titanium dioxide films on microcantilevers was performed by sputtering from a TiO_2 target using a RF (13.56MHz) plasma discharge, by using an ad-hoc developed carrousel sample holder allowing multiple deposition of material with different properties in the same deposition run. A constant dc self bias on the cathode was maintained at -750 V, corresponding to an effective load of 106 W. During the deposition the pressure was 0.05 Torr and an Ar-O_2 mixture gas was used. The O_2 and Ar concentration in the feed gas was 3% and 97%, respectively. The film was grown at a floating potential given by plasma and at room temperature. Both the cathode and the sample holder were water cooled. A set of depositions of TiO_2 films with different thicknesses was performed and film thicknesses were measured by using a stylus profilometer. The deposition time ranged from 25 min to 350 min, corresponding to thicknesses from 38 nm to 200nm, with an almost constant deposition rate of (0.63±0.08) nm/min. The sputtered TiO_2 thin films were characterized in terms of crystallographic structure by XRD technique. Measurements were performed using the Italstructures APD 2000 diffractometer in the Seeman-Bohlin geometry (grazing angle configuration). A Cu K_α (0.1540598 nm) radiation source operated at 40 KeV and 30 mA and at an incident angle of 3° has been used. XRD patterns were acquired in the 25° -90° range, 0.02° step and 5 seconds of acquisition time. The film exhibited anatase structure with (101) preferential orientation, which is the typical crystallographic phase for coatings grown at low temperature [Zhang 2002].

6.4. Experimental results

The characterization of the fabricated devices was focused on the sensitivity to the bending and the measurement of the curvature of the suspended beams by means of a mechanical profilometer. Mechanical properties of the film were calculated, starting from the results of the profilometer scanning at 1, 2 and 5mg along the microcantilevers.

Results are reported in Figure 6.6, as well as the extrapolated displacement at null load (δ_0) and beam compliance (K^{-1}). Similar results were also calculated before the film deposition.

In order to provide a robust technique to evaluate the spring constant, especially insensitive to the alignment of the structure (x coordinate in the K expression), to the poorly representative region at the beam root showing a tri-axial stress distribution, it is more convenient to perform a linear fitting of the variable $K^{-1/3}$ [He 2005]. Then, the extraction of the Young's modulus of the film has been performed starting from the results of the fit:

$$K^{-1/3}(x) = \frac{1}{(3 \cdot C)^{1/3}} x = A + B \cdot x \qquad 6.6$$

Results are reported in Figure 6.7 and Table 6.3.

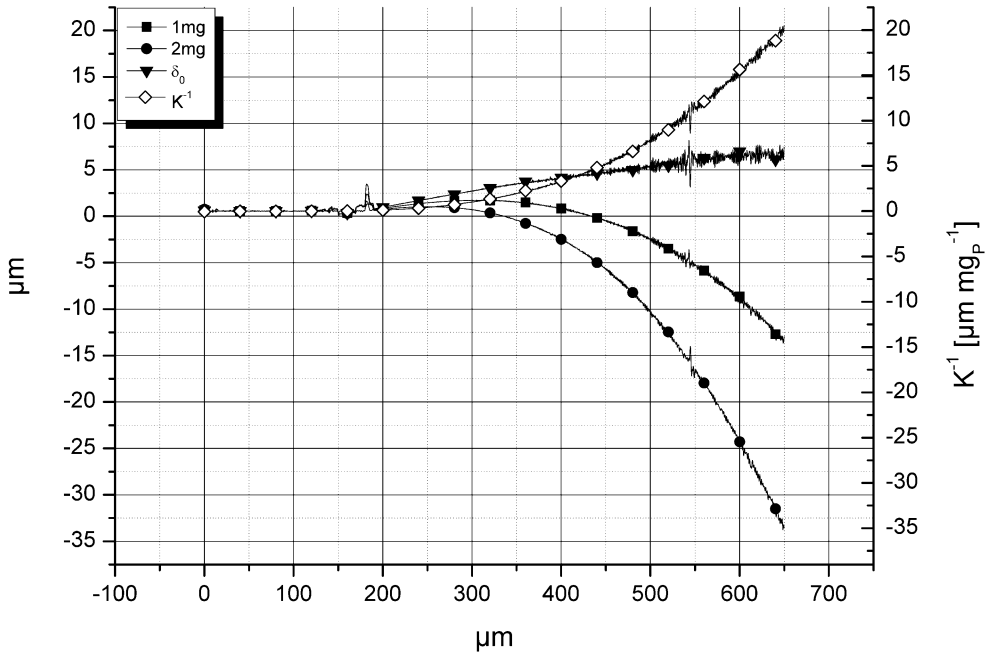

Figure 6.6. Mechanical characterization of final devices (2µm thickness): Chip number 6, deformation at 1 and 2 mg load, extrapolated deformation at null load (δ0) and beam compliance (K-1).

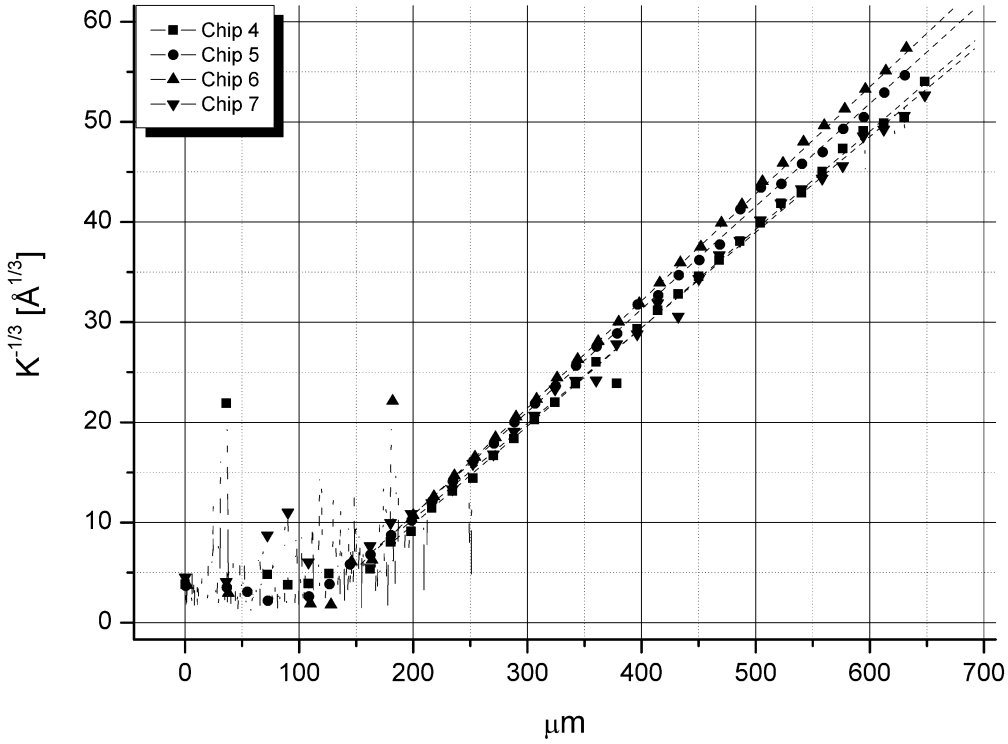

Figure 6.7. Fitting results for $K^{-1/3}$. Chips 4 to 7.

Table 6.3. Fitting results for $K^{-1/3}$. Chips 4 to 7 and dummy samples.

Chip	Film t [nm]	A [Å / mg_p]$^{1/3}$	B [(Å / mg_p)$^{1/3}$ µm^{-1}]	C [N m^2]	E [GPa]
Dummy 1	0	-9.77 ± 0.07	0.1063 ± 1 10^{-4}	(2.72 ± 0.01) 10^{-11}	-
Dummy 2	0	-9.75 ± 0.08	0.1033 ± 1 10^{-4}	(2.96 ± 0.02) 10^{-11}	-
4	192 ± 10	-9.82 ± 0.06	0.0982 ± 1 10^{-4}	(3.45 ± 0.02) 10^{-11}	237 ± 42.5
5	73.8 ± 10	-9.77 ± 0.04	0.10271 ± 0.9 10^{-4}	(3.02 ± 0.02) 10^{-11}	259 ± 89.6
6	35.3 ± 10	-10.62 ± 0.02	0.10689 ± 0.5 10^{-4}	(2.68 ± 0.02) 10^{-11}	266 ± 171
7	114.3 ± 10	-8.78 ± 0.07	0.0955 ± 2 10^{-4}	(3.76 ± 0.02) 10^{-11}	251 ± 62.8

The Young's modulus was estimated with the equation (6.4), where the stiffness variation was calculated against the average K of devices without deposited films, in order to evaluate the sensitivity of the method to the fabrication tolerances. By performing a beam calibration by measuring K of the specific chip before the film deposition, higher precision is expected for Young's modulus. The accuracy of deflection measurement with the profilometer is quite good with respect to the total deflection in the considered application, since the total accuracy on deposited films, also including other sources of errors such as the film roughness, can be estimated in the tens of nanometers, against deflections typically in the microns range. Thus, the relative error on deflection can be estimated about 1%. Using different techniques for improving the deflection measurement can also improve the evaluation of the material properties, although the improvement may be minor with respect to other sources of errors in the procedure. For instance, Young's modulus shows an increase of error bars at low film thicknesses due to film thickness uncertainness. In any case, other instrumentation with higher force and deflection accuracy, such AFM for instance, may be available to measure the Young's modulus of materials with the proposed method. Optical methods (e.g. interferometric detection and laser scanning detection) cannot apply loads and can be used only for residual stresses measurements.

Then, the residual stresses were calculated from the displacement variation between measurements before and after film deposition. Since the displacement at null load before the deposition could not be calculated due to experimental issues, the beam deflection $\delta_0(x)$, related to the TiO_2 film stress, was calculated from profilometer scanning at 1mg, by applying the following correction for K^{-1} variation:

$$\Delta\delta(x) = \Delta\delta_0(x) - F \cdot \Delta K^{-1}(x) \qquad 6.7$$

Then, fitting of the $\Delta\delta_0(x)$ deflection after the film deposition can be performed with a strategy similar to the approach for the experimental K(x) measurement, allowing a high independence on alignment and non-ideal effects at the beam root.

$$\Delta\delta_0^{0.5}(x) = \left(\frac{\sigma_{film} t_{film} h_{film}}{2 \cdot C}\right)^{0.5} \cdot x = A + B \cdot X \qquad 6.8$$

$$\sigma_{film} = B^2 \frac{2 \cdot C}{h_F \cdot t_{film}} \qquad 6.9$$

Results are summarized in Figure 6.8 and Table 6.4, showing tensile stress states for all the samples, as expected for anatase-phase TiO_2, especially for films with density lower than pure anatase bulk material [Ottermann 1996]. Furthermore, the residual stress strongly decreases when the film thickness increases. The stress reaches the lower value (80 MPa) for 192 nm-thick coating. Again, error bars of residual stresses in the Figure 6.8 (residual stress vs. film thickness) are mostly due to the accuracy of film thickness, which is used to evaluate the material properties in eq. 6.4 and 6.9. This results in larger error bars at lower film thickness.

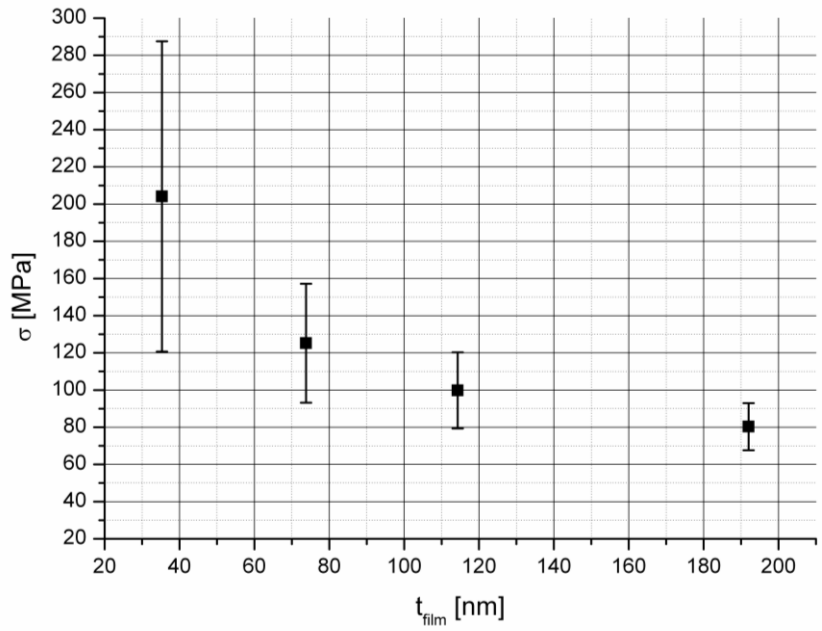

Figure 6.8. Residual stress as a function of different film thicknesses.

Table 6.4. Fitting of δ0.5 for chips from 4 to 7 and calculated residual stresses.

Chip	A [Å$^{1/2}$]	B [Å$^{1/2}$ µm^{-1}]	σ [MPa]
4	-15.5 ± 0.4	0.601 ± 1e-3	80 ± 12
5	-3.5 ± 0.5	0.478 ± 1e-3	125 ± 32
6	-6.7 ± 0.5	0.442 ± 1e-3	204 ± 83
7	-13.7 ± 0.8	0.483 ± 2e-3	99 ± 20

The integrated piezoresistive read-out was used in order to evaluate the residual stresses and to compare the results with the measurement performed with the profilometer. The resistances of the Wheatstone bridge, integrated on the beams, were measured before and after the deposition, in order to evaluate the relative resistance variation (ΔR/R). Since the read-out output is proportional to the stress on the piezore-

sistors, the plot of $\Delta R/R$ was performed vs. the applied momentum ($m = \sigma_{film}\, t_{film}\, W\, t_{beam}/2$), which is in turn proportional to the stress on piezoresistors. The residual stress calculated in the previous paragraph was used. A linear relationship can be found, as shown in Figure 6.9.

Here, the major source of errors bars is the initial value of resistance, which is used to evaluate the relative resistance increase. Although other approaches may be more accurate, piezoresistive detection has advantages in terms of cost and simplicity of the instrumentation with respect to high accuracy methods for measuring the curvature of a substrate and it is also suitable for on-line measurement of stress.

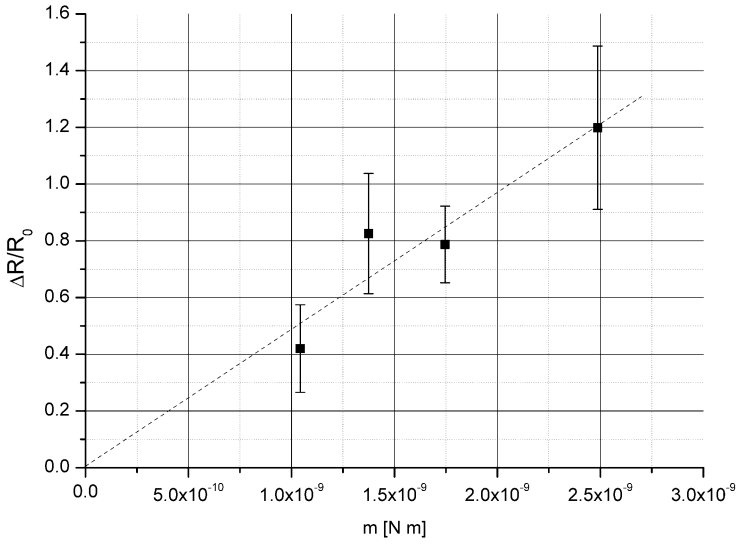

Figure 6.9 Relative resistance variation between measurement before and after the film deposition, vs. the momentum applied to the structure by the residual stress in the film.

6.5. Discussion

MEMS-based cantilevers were designed and realized through the development of analytical as well as numerical models. TiO_2 films with different thickness were successfully deposited on MEMS-based cantilevers by sputtering from a TiO_2 target using an RF plasma discharge. The films were confirmed to be in anatase phase from XRD analysis, with (101) preferential orientation. Mechanical properties of the film were calculated, starting from the results of the profilometer scanning along the microcantilevers. Measured Young's modulus of TiO_2 thin films is around 250 GPa for all deposited films.

Electrical measurements were been carried out on microcantilevers, in order to evaluate the residual stresses and to compare the results with the measurement performed with the profilometer. As expected, a linear relationship was found between applied momentum and the relative resistance variation.

With the realized MEMS structure, the characterization of residual stress and Young's modulus of thin film materials can be performed, as demonstrated by the mechanical characterization. Furthermore, the

integrated read-out piezoresistors can allow the on-line measurement of residual stress during the material deposition. This class of devices is a promising tool for material characterization, allowing an high parallelism in measurement for high throughput characterization systems. Future work will deal with the experimental characterisation of the stress-intensifier structures for the electrical measurement of residual stresses.

Chapter 7

7. Conclusions

The development of several cantilever structures was performed for applications ranging from gas sensing, biosensors and material characterisation. Specific requirements led to the optimisation of geometries, technological processes and operative conditions for each application, through the analysis of analytical and numerical models. The evaluated technological processes were focused on the realisation of beams with different thicknesses, in particular 10 and 2 μm thickness with p-type piezoresistors for gas sensing applications and material characterisation, while a further process was studied for the implementation of DNA sensors with 340nm thick beams with n-type piezoresistors. Simulation and evaluation of specific technological aspects such as residual stress balancing and piezoresistors' implantation parameters allowed the optimisation of fabrication processes.

Cantilever-based gas sensors were developed with optimal performances in terms of mass sensitivity and resolution of the substrates. For 10μm beams, sensitivity was evaluated about -190 [$cm^2\ g^{-1}$] and mass resolution about 9.4 10^{-8} [$g\ cm^{-2}\ Hz^{-1}$], while 2μm beams provided better performances, estimated in the order of -669 [$cm^2\ g^{-1}$] for mass sensitivity and 1.1 10^{-8} [$g\ cm^{-2}\ Hz^{-1}$] for resolution. Here the properties of the electromechanical structures are expressed in terms of mass resolution per Hz of shift of the resonance frequency, while overall mass resolution must also consider the specifications of the implemented readout electronics. The resolution and sensitivity of cantilever sensors to ammines were estimated by using the adsorption properties of the phthalocyanines layers. The calculated resolution for devices realised by the first process (thicker structure) was in the order of 10-100 ppm for NH_3, DMA e TMA, by using the properties of sensitive materials without thickness normalisation. Preliminary experimental characterisation, providing 45ppm resolution for NH_3, validated the modelling results. For devices designed for the second process the estimated NH_3 resolution is in the order of 1-10 ppm, and experimental characterisation of the electromechanical properties of cantilever beams showed the improvement of performances, in terms of resonance quality factor, of the devices designed to work at higher-mode resonance.

In the field of static-mode biosensors, performances achievable with different technological options were evaluated for the selection of best DNA cantilever sensors. In particular, according to the analysis performed, the best sensitivity and SNR can be achieved with single crystal silicon beams, using implanted n-type piezoresistors and SOI wafer for suspended structure realisation. This is due to high sensitivity of single crystal piezoresistors with respect to other options (poly-silicon resistors, strain gauges), which is overcoming the advantages of other approaches, such as the use of high compliance beams made of

polymeric materials. The designed configuration is based on arrays with up to 16 elements composed by 2 beams each (1 reference beam and 1 measurement), in a Wheatstone bridge configuration. The use of the reference beam can provide the rejection of several "common" signals not related to specific DNA hybridisation with single nucleotide mismatch. Detection of SNPs is expected, with differential signals in the order of tens μV. Devices are expected to be fabricated in the next period for experimental testing.

The case study for MEMS-based cantilevers for material characterisation was the analysis of TiO_2 films with different thickness deposited on MEMS-based cantilevers by sputtering from a TiO_2 target using an RF plasma discharge. The characterization of residual stress and Young's modulus of thin film materials was performed with the realized 2μm-thick MEMS structures, thus demonstrating the suitability of this approach. This class of devices is a promising tool for material characterization, allowing an high parallelism in measurement for high throughput characterization systems, also enabling the on-line measurement of residual stress during the material deposition by means of the integrated read-out piezoresistors.

In conclusion, the suitability of MEMS-based piezoresistive arrays for a range of sensing applications was demonstrated with suitable sensitivity and selectivity. The possibility to perform measurement without the requirement for complex readout setups enables the use of this class of detectors for portable systems, which are expected to have an increasing diffusion in several fields including biomedical and agrofood applications.

Acknowledgments

This work has been developed at the Fondazione Bruno Kessler (FBK) in Trento, and in particular in collaboration with the BioMEMS Research Unit, under the supervision of Dr. Leandro Lorenzelli. All the devices presented in this work have been fabricated by the BioMEMS group, and in particular by Massimiliano Decarli, using the FBK's clean room facilities.

This work has been partially funded by the European projects "GOODFOOD" (FP6-IST-1-508744-IP) and "POCEMON" (Point-Of-Care MONitoring and Diagnostics for Autoimmune Diseases, FP7-ICT-2007-216088), respectively dealing with the development of cantilever sensors for gas sensing and biosensors. Cantilever-based gas sensors were based on sensitive materials deposited by the University of Valladolid and tested in collaboration with the BioMEMS group and the N.S. Kournakov Institute of Common and Inorganic Chemistry RAS in Moscow (Russia). Actuation and readout electronics were developed by Mattia Malfatti of the Sistemi Ottici Integrati (SOI) Research Unit of the FBK.

The development of devices and methods for material characterisation has been funded by the Provincia Autonoma di Trento in the framework of the MICROCOMBI Project. This activity has been carried out in collaboration with the Plasma Advanced Materials Research Unit of FBK, and in particular with Ruben Bartali and Nadhira Bensaada Laidani for the part related to TiO_2 deposition and crystallographic characterization.

Bibliography

[Abdulhaim 2008] I. Abdulhaim, M. Zourob and A. Lakhtakia – Surface Plasmon Resonance for Biosensing: A Mini-review – Electromagnetics, 28 (2008), 214-242.

[Abgrall 2007] P. Abgrall and A. M. Gué - Lab-on-chip technologies: making a microfluidic network and coupling it into a complete microsystem - a review - Journal of Micromechanics and Microengineering, 17 (2007), R15-R49.

[Alvarez 2004] M. Alvarez, L. G. Carascosa, M. Moreno, A. Calle, A. Zaballos, L. M. Lechuga, C. Martinez-A, and J. Tamayo – Nanomechanics of the formation of DNA self-assembled monolayers and hybridisation on microcantilevers – Langmuir 20 (2004), 9663-9668.

[Bagolini 2004] A. Bagolini, B. Margesin, A. Faes, G. Turco, F. Giacomozzi - Novel test structures for stress diagnosis in micromechanics - Sensors and Actuators A 115 (2004) 494–500.

[Baller 2000] M.K. Baller, H.P. Lang, J. Fritz, Ch. Gerber, J.K. Gimzewski, U. Drechsler, H. Rothuizen, M. Despont, P. Vettiger, F.M. Battiston, J.P. Ramseyer, P. Fornaro, E. Meyer, H.-J. Güntherodt - A cantilever array-based artificial nose – Ultramicroscopy 82 (2000), 1-9.

[Barrettino 2007] D. Barrettino, P. Malcovati, M. Graf, S. Hafizovic, and A, Hierlemann – CMOS-based monolithic controllers for smart sensors comprising micromembranes and microcantilevers – IEEE Transactions on Circuits and Systems – 1, Vol. 54, No. 1 (2007), 141-152.

[Bashir 2004] R. Bashir – BioMEMS: state-of-the-art in detection, opportunities and prospects – Advanced Drug Delivery Reviews 56 (2004) 1565-1586.

[Battiston 2001] F. M. Battiston, J.-P. Ramseyer, H. P. Lang, M. K. Baller, Ch. Gerber, J. K. Gimzewski, E. Meyer, H.-J. Guntherodt – A chemical sensor based on a microfabricated cantilever array with simultaneous resonance-frequency and bending readout – Sensors and Actuators B 77 (2001), 122-131.

[Binning 1982] G. Binnig, H. Rohrer, Ch. Gerber, and E. Weibel - Surface Studies by Scanning Tunneling Microscopy - Physical Review Letters 49, 9 (1982), 57-61.

[Binning 1986] G. Binning and C. F. Quate, Ch. Gerber – Atomic Force Microscope – Physical Review Letters 56, 9 (1986), 930-933.

[Biswal 2006] S. L. Biswal, D. Raorane, A. Chaiken, H. Birecki, A. Majumdar - Nanomechanical Detection of DNA Melting on Microcantilever Surfaces - Analytical Chemistry 78 (2006), 7104-7109.

[Biswal 2007] S. L. Biswal, D. Raorane, A. Chaiken, A. Majumdar - Using a Microcantilever Array for Detecting Phase Transitions and Stability of DNA – Clinics in Laboratory Medicine 27 (2007), 163–171.

[Burg 2007] T. P. Burg, M. Godin, S. M. Knudsen, W. Shen, G. Carlson, J. S. Foster, K. Babcock and S. R. Manalis - Weighing of biomolecules, single cells and single nanoparticles in fluid - Nature 446 (2007), 1066-1069.

[Buser 1994] R. A. Buser – Resonant sensors – in "Sensors" edited by W. Göpel, J. Hesse, J. N. Zenel –vol. 7, 205- 284, VCH, 1994.

[Butt 1995] H. J. Butt and M. Jashke – Calculation of thermal noise in atomic force microscopy – Nanotechnology 6 (1995), 1-7.

[Cai 1995] X. Cai, H. Bangert – Hardness measurement of thin films – determining the critical ratio of depth to thickness using FEM – Thin Solid Films 264 (1995), 59-71.

[Calleja 2005] M. Calleja, M. Nordstr, M. Alvarez, J. Tamayo, L.M. Lechuga, A. Boisen Highly sensitive polymer-based cantilever-sensors for DNA detection - Ultramicroscopy 105 (2005), 215–222.

[Capone 2003] S. Capone, A. Forleo, L. Francioso, R. Rella, P. Siciliano, J. Spadavecchia, D. S. Presicce, A. M. Taurino - Solid state gas sensors: state of the art and future activities Journal of Optoelectronics and Advanced Materials 5 (5) (2003), 1335 – 1348.

[Carbone 2006] R. Carbone, I. Marangi, A. Zanardi, L. Giorgetti, E. Chierici, G. Berlanda, A. Podestà, F. Fiorentini, G. Bongiorno, P. Piseri, P. G. Pelicci, P. Milani - Biocompatibility of cluster-assembled nanostructured TiO_2 with primary and cancer cells - Biomaterials 27 (2006), 3221–3229.

[Chapman 2007] P. J. Chapman, F. Vogt, P. Dutta, P. G. Datskos, G. L. Devault, and M. J. Sepaniak - Facile Hyphenation of Gas Chromatography and a Microcantilever Array Sensor for Enhanced Selectivity - Analytical Chemistry 79 (2007), 364-370.

[Chen 1994] G. Y. Chen, R. J. Warmack, T. Thundat, and D. P. Allison – Resonance response of scanning force microscopy cantilevers – Review of Scientific Instruments 65 (8) (1994), 2532.

[Chen 1995] G. Y. Chen, T. Thundat, E. A. Wachter, and R. J. Warmack – Adsorption-induced surface stress and its effects on resonance frequency of microcantilever – Journal of Applied Physics 77 (8) (1995), 3618-3622.

[Choudhury 2007] A. Choudhury, P. J. Hesketh, T. Thundat and Z. Hu – A piezoresistive microcantilever array for surface stress measurement: curvature model and fabrication - Journal of Micromechanics and Microengineering 17 (2007), 2065-2076.

[Creemer 2001] J. Fredirk Creemer, F. Fruett, G. C. M. Mejer, P. J. French – The Piezojunction Effect in Silicon Sensors and Circuits and its Relation to Piezoresistance – IEEE Sensors Journal 1 (2) (2001), 98-108.

[Datskos 1999] P. G. Datskos, I. Sauers - Detection of 2-mercaptoethanol using gold-coated micromachined cantilevers - Sensor and Actuators B 61 (1999), 75-82.

[Datskos 2004] P. G. Datskos, T. Thundat, N. V. Lavrik – Micro and Nanocantilever Sensors – in Encyclopedia of Nanoscience and Nanotechnology 10, 1-10, edited by H. S. Nalwa, American Scientific Publishers, 2004.

[Fadel 2004] L. Fadel, F. Lochon, I. Dufour and O. Francais - Chemical sensing: millimeter size resonant microcantilever performance - Journal of Micromechanics and Microengineering 14 (2004), S23–S30.

[Fischer] A.C Fischer-Cripps, Nanoindentation, II edition, Springer-Verlag, New York, LLC, 2004.

[French 1988] P. J. French and A. G. R. Evans – Piezoresistance in single crystal and polycrystalline Si – in “Properties of Silicon”, ISPEC, London, 1988.

[French 2002] P. J. French – Polysilicon: a versatile material for microsystems – Sensors and Actuators A 99 (2002), 3-12.

[Fritz 2000] J. Fritz, M. K. Baller, H. P. Lang, H. Rothuizen, P. Vettiger, E. Meyer, H.-J. Guntherodt, Ch. Gerber, and J. K. Gimzewski - Translating Biomolecular Recognition into Nanomechanics, Science 288 (2000), 316-318.

[Fritz 2002] J. Fritz, E. B. Cooper, S. Gaudet, P. K. Sorger and S. R. Manalis – Electronic detection of DNA by its intrinsic molecular charge – PNAS 99 (22) (2002), 14142-14146.

[Fritz 2008] J. Fritz – Cantilever biosensors – Analyst, 133 (2008), 855-863.

[Fukuda 2002] H. Fukuda, S. Maeda, K. Salam, S. Nomura - Synthesis of High Dielectric Constant Titanium Oxide Thin Films by Metalorganic Decomposition - Japanese Journal of Applied Physics – Part 1 41 (2002), 6912–6915.

[Gabrielson 1993] T. B. Gabrielson – Mechanical-Thermal noise in micromachined acoustic and vibration sensors – IEEE Transactions on Electron Devices 40 (5) (1993), 903-909.

[Gammelgaard 2006] L. Gammelgaard, P.A. Rassmusen, M. Calleja, P. Vettiger and A. Boisen - Microfabricated photoplastic cantilever with integrated photoplastic/carbon based piezoresistive strain sensor - Applied Physics Letters 88 (2006), 113508.

[Ghatkesar 2008] M. K. Ghatkesar, T. Braun, V. Barwich, J. Ramseyer, C. Gerber, M. Hegner, and H. P. Lang - Resonating modes of vibrating microcantilevers in liquid – Applied Physics Letters 92 (2008), 043106.

[Gridchin 1995] V. A. Gridchin, V. M. Lubimsky, M. P. Sarina – Piezoresistive properties of polysilicon films – Sensors and Actuators A 49 (1995), 67-72.

[Hagan 2002] M. F. Hagan, A. Majumdar, and A. K. Chakraborty – Nanomechanical forces generated by surface grafted DNA – Journal of Physical Chemistry B 106 (2002), 10163-10173.

[Hansen 2001] K. M. Hansen, H.-F. Ji, G. Wu, R. Datar, R. Cote, A. Majumdar, and T. Thundat – Cantilever-based optical deflection assay for discrimination of DNA single-nucleotide mismatches – Analytical Chemistry 73 (2001), 1567-1571.

[He 2005] J. H. He, J. K. Luo, H. R. Le and D. F. Moore - MEMS/NEMS Mechanical Characterization on Different Thin Film Materials by Scanning along Micromachined Cantilevers - Smart Sensors, Actuators, and MEMS II, edited by Carles Cané, Jung-Chih Chiao, Fernando Vidal Verdú, Proceedings of SPIE 5836 (2005), 208-219.

[Humphris 2005] A. D. L. Humphris, M. J. Miles, and J. K. Hobbs - A mechanical microscope: High-speed atomic force microscopy - Applied Physics Letters 86 (2005), 034106.

[Ilic 2005] B. Ilic, Y. Yang, K. Aubin, R. Reichenbach, S. Krylov, and H. G. Craighead - Enumeration of DNA Molecules Bound to a Nanomechanical Oscillator - Nano Letters 5 (5) (2005), 925–929.

[Ingebrandt 2007] S. Ingebrandt, Y. Han, F. Nakamura, A. Poghossian, M. J. Schoning, A. Offenhausser – Label-free detection of single nucleotide polymorphisms utilizing the differential transfer function of field-effect transistors – Biosensors and Bioelectronics 22 (2007), 2834-2840.

[Jin 2006] D. Jin, X. Li, J. Liu, G. Zuo, Y.Wang, M. Liu and H. Yu - High-mode resonant piezoresistive cantilever sensors for tens-femtogram resoluble mass sensing in air - Journal of Micromechanics and Microengineering 16 (2006), 1017–1023.

[Johansson 2005] A. Johansson, M. Calleja, P.A. Rasmussen, A. Boisen - SU-8 cantilever sensor system with integrated readout - Sensors and Actuators A 123–124 (2005), 111–115.

[Kanda 1982] Y. Kanda – A graphical representation of the piezoresistance coefficients in Silicon – IEEE Transactions on Electron Devices, ED-29 (1) (1982), 64-70.

[Kim 2004] D. Kim, Y. Jeong, H. Park, J. Shin, P. Choi, J. Lee, G. Lim – An FET-type charge sensor for highly sensitive detection of DNA sequence – Biosensor and Bioelectronics 20 (2004), 69-74.

[Lange 2002] D. Lange, O. Brand, H. Baltes - CMOS Cantilever Sensor Systems - Atomic-Force Microscopy and Gas Sensing Applications – Springer, 2002.

[Lange 2003] D. Lange, C. Hagleitner, C. Herzog, O. Brand, H. Baltes - Electromagnetic actuation and MOS-transistor sensing for CMOS-integrated micromechanical resonators - Sensors and Actuators A 103 (2003), 150–155.

[Lee 2004] J. H. Lee, K. H. Yoon, K. S. Hwang, J. Park, S. Ahn, T. S. Kim, Label free novel electrical detection using micromachined PZT monolithic thin film cantilever for the detection of C-reactive protein - Biosensors and Bioelectronics 20 (2004), 269–275.

[Lee 2004/2] S. H. Lee, S. S. Lee, J.-J. C., J. U. Jeon and K. Ro - Fabrication of a High-Aspect-Ratio Nano Tip Integrated Micro Cantilever with a ZnO Piezoelectric Actuator - Key Engineering Materials (270-273) (2004), 1095-1100.

[Li 2006] P. Li, X. Li, G. Zuo, J. Liu, Y. Wang, M. Liu, and D. Jin - Silicon dioxide microcantilever with piezoresistive element integrated for portable ultraresoluble gaseous detection - Applied Physics Letters 89 (2006), 074104.

[Li 2006/2] Y. Li, M. Ho, S. Hung, M. Chen and M. Lu - CMOS micromachined capacitive cantilevers for mass sensing - Journal of Micromechanics and Microengineering 16 (2006), 2659–2665.

[Li 2007] M. Li, H. X. Tang And M. L. Roukes - Ultra-sensitive NEMS-based cantilevers for sensing, scanned probe and very high-frequency applications - Nature Nanotechnology 2 (2007), 114-120.

[Li 2009] X. Li, H. Yu, X. Gan, X. Xia, P. Xu, J. Li, M. Liu, and Y. Li - Integrated MEMS/NEMS Resonant Cantilevers for Ultrasensitive Biological Detection - Journal of Sensors 2009, 637874.

[Lillemose 2008] M. Lillemose, M. Spieser, N.O. Christiansen, A. Christensen and A. Boisen - Intrinsically conductive polymer thin film piezoresistors - Microelectronic Engineering 85 (5-6) (2008), 969-971.

[Linder 2007] V. Linder - Microfluidics at the crossroad with point-of care diagnostics - The Analyst 132 (2007), 1186–1192.

[Liu 2003] F. Liu, Y. Zhang, Z. Ou-Yang – Flexoelectric origin of nanomechanical deflection in DNA-microcantilever system – Biosensors and Bioelectronics 18 (2003), 655-660.

[Ludwig 2005] A. Ludwig, J. Cao, J. Brugger and I. Takeuchi - MEMS tools for combinatorial materials processing and high-throughput characterization – Measurement Science and Technology 16 (2005), 111–118.

[Madou 2002] M. J. Madou – Fundamentals of microfabrication – CRC Press LLC, 2002.

[Mallick 1993] P.K. Mallick, Fiber-reinforced Composites: Materials, Manufacturing, and Design, CRC Press, 1993.

[McKendry 2002] R. McKendry, J. Zhang, Y. Arntz, T. Strunz, M. Hegner, H. P. Lang, M. K. Baller, U. Certa, E. Meyer, H.-J. Guntherodt and C. Gerber - Multiple label-free biodetection and quantitative DNA-binding assays on a nanomechanical cantilever array – PNAS 99 (15) (2002), 9783–9788.

[McShane 2006] G. J. McShane, M. Boutchich, A. Srikantha Phani, D. F. Moore and T. J. Lu - Young's modulus measurement of thin-film materials using micro-cantilevers- Journal of Micromechanics and Microengineering 16 (2006), 1926–1934.

[Mertens 2005] J. Mertens, M. Alvarez and J. Tamayo – Real-time profile of microcantilevers for sensing applications – Applied Physics Letters 87 (2005), 234102.

[Minne 1995] S. C. Minne, S. R. Manalis, and C. F. Quate - Parallel atomic force microscopy using cantilevers with integrated piezoresistive sensors and integrated piezoelectric actuators - Applied Physics Letters 26 (1995), 3918-3920.

[Mukhopadhyay 2005] R. Mukhopadhyay, M. Lorentzen, J. Kjems and F. Besenbacher – Nanomechanical sensing of DNA sequences using piezoresistive cantilevers – Langmuir 21 (2005), 8400-8408.

[Muralidharan 2003] G. Muralidharan, A. Wig, L.A. Pinnaduwage, D. Hedden, T. Thundat, R. T. Lareau - Adsorption–desorption characteristics of explosive vapors investigated with microcantilevers -Ultramicroscopy 97 (2003), 433–439.

[Ottermann 1996] C.R. Ottermann. K. Bange - Correlation between the density of TiO_2 films and heir properties - Thin Solid film 286 (1996), 32-34.

[Pinnaduwage 2004] L.A. Pinnaduwage, T. Thundat, J.E. Hawk, D.L. Hedden, P.F. Britt, E.J. Houser, S. Stepnowski, R.A. McGill, D. Bubb - Detection of 2,4-dinitrotoluene using microcantilever sensors - Sensors and Actuators B 99 (2004), 223–229.

[Passian 2003] A. Passian, G. Muralidharan, A. Mehta, H. Simpson, T.L. Ferrell, T. Thundat - Manipulation of microcantilever oscillations - Ultramicroscopy 97 (2003), 391–399.

[Price 2007] C. P. Price and L. J. Kricka - Improving Healthcare Accessibility through Point-of-Care Technologies - Clinical Chemistry 53 (9) (2007), 1665–1675.

[Raiteri 2001] R. Raiteri, M. Grattarola, H.-J. Butt, P. Skládal – Micromechanical cantilever-based biosensors – Sensors and Actuators B 79 (2001), 115-126.

[Rasmussen 2003] P.A. Rasmussen, J. Thaysen, O. Hansen, S.C. Eriksen, A. Boisen - Optimised cantilever biosensor with piezoresistive read-out - Ultramicroscopy 97 (2003), 371–376.

[Rasmussen 2004] P. A. Rasmussen, O. Hansen, and A. Boisen - Cantilever surface stress sensors with single-crystalline silicon piezoresistors - Applied Physics Letters 86 (2005), 203502.

[Ren 2004] Q. Ren, Y.-P. Zhao - Influence of surface stress on frequency of microcantilever-based biosensors - Microsystem Technologies 10 (2004), 307–314.

[Rogers 2003] B. Rogers, L. Manning, M. Jones, T. Sulchek, K. Murray, B. Beneschott, and J. D. Adams, Z. Hu and T. Thundat, H. Cavazos and S. C. Minne - Mercury vapor detection with a self-sensing, resonating piezoelectric cantilever - Review Scientific Instruments 74 (2003), 4899.

[Roukes 2007] M. L. Roukes, A. Naik, M. S. Hanay – Single molecule mass spectroscopy enabled by nanoelectromechanical systems (NEMS-MS) – US Patent US 2009/0261241 A1.

[Shekhawat 2006] G. Shekhawat, S-H. Tark, V. P. Dravid – MOSFET-Embedded Microcantilevers for Measuring Deflection in Biomolecular Sensors – Science 311 (2006), 1592-1595.

[Srikar 2003] V.T. Srikar and S.M. Spearing - A Critical Review of Microscale Mechanical Testing Methods Used in the Design of Microelectromechanical Systems – Experimental Mechanics 43 (3) (2003), 238-247.

[Shui 1996] X. Shui and D.D.L. Chung - A piezoresistive carbon filament polymer-matrix composite strain sensor - Smart Materials and Structures 5 (1996), 243.

[Stachowiak 2006] J. C. Stackowiak, M. Yue, K. Castelino, A. Chakraborty, and A. Majumdar – Chemomechanics of surface stress induced by DNA hybridisation – Langmuir 22 (2006), 263-268.

[Stoney 1909] G. G. Stoney – The tension of metallic films deposited by electrolysis – Proceeding of the Royal Society of London A 82 (1909), 172-175.

[Tang 2007] Y. J. Tang, J. Chen, Y. B. Huang, D. C. Li, S. S.Wang, Z. H. Li and W. D. Zhang - Ultra-sensitive, highly reproducible film stress characterization using flexible suspended thin silicon plates and local curvature measurements - Journal Micromechanics and Microengineering 17 (2007), 1923–1930.

[Thaysen 2002] J. Thaysen, A. D. Yalcinkaya, P. Vettiger and A. Menon - Polymer-based stress sensor with integrated readout – Journal of Physics D: Applied Physics 35 (2002), 2698–2703.

[Tseytlin 2005] Y. M. Tseytlin - High resonant mass sensor evaluation: An effective method - Review of Scientific Instruments 76 (2005), 115101.

[Verd 2005] J. Verd, G. Abadal, J. Teva, M. V. Gaudó, A. Uranga, X. Borrisé, F. Campabadal, J. Esteve, E. Figueras Costa, F. Pérez-Murano, Z. J. Davis, E. Forsén, A. Boisen, and N. Barniol - Design, Fabrication, and Characterization of a submicro-electromechanical Resonator With Monolithically Integrated CMOS Readout Circuit - Journal of Microelectromechanical Systems 14 (2005), 508.

[Vettiger 2002] P. Vettiger, G. Cross, M. Despont, U. Drechsler, U. Dürig, B. Gotsmann, W. Häberle, M. A. Lantz, H. E. Rothuizen, R. Stutz, and G. K. Binnig - The "Millipede"—Nanotechnology Entering Data Storage - IEEE Transactions On Nanotechnology 1 (1) (2002), 39-55.

[Vidic 2003] A. Vidic, D. Then, Ch. Ziegler – A new cantilever system for gas and liquid sensing – Ultramicroscopy 97 (2003), 407 – 416.

[Villaroya 2006] M. Villarroya, J. Verd, J. Teva, G. Abadal, E. Forsen, F. Perez Murano, A. Uranga, E. Figueras, J. Montserrat, J. Esteve, A. Boisen, N. Barniol - System on chip mass sensor based on polysilicon cantilevers arrays for multiple detection - Sensors and Actuators A 132 (2006), 154–164.

[Weihs 1988] T.P. Weihs, S. Hong, J.C. Bravman, and W. D. Nix - Mechanical deflection of cantilever microbeams: A new technique for testing the mechanical properties of thin films - Journal of Materials Research 3 (5) (1988), 931-944.

[Wu 2001] G. Wu, H. Ji, K. Hansen, T. Thundat, R. Datar, R. Cote, M. F. Hagan, A. K. Chakraborty, and A. Majumdar – Proceedings of the National Academy of Sciences 98 (4) (2001), 1560-1564.

[Yang 2000] J. Yang, T. Ono and M. Esashi – Mechanical behavior of ultrathin microcantilever - Sensors and Actuators A 82 (2000), 102-107.

[Yoshikawa 2009] G. Yoshikawa, H.-P. Lang, T. Akiyama, L. Aeschimann, U. Staufer, P. Vettiger, M. Aono., T. Sakurai and C. Gerber - Sub-ppm detection of vapors using piezoresistive microcantilever array sensors - Nanotechnology 20 (2009) 015501.

[Yi 1999] T. Yi and C. Kim - Measurement of mechanical properties for MEMS materials - Measurement Science and Technology 10 (1999), 706–716.

[Yu 2007] X. Yu, T. Yaquan, H. Zhang, T. Li, and W. Wang - Design of High-Sensitivity Cantilever and Its Monolithic Integration With CMOS Circuits - IEEE Sensors Journal 7 (2007), 489.

[Yu 2008] X. Yu, Y. Tang, H. Zhang – Monolithic integration of micromachined sensors and CMOS circuits based on SOI technologies – Journal of Micromechanics and Microengineering 18 (2008), 037002.

[Ziegler 2004] C. Ziegler – Cantilever-based biosensors – Analytical And Bioanalytical Chemistry 379 (2004), 946-959.

[Waggoner 2007] P. S. Waggoner and H. G. Craighead – Micro- and nanomechanical sensors for environmental, chemical, and biological detection – Lab on a Chip 7 (2007), 1238-1255.

[Wang 1993] Z.Z. Wang, J. Suski, D. Collard - Piezoresistive simulation in MOSFETs – Sensors and Actuators A 37–38 (1993), 357–364.

[Wehrmeister 2007] J. Wehrmeister, A. Fuß, F. Saurenbach, R. Berger, M. Helm – Readout of micromechanical cantilever sensor arrays by Fabry-Perot interferometry – Review Scientific Instruments 78 (2007), 104105.

[Zhang 2002] W.J. Zhang, Y. Li, F.H. Wang - Properties of TiO_2 Thin Films Prepared by Magnetron Sputtering - Journal of Materials Sciences and Technology 18 (2002), 101.

[Zhang 2004] W. Zhang, Y. Li, S. Zhu, F. Wang - Influence of argon flow rate on TiO_2 photocatalyst film deposited by dc reactive magnetron sputtering - Surface and Coatings Technology 182 (2004), 192.

[Zhang 2004/2] Y. Zhang, Q. Ren and Y. Zhao - Modelling analysis of surface stress on a rectangular cantilever beam - Journal of Physics D: Applied Physics 37 (2004), 2140–2145.

[Zhang 2006] J. Zhang, H. P. Lang, F. Huber, A. Bietsch, W. Grange, U. Certa, R. Mckendry, H.-J. Güntherodt, M. Hegner and Ch. Gerber - Rapid and label-free nanomechanical detection of biomarker transcripts in human RNA – Nature Nanotechnology 1 (2006), 214 – 220.

[Zhang 2007] M. Zhang, G. Lin, C. Dong, L. Wen - Amorphous TiO_2 films with high refractive index deposited by pulsed bias arc ion plating - Surface and Coatings Technology 201 (2007), 7252–7258.

[Zhang 2008] N. H. Zhang, J. Y. Shan – An energy model for nanomechanical deflection of cantilever-DNA chip – Journal of the Mechanics and Physics of Solids 56 (2008), 2328-2337.

Appendix A: List of related publications

- **A. Adami**, M. Decarli, R. Bartali, V. Micheli, N. Laidani, L. Lorenzelli - *Mechanical characterization of thin TiO_2 films by means of MEMS-based cantilevers* – Review of Scientific Instruments – Vol. 81 (1) (2010), pp. 015109.

This work presents the results of the developed method for material characterisation based on cantilever devices, applied to sputtered thin TiO_2 films.

- F. Kalatzis, N. Giannakeas, T. P. Exarchos, L. Lorenzelli, A. Adami, M. Decarli, S. Lupoli, F. Macciardi, S. Markoula, I. Georgiou, D. I. Fotiadis - *Developing a genomic-based point-of-care diagnostic system for rheumatoid arthritis and multiple sclerosis* - IEEE EMBS 2009 Conference - Minneapolis, Minnesota, USA, 2nd - 6th September, 2009.

In this paper it is presented the methodology of designing a genomic-based point-of-care diagnostic system composed of a microfluidic Lab-On-Chip, algorithms for microarray image information extraction and knowledge modelling of genomic and clinical patient data.

- K. Schicho, H. Gruessinger, L. Lorenzelli, M. Decarli, A. Adami, L. Odorizzi, F. Macciardi, F. Kalatzis – *Lab-on-chip, Innovative approach towards telemedicine in primary care* - Asian Hospital & Healthcare Management, Issue 19 (2009), pp 66-67.

This work present the potential of LOC system based on MEMS technologies and cantilever detectors on healthcare cost and management.

- E. Morganti, C. Collini, C. Ress, A. Adami, L. Lorenzelli - *Design and fabrication of a micro PCR module for POC applications* – Lab-on-a-Chip European Congress, 19-20 May 2009 – Stockholm, Sweden. Published on "The Online Journal of Scientific Posters" (ISSN 1754-1417).

This work presents the development of microfluidic PCR modules, finalised to the development of cantilever-based LOC for the analysis of DNA single-base polymorphism related to autoimmune diseases.

- Adami, M. Decarli, L. Odorizzi, L. Lorenzelli, K. Fincati, K. Schicho, H. Gruessinger – *Development of MEMS microcantilever arrays for DNA single nucleotide polymorphism detection in autoimmune diseases diagnostic* – Book of Abstract of the conference: AISEM 2009, 14th National Conference on Sensors and Microsystems, 24-26 February 2009, Pavia.

In this work, the development of a cantilever-based detector arrays for LOC application is presented, especially aimed to the integration in point of care systems for early diagnosis and screening of autoimmune disorders based on typing of Human Leukocyte Antigen (HLA). The design and technological implementation of single crystal cantilevers with very low thickness are presented, finalised to the

evaluation of technologies and functionalisation procedures for high-density and high sensitivity detector arrays with piezoresistive readout.

- M. Decarli, A. Adami, L. Odorizzi, L. Lorenzelli and K. Fincati - *Development of a microfabrication technology for microcantilever-based detection modules in Lab-On-a-Chip application* – Proceeding of the NNC National Nanomedicine Congress 2008, 28-29 November 2008, Genova, Italy.

In this work, the design and realization of the first prototypes of microcantilever are presented, finalised to the pre-screenings of autoimmune diseases such as multiple sclerosis and rheumatoid arthritis with LOC systems in point-of-care applications.

- Adami, M. Decarli, L. Lorenzelli, F. G. Kalatzis, F. Macciardi, H. Gruessinger, K. Schicho - *The EU FP7 IP Project POCEMON: Point-Of-Care MONitoring and Diagnostics for Autoimmune Diseases* - Third International Workshop on Multianalyte Biosensing Devices, Athens, September 18-19, 2008.

In this work, a novel approach to the point of care diagnosis and screening will be described, based on typing of Human Leukocyte Antigen (HLA) with Lab-on-Chip (LOC) technologies and computer based artificial intelligent algorithms for the early prognosis and diagnosis of Autoimmune Disorders. HLA-typing will be based on LOC systems with Polymerase Chain Reaction (PCR) modules and cantilever array detectors integrated with Personal Digital Assistants (PDA) and diagnostic software for the realisation of an automated and portable diagnostic system. This hardware platform will allow complex analysis and diagnosis at any point of care, while the diagnostic software will be developed with advanced programming environments and deployment of artificial intelligent algorithms.

- Adami, M. Decarli, L. Lorenzelli, V. Guarnieri, M. Malfatti, C. Apetrei, M. L. Rodriguez Mendez - *Microcantilever-based sensor array for amine detection in agro-food applications* – Proceedings of the conference Smart Systems Integration 2008, 9-10 April 2008, Barcelona, Spain, VDE Verlag GMBH, pp. 375-377.

This work presents the development of silicon microcantilever-based sensor arrays for food quality monitoring applications. The devices, realised with a CMOS-compatible process, allow the detection of amines by monitoring the shift of resonance frequency due to analyte adsorption. Investigation of sensitivity properties and piezoresistive read-out performances has been carried out by both finite element analysis and analytical models.

- M. Decarli, A. Adami, L. Lorenzelli, N. Laidani - *MEMS-based Silicon Cantilevers Arrays for combinatorial analysis of thin-film materials* – Proceedings of the conference: Eurosensors XX, Gothenburg, Sweden, 17-20 September 2006.

Appendix A: List of related publications

This research work presents the modelling, design and fabrication of silicon microcantilevers arrays, suitable for the mechanical characterization of thin-film materials, deposited with combinatorial methods. Microcantilevers are realized with micromachining technology and are used for the on-line evaluation of the residual stress and Young's Modulus of thin-films during their depositions by revealing the beam bending profile.

Appendix B: Other related publications

Other activities not related to cantilever detectors have been developed in order to explore the suitability of MEMS-based approach to the realisation of instrumentations for on-field analyses, especially in the agro-food field. Such studies can be considered as an exploration of MEMS systems for portable application that can take advantage of the developed cantilever sensors, for instance chromatographic systems, or be used in parallel to increase the system functionalities (for instance gas sensors). Papers published in these topics are reported here as "Other relevant publications", although the activities are not described in detail in this thesis.

- A. Adami, E. Morganti, L. Lorenzelli, L. Francioso, P. Siciliano - *A novel approach to data analysis for semiconductor metal-oxide gas sensors in chromatographic systems* – In revision phase for the publication on Sensors and Actuators B.
- C. Ress, A. Tindiani, A. Adami, C. Collini, S. Pedrotti, L. Odorizzi, L. Lorenzelli - *Wine yeast quality assessment with integrated multiparametric microsensors* – Book of abstract of the conference: Biosensors 2010 - 20th World Congress on Biosensors, 26-28 May 2010, Glasgow, UK.
- C. Ress, A. Tindiani, A. Adami, C. Collini, S. Pedrotti, L. Odorizzi, L. Lorenzelli - *A multiparametric electrochemical microsensor for wine yeast quality assessment* – Proceedings of the conference Smart System Integration, 23-24 March 2010, Como, Italy.
- C. Ress, A. Adami, L. Lorenzelli, C. Collini, A. Tindiani, A. Maglione, G. Soncini - *Development and characterization of a multiparametric microsensor for yeast cell growth monitoring* - Procedia Chemistry, Volume 1, Issue 1, (2009), pp. 1059-1062. (Eurosensors XXIII, Lausanne 6-10 September 2009)
- L. Francioso, A. Forleo, A.M. Taurino, P. Siciliano, L. Lorenzelli, V. Guarnieri, A. Adami, G. Agnusdei - *Linear temperature microhotplate gas sensor array for automotive cabin air quality monitoring* - Sensors and Actuators B: Chemical, Vol. 134, Issue 2, 25 September 2008, pp. 660-665.
- Adami, L. Lorenzelli, D. Presicce, M. Malfatti, V. Guarnieri, L. Francioso, P. Siciliano, G. Agnusdei, M. Zen - *A Cr-doped WO_3 sensor for chromatographic systems in wine quality applications* – Proceedings of the conference IEEE Sensors 2008, 26-29 October 2008, Lecce, Italy, pp. 1378 - 1381.
- D.S. Presicce, L. Francioso, P. Siciliano, A. Adami, L. Lorenzelli, M. Malfatti, V. Guarnieri, M. Zen – *Development of a new portable microsystem for wine quality analysis* – Proceedings of the 12th Italian Conference on Sensors and Microsystems [AISEM 2007, 12-14 February 2007, Na-

poli], Ed. G. Di Francia, P. Maddalena, I. Rendina, C. Di Natale and A. D'Amico, pp. 245-250, World Scientific Publishing, 2008.

- Benvenuto, L. Lorenzelli, C. Collini, V. Guarnieri, A. Adami, E. Morganti - *A liquid chromatography miniaturised system for agrofood applications* - Microsystem technologies, Vol. 14, Numbers 4-5, pp. 551-556, April 2008.
- Benvenuto, V. Guarnieri, L. Lorenzelli, C. Collini, M. Decarli, A. Adami, C. Potrich, L. Lunelli , R. Canteri, C. Pederzolli - *Fabrication of a MEMS-based separation module for liquid chromatography* – Sensors and Actuators B, Vol. 130, Issue 1, pp. 181-186, March 2008.
- Adami, C. Collini, L. Lorenzelli, F. Verlato, P. Bouvier, A. Maglione - *Development and characterisation of a multianalyte sensing platform* - Third International Workshop on Multianalyte Biosensing Devices, Athens, September 18-19, 2008.
- Benvenuto A., Lorenzelli L., Collini C., Guarnieri V., Adami A., Morganti E., - *Development of MEMS-based liquid chromatography modules for agrofood applications.* - In: Smart Sensors, Actuators, and MEMS III (SPIE Europe Microtechnologies for the New Millennium, 2 - 4 May 2007, Maspalomas, Gran Canaria, Spain). Thomas Becker; Carles Cané; N. Scott Barker (eds.) Proc. SPIE Vol 6589, 65890D, 8 pp., 2007.